General Disclaimer

One or more of the Following Statements may affect this Document

- This document has been reproduced from the best copy furnished by the organizational source. It is being released in the interest of making available as much information as possible.

- This document may contain data, which exceeds the sheet parameters. It was furnished in this condition by the organizational source and is the best copy available.

- This document may contain tone-on-tone or color graphs, charts and/or pictures, which have been reproduced in black and white.

- This document is paginated as submitted by the original source.

- Portions of this document are not fully legible due to the historical nature of some of the material. However, it is the best reproduction available from the original submission.

Produced by the NASA Center for Aerospace Information (CASI)

NASA CR-135079

(NASA-CR-135079) SYSTEM ANALYSIS OF PLASMA CENTRIFUGES AND SPUTTERING Final Report, 1 Nov. 1976 - 31 Oct. 1977 (Colorado State Univ.) 141 p HC A07/MF A01 CSCL 20I

N78-29916

Unclas

G3/75 29059

FINAL REPORT

SYSTEM ANALYSIS OF PLASMA CENTRIFUGES AND SPUTTERING

COVERING THE PERIOD

1 NOVEMBER 1976 - 31 OCTOBER 1977

FOR:

LEWIS RESEARCH CENTER

NATIONAL AERONAUTICS AND SPACE ADMINISTRATION

GRANT NGR-06-002-147

SEP 1978

RECEIVED

NASA STI FACILITY

MAY 1978

DEPARTMENT OF ELECTRICAL ENGINEERING

COLORADO STATE UNIVERSITY

FORT COLLINS, COLORADO 80523

TABLE OF CONTENTS

Chapter		Page
I.	INTRODUCTION	1
II.	SOLUTION OF EXTERNAL BOUNDARY-VALUE PROBLEM FOR DEPOSITION OF SPUTTERING PRODUCTS	3
	2.1 Boundary-Value Problem	7
	2.2 Integral Equation and Solution	13
III.	PLASMA ROTATION BY LORENTZ FORCES IN A DIVERGING PLASMA CENTRIFUGE WITH HALL EFFECT	17
	3.1 Model of Diverging Plasma Centrifuge	17
	3.2 Boundary-value Problem for Velocity and Electric Potential	20
	3.3 Fourier-Bessel and Dini Series Solutions	22
	3.4 Numerical Illustrations and Results	30
IV.	EFFECT OF INDUCED MAGNETIC FIELD ON DIVERGING PLASMA CENTRIFUGE WITH ARBITRARY MAGNETIC REYNOLDS NUMBERS	49
	4.1 Boundary-value Problem for Velocity and Induced Magnetic Field	49
	4.2 Analytical Solutions in Terms of Fourier-Bessel Series	52
	4.3 Numerical Illustrations and Results	61
V.	PLASMA COUNTER-ROTATION IN MULTI-DISCHARGE CENTRIFUGE	80
	5.1 Model for Multi-discharge Centrifuge	80
	5.2 Boundary-value Problem for Velocity and Radial Current Density	83
	5.3 Fourier Series Solutions in Terms of Bessel Functions of Complex Arguments	86
	5.4 Numerical Illustrations and Results	91
VI.	APPLICATION TO ISOTOPE SEPARATION	104
VII.	COMPRESSIBLE PLASMA CENTRIFUGE WITH SECONDARY FLOWS	107
	7.1 Plasma Centrifuge Model with Secondary Flows	107
	7.2 Analytical Method	111
	7.3 Theoretical Formulation	112
	7.4 Solutions for Primary Fields	115
	7.5 Eigen-value Problem for Secondary Fields	116

VIII. COLLISIONLESS PLASMA CENTRIFUGE 121

8.1 Model 121
8.2 Boundary-value Problem for Vlasov-Maxwell Equations 123
8.3 Quasi-neutral Solutions 127

IX. APPENDIX: PREVIOUS RESEARCH ON ISOTOPE SEPARATION . . . 130

CHAPTER I

INTRODUCTION

The Research Grant NGR-06-002-147 is concerned with the system analysis of collision-dominated and collisionless plasma centrifuges and the theory of sputtering and deposition of sputtering products on surfaces. The period of the grant extended from 1 November 1976 to 31 October 1977. This is the final report on the research carried through in this period.

In Chapter II, an analytical theory is developed describing the deposition of sputtered atoms on system surfaces which cannot be seen along straight paths from the emitting surface. The boundary-value problem describing the diffusion of the sputtered atoms through the surrounding rarefied electron-ion plasma to the "hidden" system surfaces is formulated and treated analytically. It is shown that outer boundary-value problems of this type lead to a Fredholm integral equation. The latter is solved by the method of successive approximations. A quantum theory of sputtering of metal surfaces by low energy ions (<100eV) has been developed and submitted for publication. This work will be communicated at a later date.

In Chapters III and IV, centrifuge models employing ring electrodes of different radii located in the end plates of a cylindrical discharge chamber, are analyzed which avoid the boundary layers at the inner electrode cylinder and (probably) the secondary flows and instabilities occurring in the magnetohydrodynamic flow between concentric cylinders (Chandrasekhar 1961). Complete two-dimensional solutions are derived which show that the Hall effect enhances plasma rotation (Chapter III) and that the induced magnetic field does not interfere with the rotation due to the external magnetic field (Chapter IV). These schemes exhibit velocity end losses due to the boundary layers in the cathode and anode planes.

For this reason, an improved centrifuge system is conceived, which essentially avoids the velocity end losses caused by boundary layers at the electrode plates (Chapter V). In view of the circumferential electrode arrangement, a multidischarge counter-rotating centrifuge can be set up in a long insulating cylinder to rotate large volume of isotope mixtures. In Chapter VI, the theory is applied to the separation of U_{238} and U_{235}. The difficult problem of compressible plasma centrifuge analysis is formulated in Chapter VII and solved by means of Lyapunov-Schmidt series expansions. In Chapter VII, a simple theory for a collisionless plasma centrifuge is formulated based on the coupled Vlasov-Maxwell equations for the electron and ion components.

CHAPTER II

SOLUTION OF EXTERNAL BOUNDARY-VALUE PROBLEM FOR DEPOSITION OF SPUTTERING PRODUCTS

In an ideal vacuum, sputtered atoms travel undeflected along straight paths determined by their initial velocities at the point of emission. Within this free particle flow, a system surface is reached by the sputtered atoms only if it can be seen along a straight line from the emitting surface. In reality, ion propulsion systems are surrounded by a very rarefied plasma consisting of escaped beam ions, recombined ions, and electrons. For this reason, always some of the sputtered atoms will be deflected out of their initial paths by interacting through long-range forces (polarization forces) with the plasma particles so that they can reach system surfaces which are not seen along a straight line from the emitter.

An idealized propulsion system exhibits an emitting plane $z = 0$, $0 \leq r \leq a$ (accelerating grid), the rocket surfaces $r = a$, $-c \leq z \leq 0$ and $z = -c$, $0 \leq r \leq a$, and the plane $z = -d$, $a \leq r \leq b$ of the solar energy collectors. All these system surfaces can be reached by the atoms sputtered from the emitter by diffusion through the rarefied plasma. The diffusion coefficient D is determined by the Vlasov equation for the sputtered atoms interacting through weak long-range forces with the plasma particles. In view of the mathematical difficulties associated with the solution of boundary-value problems for this geometry, a somewhat simpler system is studied here consisting of an emitting plane ($z = 0$, $0 \leq r \leq a$), the upper rocket surface ($r = a$, $-c \leq z \leq 0$) and the plane ($z = -c$, $a \leq r \leq \infty$) of the solar energy collectors (Fig. 1). The latter is assumed to have infinite radial extension.

Ordinary boundary-value problems are defined for a space bounded

on the "outside" by boundaries, whereas external boundary-value problems are defined for the space surrounding "inner" boundaries. In terms of cylindrical coordinates (r,θ,z), the space in Fig. 1 consists of the adjacent regions,

$$\text{I:} \quad 0 \leq z \leq \infty, \; 0 \leq r \leq \infty;$$

$$\text{II:} \quad -c \leq z \leq 0, \; a \leq r \leq \infty.$$

In this case, the "inner" boundaries are formed by the cylindrical wall $(r = a, -c \leq z \leq 0)$ and the circular end-surface $(0 \leq r \leq a, z = 0)$ of a cylinder of radius $r = a$ extending from the plane $z = -c$ to the height $z = 0$. On the other hand, the plane $z = -c$, $a \leq r \leq \infty$ represents an external boundary of the space II.

We consider herein the external boundary-value problem for the steady-state diffusion (Laplace) equation and the space I + II shown in Fig. 1 when the end-surface $(0 \leq r \leq a, z = 0)$ of the cylinder emits particles at a given rate $I(r)$. At the inner, cylindrical boundary $(r = a, -c \leq z \leq 0)$ and the bottom plane $(z = -c, a \leq r \leq \infty)$ the particles are assumed to be deposited by adsorption or absorption.

Various other transport processes for particles or heat in technical, physical, and biological systems lead to external boundary-value problems of this type. We mention as examples i) the emission of particles from a cylindrical chimney into a gaseous atmosphere, and ii) the injection of a liquid from a cylindrical probe into a biological medium.

Analytical or numerical solutions of external boundary-value problems have apparently not been given in the literature. We will demonstrate that the considered external boundary-value problem can be solved analytically by means of a Weber transform. In this analytical solution a matching function $\psi(r)$, $a \leq r \leq \infty$ (at the interface of the regions I and

II), occurs which is determined by an inhomogeneous Fredholm integral equation of the first kind. This integral equation is discussed and transformed into an inhomogeneous Fredholm equation of the second kind, which is solved by the method of successive approximations.[1)]

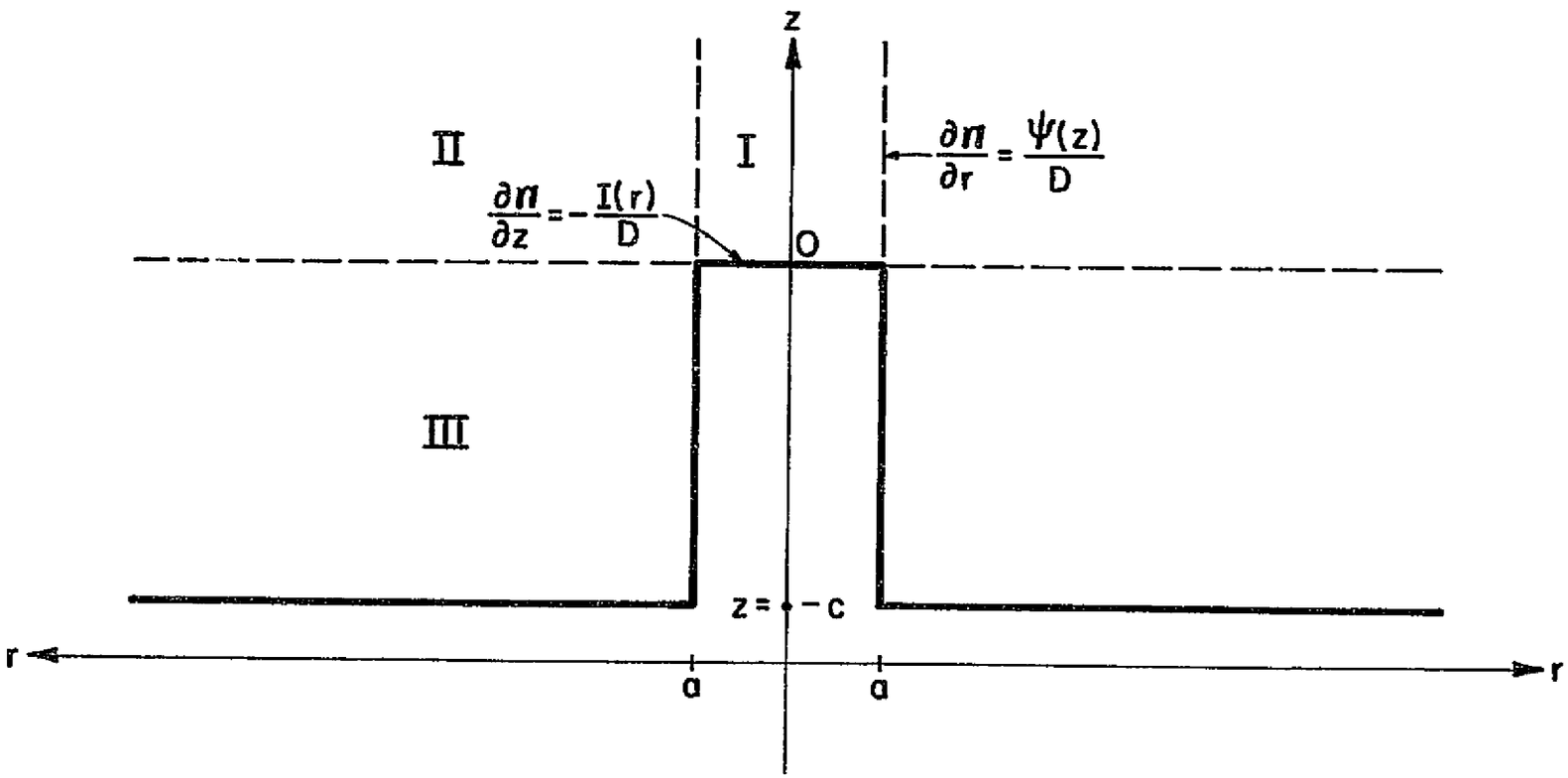
z
II
I
$\frac{\partial n}{\partial z} = -\frac{I(r)}{D}$
$\frac{\partial n}{\partial r} = \frac{\psi(z)}{D}$
O
III
z = -c
r
a
a
r

Figure 1

BOUNDARY-VALUE PROBLEM

In the space $z \geq -c$, let the density of the diffusing particles be designated by $n(r,z)$ [cm^{-3}] and the flux of emitted atoms at the emitter surface by $I(r)$ [$cm^{-3} \cdot cm\ sec^{-1}$]. In steady state, the spatial distribution $n = n(r,z)$ of particles is determined by the external boundary-value problem for the Laplace equation (Fig. 1):

$$\frac{\partial^2 n}{\partial r^2} + \frac{1}{r}\frac{\partial n}{\partial r} + \frac{\partial^2 n}{\partial z^2} = 0 \tag{1}$$

with

$$[\partial n(r,z)/\partial z]_{z=0} = -I(r)D^{-1}, \qquad 0 \leq r \leq a \quad , \tag{2}$$

$$n(r,z)_{r=a} = 0, \ -c \leq z \leq 0 \quad , \tag{3}$$

$$n(r,z)_{z=-c} = 0, \ a \leq r \leq \infty \quad , \tag{4}$$

and

$$n(r,z) \to 0, \qquad (r^2 + z^2) \to \infty \quad , \tag{5}$$

as the proper and improper boundary conditions, respectively. D designates the diffusion coefficient of the particles.

The boundary conditions (3)-(4) imply that particles arriving at the indicated surfaces are deposited there, i.e., do not return into the diffusion space. The fluxes $\Phi_i = -D\ \nabla_i n$ of particles arriving at the system surfaces $r = a$, $-c \leq z \leq 0$ and $z = -c$, $a \leq r \leq \infty$ are given by (Fig. 1):

$$\Phi_r(r = a,z) = -D\ \partial n(r = a,z)/\partial r, \qquad -c \leq z \leq 0 \quad , \tag{6}$$

$$\Phi_z(z = -c,r) = -D\ \partial n(z = -c,r)/\partial z, \qquad a \leq r \leq \infty \quad , \tag{7}$$

Accordingly,

$$\dot{N}_{r=a} = -2\pi a D \int_{-c}^{0} [\partial n(r = a,z)/\partial r]dz \quad , \tag{8}$$

$$\dot{N}_{z=-c} = -2\pi D \int_a^\infty [\partial n(r,z = -c)/\partial z] r dr \quad , \qquad (9)$$

are the numbers of particles deposited per unit time on the system surfaces $r = a$, $-c \leq z \leq 0$ and $z = -c$, $a \leq r \leq \infty$, respectively.

The above boundary-value problem cannot be solved directly, i.e., requires a decomposition of the space $z \geq -c$ into appropriate subregions I and II for which the associated boundary-value problems are solvable. In this approach, a common boundary value $[\psi(r)]$ at the decomposition plane is determined by an integral equation.

Let dimensionless independent and dependent variables be introduced in accordance with:

$$\rho = r/a, \quad 0 \leq \rho \leq \infty; \quad \zeta = z/c, \quad -1 \leq \zeta \leq \infty \quad , \qquad (10)$$

and

$$N(\rho,\zeta) = n(r,z)/n_o, \quad S(\rho) = I(r)/I_o \quad , \qquad (11)$$

with

$$n_o \equiv cI_o/D, \quad I_o \equiv I(r=0), \quad \gamma \equiv c/a \quad . \qquad (12)$$

The boundary-value problem defined in Eqs. (1)-(5) reads in dimensionless form:

$$\frac{\partial^2 N}{\partial \rho^2} + \frac{1}{\rho}\frac{\partial N}{\partial \rho} + \gamma^{-2}\frac{\partial^2 N}{\partial \zeta^2} = 0 \qquad (13)$$

where

$$[\partial N(\rho,\zeta)/\partial\zeta]_{\zeta=0} = -S(\rho), \quad 0 \leq \rho \leq 1 \quad , \qquad (14)$$

$$N(\rho,\zeta)_{\rho=1} = 0, \quad -1 \leq \zeta \leq 0 \quad , \qquad (15)$$

$$N(\rho,\zeta)_{\zeta=-1} = 0, \quad 1 \leq \rho \leq \infty \quad , \qquad (16)$$

and

$$N(\rho,\zeta) \to 0, \quad (\rho^2 + \zeta^2) \to \infty \quad . \qquad (17)$$

In Fig. 1, the space is decomposed into the regions

I($0 \leq \rho \leq \infty$, $0 \leq \zeta \leq \infty$) and II($1 \leq \rho \leq \infty$, $-1 \leq \zeta \leq 0$). At the interface $\zeta = 0$, $1 \leq \rho \leq \infty$, the partial $\partial N(\rho,\zeta = 0)/\partial\zeta = \Psi(\rho)H(\rho-1)$ is introduced as the common (unknown) boundary value $\Psi(\rho)$ of the adjacent regions I and II, $1 \leq \rho \leq \infty$. Thus, the boundary-value problem in Eqs. (13)-(17) can be decomposed into boundary-value problems for the regions I and II.

I. In region I, $N \equiv N_I(\rho,\zeta)$ is described by the ordinary boundary-value problem:

$$\frac{\partial^2 N_I}{\partial\rho^2} + \frac{1}{\rho}\frac{\partial N_I}{\partial\rho} + \gamma^{-2}\frac{\partial^2 N_I}{\partial\zeta^2} = 0, \qquad 0 \leq \rho \leq \infty, \qquad 0 \leq \zeta \leq \infty \quad , \tag{18}$$

$$[\partial N_I(\rho,\zeta)/\partial\zeta]_{\zeta=0} = -S(\rho), \qquad 0 \leq \rho \leq 1 - 0 \quad ,$$

$$= \Psi(\rho), \qquad 1 + 0 \leq \rho \leq \infty \quad , \tag{19}$$

$$N_I(\rho,\zeta) \to 0, \qquad (\rho^2 + \zeta^2) \to \infty \quad , \tag{20}$$

where

$$S(\rho \geq 1+0) \equiv 0, \ \Psi(\rho \leq 1-0) \equiv 0 \tag{21}$$

for physical reasons. Since region I is the upper half of the infinite space ($0 \leq \zeta \leq \infty$), the general solution of Eqs. (18) and (20) is given by the Fourier integral,

$$N_I(\rho,\zeta) = \int_0^\infty A(k)e^{-\gamma k\zeta} J_o(k\rho)dk \quad , \tag{22}$$

which satisfies the improper boundary condition for $\rho \to \infty$ and $\zeta \to \infty$. The Fourier amplitude $A(k)$ is determined by the boundary condition (19),

$$-\gamma \int_0^\infty A(k)\ J_o(k\rho)\ kdk = -S(\rho)H(1-\rho) + \Psi(\rho)H(\rho-1) \quad . \tag{23}$$

Application of the inverse Hankel transform to Eq. (23) gives

$$A(k) = \gamma^{-1}\int_0^1 S(\alpha)J_o(k\alpha)\ \alpha d\alpha - \gamma^{-1}\int_1^\infty \Psi(\alpha)J_o(k\alpha)\ \alpha d\alpha \quad . \tag{24}$$

Substitution of Eq. (24) into Eq. (22) results in the solution for region 1:

$$N_I(\rho,\zeta) = \gamma^{-1} \int_0^\infty dk\, e^{-\gamma k\zeta}\, J_o(k\rho)[\int_0^1 S(\alpha)J_o(k\alpha)\, \alpha d\alpha - \int_1^\infty \Psi(\alpha)J_o(k\alpha)\, \alpha d\alpha],$$

$$0 \le \rho \le \infty, \quad 0 \le \zeta \le \infty \quad . \tag{25}$$

II. In region II, $N \equiv N_{II}(\rho,\zeta)$ is described by the external boundary-value problem:

$$\frac{\partial^2 N_{II}}{\partial\rho^2} + \frac{1}{\rho}\frac{\partial N_{II}}{\partial\rho} + \gamma^{-2}\frac{\partial^2 N_{II}}{\partial\zeta^2} = 0, \quad 1 \le \rho \le \infty, \quad -1 \le \zeta \le 0, \tag{26}$$

$$[\partial N_{II}(\rho,\zeta)/\partial\zeta]_{\zeta=0} = \Psi(\rho), \quad 1 \le \rho \le \infty \quad , \tag{27}$$

$$N_{II}(\rho,\zeta)_{\rho=1} = 0, \quad -1 \le \zeta \le 0 \quad , \tag{28}$$

$$N_{II}(\rho,\zeta)_{\zeta=-1} = 0, \quad 1 \le \rho \le \infty \quad , \tag{29}$$

$$N_{II}(\rho,\zeta) \to 0, \quad \rho \to \infty, \quad -1 \le \zeta \le 0 \quad . \tag{30}$$

According to Eq. (28), region II has an inner, cylindrical boundary at $\rho = 1$ where $N_{II}(\rho,\zeta)$ vanishes. For this reason, a Fourier integral representation of $N_{II}(\rho,\zeta)$ is needed for $1 \le \rho \le \infty$ which vanishes at $\rho = 1$. According to Weber's integral theorem, an arbitrary function $f(\rho)$, $a \le \rho \le \infty$, with $f(\rho = a, \infty) = 0$ satisfies the integral equation:[2,3]

$$f(\rho) = \int_0^\infty \frac{kdk\, W_k^\nu(\rho)}{J_\nu^2(ka)+Y_\nu^2(ka)} \int_a^\infty f(\alpha)W_k^\nu(\alpha)\, \alpha d\alpha, \quad a \le \rho \le \infty \quad , \tag{31}$$

where

$$W_k^\nu(\rho) \equiv J_\nu(k\rho)Y_\nu(ka) - J_\nu(ka)Y_\nu(k\rho) \quad , \tag{32}$$

and $J_\nu(k\rho)$ and $Y_\nu(k\rho)$ are Bessel functions of order ν of the first and second kind, respectively. In view of Eqs. (31)-(32), a Fourier integral solution of Eqs. (26)-(30) is sought in the form,

$$N_{II}(\rho,\zeta) = \int_0^\infty B(k)W_k(\rho)\ \sinh[\gamma k(\zeta+1)]dk \quad , \tag{33}$$

$$W_k(\rho) \equiv J_o(k\rho)Y_o(k) - J_o(k)Y_o(k\rho) \quad , \tag{34}$$

which obviously satisfies the boundary conditions (28)-(30). The Fourier amplitude B(k) is determined by the boundary condition (27),

$$\gamma \int_0^\infty B(k)W_k(\rho)\ \cosh\gamma k\ kdk = \Psi(\rho), \qquad 1 \leq \rho \leq \infty \quad , \tag{35}$$

which gives

$$B(k) = \{\gamma\cosh\gamma k\cdot[J_o^2(k)+Y_o^2(k)]\}^{-1} \int_1^\infty \Psi(\alpha)W_k(\alpha)\ \alpha d\alpha \quad , \tag{36}$$

by Eq. (31). Substitution of Eq. (36) into Eq. (33) results in the solution for region II:

$$N_{II}(\rho,\zeta) = \gamma^{-1} \int_0^\infty dk\ \frac{\sinh[\gamma k(\zeta+1)]}{\cosh\gamma k} \cdot \frac{W_k(\rho)}{J_o^2(k)+Y_o^2(k)} \int_1^\infty \Psi(\alpha)W_k(\alpha)\ \alpha d\alpha,$$

$$1 \leq \rho \leq \infty, \qquad -1 \leq \zeta \leq 0 \quad . \tag{37}$$

The solutions $N_I(\rho,\zeta)$, Eq. (25), and $N_{II}(\rho,\zeta)$ Eq. (37), contain the yet unknown boundary-value $\Psi(\alpha)$, $1 \leq \alpha \leq \infty$. $\Psi(\alpha)$ is determined by the continuity condition at the interface of regions I and II,

$$N_I(\rho,\zeta)_{\zeta=0} = N_{II}(\rho,\zeta)_{\zeta=0}, \qquad 1 \leq \rho \leq \infty \quad , \tag{38}$$

which gives

$$\int_0^\infty dk\ J_o(k\rho)[\int_0^1 S(\alpha)J_o(k\alpha)\ \alpha d\alpha - \int_1^\infty \Psi(\alpha)J_o(k\alpha)\ \alpha d\alpha]$$

$$= \int_0^\infty dk\ \mathrm{tgh}\gamma k\ \frac{W_k(\rho)}{J_o^2(k)+Y_o^2(k)} \int_1^\infty \Psi(\alpha)W_k(\alpha)\ \alpha d\alpha, \qquad 1 \leq \rho \leq \infty. \tag{39}$$

Eq. (39) indicates that $\Psi(\alpha)$ is determined by an inhomogeneous integral equation.[1)]

Because of the boundary conditions (19) and (27), the remaining continuity condition at the interface of regions I and II,

$$[\partial N_I(\rho,\zeta)/\partial\zeta]_{\zeta=0} = [\partial N_{II}(\rho,\zeta)/\partial\zeta]_{\zeta=0}, \qquad 1 \leq \rho \leq \infty \qquad , \tag{40}$$

has already been sati ied. Indeed, substitution of Eqs. (25) and (37) into Eq. (40) yields

$$-\int_0^\infty kdk\ J_o(k\rho)[\int_0^1 S(\alpha)J_o(k\alpha)\ \alpha d\alpha - \int_1^\infty \Psi(\alpha)J_o(k\alpha)\ \alpha d\alpha]$$

$$= \int_0^\infty kdk\ \frac{W_k(\rho)}{J_o^2(k)+Y_o^2(k)} \int_1^\infty \Psi(\alpha)W_k(\alpha)\ \alpha d\alpha, \qquad 1 \leq \rho \leq \infty. \tag{41}$$

By means of the Hankel and Weber integral representations for the Dirac function $\delta(\alpha-\rho)$,

$$\int_0^\infty J_o(k\rho)J_o(k\alpha)\ kdk = \delta(\alpha-\rho)/\alpha \qquad , \tag{42}$$

$$\int_0^\infty \frac{W_k(\rho)W_k(\alpha)}{J_o^2(k)+Y_o^2(k)}\ kdk = \delta(\alpha-\rho)/\alpha \qquad , \tag{43}$$

Eq. (41) is reduced to

$$-\int_0^1 S(\alpha)\delta(\alpha-\rho)\ d\alpha + \int_1^\infty \Psi(\alpha)\delta(\alpha-\rho)\ d\alpha$$

$$= \int_1^\infty \Psi(\alpha)\delta(\alpha-\rho)\ d\alpha, \qquad 1 \leq \rho \leq \infty \qquad . \tag{44}$$

Eq. (44) gives the expected identity, $\Psi(\rho) = \Psi(\rho)$, since the first integral vanishes by Eq. (21).

INTEGRAL EQUATION

By introducing the kernel $K(\alpha,\rho)$ and the source $Q(\rho)$, the integral equation in Eq. (39) can be rewritten in the convenient form:

$$\int_1^\infty \Psi(\alpha)K(\alpha,\rho)\ \alpha d\alpha = Q(\rho), \qquad 1 \leq \rho \leq \infty \qquad , \tag{45}$$

where

$$K(\alpha,\rho) \equiv \int_0^\infty J_o(k\alpha)J_o(k\rho)dk + \int_0^\infty tgh\gamma k \frac{W_k(\alpha)W_k(\rho)}{J_o^2(k)+Y_o^2(k)}\, dk \qquad , \tag{46}$$

$$Q(\rho) = \int_0^\infty dk\ J_o(k\rho)\int_0^1 S(\alpha)J_o(k\alpha)\ \alpha d\alpha \qquad . \tag{47}$$

For simple particle emission distributions $S(\alpha)$, e.g., in the case of a homogeneous and a parabolic emission distributions, respectively, the source integral $Q(\rho)$ is readily evaluated,

$$Q(\rho) = \frac{2}{\pi}\rho[E(\tfrac{1}{\rho}) - (1 - \frac{1}{\rho^2})K(\tfrac{1}{\rho})], \qquad 1 \leq \rho \leq \infty \qquad ,$$

$$\text{for } S(\alpha) = 1, \qquad 0 \leq \alpha \leq 1 \qquad , \tag{48}$$

and

$$Q(\rho) = \frac{4\rho}{9\pi}\ [(4-2\rho^2)E(\tfrac{1}{\rho})-(1-\frac{1}{\rho^2})(3-2\rho^2)K(\tfrac{1}{\rho})] \qquad ,$$

$$\text{for } S(\alpha) = 1-\alpha^2, \qquad 0 \leq \alpha \leq 1 \qquad . \tag{49}$$

$K(\frac{1}{\rho})$ and $E(\frac{1}{\rho})$ are the complete elliptic integrals of the first and second kind, respectively [$K(1) = \infty$, $E(1) = 1$].[4] Eq. (45) reduces the external boundary-value problem to the resolution of an inhomogeneous Fredholm integral equation of the first kind for the unknown boundary-value $\Psi(\rho)$, $1 \leq \rho \leq \infty$.

Comparison of the integrals in Eq. (46) with Eqs. (42)-(43) indicates that the kernel $K(\alpha,\rho)$ is the sum of two integral functionals

which are singular at $\alpha = \rho$, similar to the Dirac function.* It follows that the solution of the integral equation (45) is $\Psi(\rho) \cong \Psi_0(\rho) = \frac{1}{2} Q(\rho)$ in the lowest approximation. By means of Eqs. (42)-(43), we transform Eq. (45) into the Fredholm integral equation of the second kind:[1)]

$$\Psi(\rho) = \tilde{Q}(\rho) + \frac{1}{2}\int_1^\infty \Psi(\alpha)\, \tilde{K}(\alpha,\rho)\, d\alpha, \qquad 1 \leq \rho \leq \infty \qquad , \tag{50}$$

where

$$\tilde{K}(\alpha,\rho) = \alpha\int_0^\infty J_o(k\alpha)J_o(k\rho)(k-1)dk + \alpha \int_0^\infty \frac{W_k(\alpha)W_k(\rho)}{J_o^2(k)+Y_o^2(k)} (k-\mathrm{tgh}\gamma k)\, dk \ , \tag{51}$$

$$\tilde{Q}(\rho) = \frac{1}{2} Q(\rho) \qquad . \tag{52}$$

It is seen that the parameter of the integral equation (50) is $\lambda = 1/2$. The kernel $\tilde{K}(\alpha,\rho)$ in Eq. (51) consists of two integrals, each of which is the difference of two integral functionals which go to ∞ for $\alpha \to \rho$. Eq. (50) is solved by the method of successive approximations which gives:[1)]

$$\Psi(\rho) = \lim_{n\to\infty} \Psi_n(\rho) \ , \qquad 1 \leq \rho \leq \infty \qquad , \tag{53}$$

where

$$\Psi_0(\rho) = \tilde{Q}(\rho) \qquad ,$$

$$\Psi_1(\rho) = \Psi_o(\rho) + (\tfrac{1}{2})^1 \int_1^\infty \tilde{Q}(\alpha_1)\tilde{K}(\alpha_1,\rho)d\alpha_1 \qquad ,$$

---

*) The singular behavior of $K(\alpha,\rho)$ is demonstrated by evaluating the integrals in Eq. (46), e.g.,

$$\int_0^\infty J_o(k\alpha)J_o(k\rho)dk = (2/\pi)\rho^{-1}K(\alpha/\rho), \qquad 0 < \alpha < \rho < \infty \qquad ,$$

$$= (2/\pi)\alpha^{-1}K(\rho/\alpha), \qquad 0 < \rho < \alpha < \infty \qquad ,$$

where

$$K(1) = \infty \qquad .$$

$$\Psi_2(\rho) = \Psi_1(\rho) + (\tfrac{1}{2})^2 \int_1^\infty \int_1^\infty \tilde{Q}(\alpha_2)\tilde{K}(\alpha_2,\alpha_1)\tilde{K}(\alpha_1,\rho)d\alpha_2 d\alpha_1 \quad ,$$

- -

$$\Psi_n(\rho) = \Psi_{n-1}(\rho) + (\tfrac{1}{2})^n \int_1^\infty \cdots \int_1^\infty \tilde{Q}(\alpha_n)\tilde{K}(\alpha_n,\alpha_{n-1})\cdots\tilde{K}(\alpha_2,\alpha_1)\tilde{K}(\alpha_1,\rho)d\alpha_n\cdots d\alpha_1 \ . \tag{54}$$

Combining of Eqs. (53) and (54) yields the solution of the nth approximation in the form:

$$\Psi_n(\rho) = \sum_{i=0}^{n} u_i(\rho), \qquad n = 0,1,2,\ldots \infty \quad , \quad 1 \le \rho \le \infty \quad , \tag{55}$$

where

$$u_0(\rho) = \tilde{Q}(\rho) \quad ,$$

$$u_1(\rho) = (\tfrac{1}{2})^1 \int_1^\infty \tilde{Q}(\alpha_1)\tilde{K}(\alpha_1,\rho)d\alpha_1 \quad ,$$

$$u_2(\rho) = (\tfrac{1}{2})^2 \int_1^\infty \int_1^\infty \tilde{Q}(\alpha_2)\tilde{K}(\alpha_2,\alpha_1)\tilde{K}(\alpha_1,\rho)d\alpha_2 d\alpha_1 \quad ,$$

- -

$$u_n(\rho) = (\tfrac{1}{2})^n \int_1^\infty \cdots \int_1^\infty \tilde{Q}(\alpha_n)\tilde{K}(\alpha_n,\alpha_{n-1})\cdots\tilde{K}(\alpha_2,\alpha_1)\tilde{K}(\alpha_1,\rho)d\alpha_n\cdots d\alpha_1 \ . \tag{56}$$

It is readily shown that the Neumann series in Eq. (55) converges to $\Psi(\rho)$ in the limit $n \to \infty$.[1)] It should be noted that $\Psi(1+0)$ is not necessarily $S(1-0)$ in any approximation n, i.e. $\partial N(\rho,0)/\partial\zeta$ may be discontinuous at $\rho = 1$. With $\Psi(\rho)$ given by Eqs. (55)-(56), the particle density fields $N_I(\rho,\zeta)$ and $N_{II}(\rho,\zeta)$ are given by Eqs. (25) and (37), respectively. Thus, we complete the analytical solution of the external boundary-value problem under consideration.

Citations

1. F. G. Tricomi, Integral Equations (Interscience Publ., Inc., New York 1957).

2. H. Weber, Math. Annalen 6, 154 (1873).

3. E. C. Titchmarsh, Proc. Lond. Math. Soc. 22, 15 (1923).

4. M. Abramowitz and I. A. Stegun, Handbook of Mathematical Functions (Dover Publications, New York 1964).

CHAPTER III

PLASMA ROTATION BY LORENTZ FORCES IN A DIVERGING PLASMA CENTRIFUGE WITH HALL EFFECT

In this chapter, a system analysis for a collision-dominated plasma centrifuge is presented in which the plasma rotates under the influence of the Lorentz forces due to the interaction of a spatially diverging current density field with an axial external magnetic field. The associated boundary-value problem for the coupled partial differential equations, which describe the electric potential and the plasma velocity fields, is solved in closed form. The electric field, current density, and velocity distributions are discussed in terms of the Hartmann number H and the Hall coefficient $\omega\tau$. As a result of the Lorentz forces, the plasma rotates with speeds as high as 10^4 m/sec around its axis of symmetry at sufficiently large values of H and $\omega\tau$. It is remarkable that the Hall effect supports the plasma rotation.

3.1. Model of Diverging Plasma Centrifuge

An electrical discharge in a cylindrical container rotates if the Lorentz force has a nonvanishing component in the azimuthal direction. For example, arc experiments in an axial external magnetic field B_z indicate that the discharge plasma rotates (Schwenn 1970; Vedenov et al. 1961) since the current field lines $\vec{J}$ have a nonvanishing radial component J_r so that $(\vec{J} \times \vec{B})_\theta = - J_r B_z \neq 0$. In a stable arc discharge,

the J_r-component is caused by the concentration of field lines ($\vec{J}$) at the electrodes and a dilatation (repulsion of currents in the same direction) of the field lines $\vec{J}$ in the interelectrode space.

A theoretical model for the production of a high-density plasma centrifuge, which has a radial current density J_r which is in magnitude comparable with the axial current density J_z, is shown in Figure 3.1. The radial spreading of the current field lines $\vec{J}$ is forced by means of electrodes of considerably different radii R_+ and R_- ($R_+ >> R_-$) in the end plates $z = \pm c$ of an electrically isolating centrifuge chamber of radius R_o. The field lines of the current density $\vec{J}$ and of the external axial magnetic field $\vec{B}_o$ cross under a nonvanishing angle (except at the chamber axis) so that the resultant Lorentz force $\vec{J} \times \vec{B}_o$ rotates charged particles around its axis of symmetry. In the steady state, the magnetic body forces in the azimuthal direction are balanced by the viscous forces (boundary layers at the chamber walls). As opposed to the centrifuge with radial electric current flow between an inner and outer cylinder electrode, the centrifuge scheme in Figure 3.1 avoids the boundary layer and losses at the inner cylinder surface.

In the following, the steady-state rotation of the spatially diverging plasma contained by an insulating cylinder in the external axial magnetic field $\vec{B}_o$ (Fig. 3.1) is treated theoretically. The analysis is based on the magnetogasdynamic approximation, in which two characteristic dimensionless parameters occur, the Hartman number H and the Hall coefficient $\omega\tau$. The magnetic fields associated with the discharge currents $\vec{J} = \{J_r, J_\theta, J_z\}$ are neglected for small magnetic Reynolds numbers $[\sigma_\perp = \sigma/(1+\omega^2\tau^2)]$,

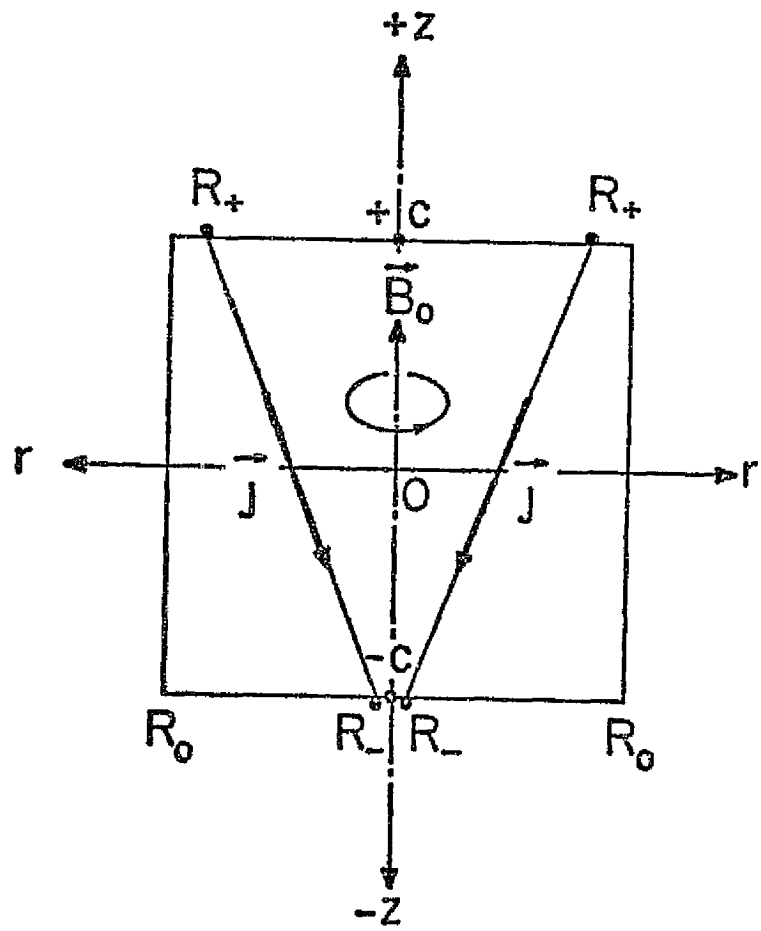

Fig. 3.1. Scheme of plasma centrifuge of radius R_o and height 2c with cathode (R_-), anode (R_+), and axial magnetic field $\vec{B}_o$ ($R_+ >> R_-$).

$$R_r = O[B_r/B_o] = \mu_o \omega\tau\sigma_\perp V_o << 1 \quad ,$$

$$R_\theta = O[B_\theta/B_o] = |\mu_o I/2\pi R_o|/B_o << 1 \quad , \tag{3.1}$$

$$R_z = O[B_z/B_o] = \mu_o \omega\tau\sigma_\perp V_o R_o << 1 \quad ,$$

where V_o is the characteristic velocity of rotation and I the discharge current. These inequalities are satisfied in many cases, e.g., if $R_\theta << 1$ for i) $\omega\tau >> 1$ and $R \lesssim 1$ or ii) $R << 1$ and $0 \leq \omega\tau < \infty$, where $R \equiv \mu_o \sigma \bar{v} \max (R_o; c)$.

3.2. Boundary-value Problem for Velocity and Electric Potential

For a purely azimuthal flow field $\vec{V} = \{0, V_\theta(r,z), 0\}$, the plasma behaves incompressible, $\nabla \cdot \vec{V} = 0$. From the continuity equation (2.2) for the steady state, $\nabla \cdot (\rho_p \vec{V}) = \vec{V} \cdot \nabla\rho_p = 0$, it follows then that the density gradient $\nabla\rho_p$ is everywhere perpendicular to the flow field $\vec{V}$. These ideal conditions are realized if secondary flows are absent or at least negligible (Schlichting 1960). In accordance with the steady-state magnetogasdynamic equations [Eqs. (2.1), (2.7) and (2.8)], the rotating plasma in a homogeneous magnetic field $\vec{B}_o$ (Fig. 3.1) is described by the following boundary-value problem for the azimuthal velocity $V_\theta(r,z)$ and electric potential $\phi(r,z)$ fields [induced magnetic fields neglected, Eq. (3.1)]:

$$\frac{\partial}{\partial r}\left[\frac{1}{r}\frac{\partial}{\partial r}(rV_\theta)\right] + \frac{\partial^2 V_\theta}{\partial z^2} = \frac{\sigma_\perp B_o}{\mu}\left(-\frac{\partial\phi}{\partial r} + V_\theta B_o\right) \quad , \tag{3.2}$$

$$\frac{1}{r}\frac{\partial}{\partial r}\left(r\frac{\partial\phi}{\partial\theta}\right) + \frac{\sigma}{\sigma_\perp}\frac{\partial^2\phi}{\partial z^2} = B_o \frac{1}{r}\frac{\partial}{\partial r}(r\, V_\theta) \quad , \tag{3.3}$$

where

$$V_\theta(r,z)_{r=R_o} = 0 \ , \ -c \leq z \leq +c, \tag{3.4}$$

$$V_\theta(r,z)_{z=\pm c} = 0 \ , \ 0 \leq r \leq R_o \ , \tag{3.5}$$

and

$$[\partial\phi(r,z)/\partial r]_{r=R_o} = 0 \ , \ -c \leq z \leq +c, \tag{3.6}$$

$$-\sigma[\partial\phi(r,z)/\partial z]_{z=\pm c} = I\ \delta(r - R_\pm)/2\pi r \ , \qquad 0 \leq r \leq R_o. \tag{3.7}$$

The boundary conditions (3.4), (3.5) and (3.6) consider that the plasma does not slip at the walls $r = R_o$ and $z = \pm c$, and that no current flows into the cylinder wall $r = R_o$, respectively. The boundary conditions in Equation (3.7) imply that the cathode (R_-) and anode (R_+) are ring electrodes of vanishing radial width, $\Delta r \to 0[\delta(r - R_\pm)/2\pi r$ = radial Dirac function]. The net current flowing through the centrifuge is by Equation (3.7).

$$-2\pi\sigma \int_0^{R_o} \frac{\partial\phi(r,z=\pm c)}{\partial z}\, r dr = \int_0^{R_o} \delta(r-R_\pm)\ dr = I < 0 \ , \tag{3.8}$$

since the positive current ($I < 0$) flows from the anode to the cathode (Fig. 3.1). The pressure distribution $P = P(r,z)$ is determined by the r- and z-components of the equation of motion,

$$-\rho_p \frac{V_\theta^2}{r} = -\frac{\partial P}{\partial r} + \omega\tau\ \sigma_\perp B_o \left(-\frac{\partial\phi}{\partial r} + V_\theta B_o\right) \ , \tag{3.9a}$$

$$\frac{\partial P}{\partial z} = J_r B_\theta - J_\theta B_r \to 0, \quad B_{r,\theta} \to 0. \tag{3.9b}$$

According to Equation (3.9b), it is $\partial P/\partial z = 0$ if the induced fields B_r and B_θ are neglected [Eq. (3.1)]. This means that momentum cannot be

exactly balanced in the axial direction if induced magnetic fields are neglected (in absence of secondary flows). Equation (3.9b) is in accord with the boundary-layer approximation according to which the normal pressure gradient is $\partial P/\partial z = 0$ at the electrode plates $z = \pm c$, $0 \leq r \leq R_o$.

In the absence of the Hall effect, $\omega\tau << 1$, it is $\nabla \times \vec{B} = \mu_o (J_r, 0, J_z)$. Hence, $B_r = 0$ and $B_z = 0$ because of the homogeneity of the boundary conditions for B_r and B_z, whereas $B_\theta \neq 0$ since $J_{r,z} \neq 0[B_\theta(r,z=\pm c) = (\mu_o I/2\pi r)H(r-R_\pm)]$. Consideration of the induced field $\vec{B} = \{0, B_\theta, 0\}$ leaves Equations (3.2) and (3.3) unchanged. This means that the boundary value problem in Equations (3.2)-(3.7) and the solutions $V_\theta(r,z)$ and $\phi(r,z)$ derived from it remain valid even in presence of a significant induced field $\vec{B} = \{0, B_\theta, 0\}$, $R_\theta \gtrsim 1$, as long as the Hall effect is negligible, $\omega\tau << 1$ (Chapter IV).

3.3. Fourier-Bessel and Dini Series Solutions

The characteristic dimensionless parameters of the magnetogasdynamic centrifuge problem under consideration are obtained by introducing the dimensionless independent and dependent variables,

$$\rho = r/R_o \ , \quad 0 \leq \rho \leq 1, \tag{3.10}$$

$$\zeta = z/c \ , \quad -1 \leq \zeta \leq 1, \tag{3.11}$$

and

$$V(\rho,\zeta) = V_\theta(r,z)/V_o, \quad \Phi(\rho,\zeta) = \phi(r,z)/\Phi_o \tag{3.12}$$

where

$$V_o \equiv \Phi_o/R_o B_o \ , \ \Phi_o \equiv Ic/2\pi\sigma R_o^2 \ . \tag{3.13}$$

In terms of the dimensionless space variables and fields, the boundary-value problem defined in Equations (3.2)-(3.7) assumes for $V(\rho,\zeta)$ and $\Phi(\rho,z)$ the form:

$$\frac{\partial}{\partial\rho}\left[\frac{1}{\rho}\frac{\partial}{\partial\rho}(\rho V)\right] + N^{-2}\frac{\partial^2 V}{\partial\zeta^2} - H_\perp^2 V = -H_\perp^2\frac{\partial\Phi}{\partial\rho}, \tag{3.14}$$

$$\frac{1}{\rho}\frac{\partial}{\partial\rho}\left(\rho\frac{\partial\Phi}{\partial\rho}\right) + M^{-2}\frac{\partial^2\Phi}{\partial\zeta^2} = \frac{1}{\rho}\frac{\partial}{\partial\rho}(\rho V), \tag{3.15}$$

where

$$V(\rho,\zeta)_{\rho=1} = 0, \quad -1 \le \zeta \le +1, \tag{3.16}$$

$$V(\rho,\zeta)_{\zeta=\pm1} = 0, \quad 0 \le \rho \le 1, \tag{3.17}$$

and

$$[\partial\Phi(\rho,\zeta)/\partial\rho]_{\rho=1} = 0, \quad -1 \le \zeta \le 1, \tag{3.18}$$

$$-[\partial\Phi(\rho,\zeta)/\partial\zeta]_{\zeta=\pm1} = \delta(\rho-\rho_\pm)/\rho, \quad 0 \le \rho \le 1, \tag{3.19}$$

with $\rho_\pm \equiv R_\pm/R_o$. The dimensionless constants M, N, and $H_\perp$ are defined by

$$\begin{aligned} M &\equiv (1+\omega^2\tau^2)^{-\frac{1}{2}}(c/R_o), \quad N \equiv c/R_o, \\ H_\perp &\equiv (\sigma_\perp/\mu)^{\frac{1}{2}} B_o R_o = H/(1+\omega^2\tau^2)^{\frac{1}{2}} \end{aligned} \tag{3.20}$$

In view of the similarity of the left sides of Equations (3.14) and (3.15) with Bessel's differential equation, $Z_m'' + \rho^{-1}Z_m' + (k_n^2 - \rho^{-2}m^2)Z_m = 0$, for cylinder functions $Z_m(k_n\rho)$, partial solutions of the coupled inhomogeneous equations are sought in the form,

$$V_n(\rho,\zeta) = J_1(k_n\rho)f_n(\zeta), \tag{3.21}$$

$$\Phi_n(\rho,\zeta) = J_0(k_n\rho)g_n(\zeta). \tag{3.22}$$

where $J_0'(k_n\rho) = -J_1(k_n\rho)$ and $J_1'(k_n\rho) + (k_n\rho)^{-1}J_1(k_n\rho) = J_0(k_n\rho)$. Substitution of Equations (3.21) and (3.22) into Equations (3.14) and (3.15) yields

$$f_n'' - (k_n^2 + H_\perp^2)N^2 f_n = k_n H_\perp^2 N^2 g_n \ , \tag{3.23}$$

$$g_n'' - k_n^2 M^2 g_n = k_n M^2 f_n \ , \tag{3.24}$$

where the eigen-values $k_n > 0$ are determined by the boundary conditions (3.16) and (3.18) as the real roots of the transcendental equation

$$J_1(k_n) = 0 \ , \quad n = 1,2,3,\ldots. \tag{3.25}$$

Thus, the general solution of the coupled equations (3.14) and (3.15) obtains by linear superposition as

$$V(\rho,\zeta) = \sum_{n=1}^{\infty} J_1(k_n\rho) f_n(\zeta) \ , \tag{3.26}$$

$$\Phi(\rho,\zeta) = -2\zeta + \sum_{n=1}^{\infty} J_0(k_n\rho) g_n(\zeta) \ . \tag{3.27}$$

In view of Equation (3.25), Equation (3.26) is a Fourier-Bessel series, whereas Equation (3.27) is a Fourier-Dini series in which a zero-order term, -2ζ has to be included, in accordance with the Fourier-Dini expansion [Eq. (3.32)] of the boundary value in Equation (3.19). By decoupling Equations (3.23) and (3.24) one finds for $f_n(\zeta)$ and $g_n(\zeta)$ the differential equations of 4th order,

$$f_n'''' - [k_n^2(M^2 + N^2) + N^2H_\perp^2]f_n'' + k_n^4M^2N^2 f_n = 0 \ , \tag{3.28}$$

$$g_n'''' - [k_n^2(M^2 + N^2) + N^2H_\perp^2]g_n'' + k_n^4M^2N^2 g_n = 0 \ , \tag{3.29}$$

with

$$f_n(\zeta)_{\zeta=\pm 1} = 0 \ , \tag{3.30}$$

$$-g_n'(\zeta)_{\zeta=\pm 1} = 2\ J_0(k_n\rho_\pm)/J_0^2(k_n) \ , \tag{3.31}$$

as boundary conditions by Equations (3.17) and (3.19). In deriving Equation (3.31), the Dirac function in Equation (3.19) has been expanded as the Fourier-Dini series,

$$\delta(\rho - \rho_\pm)/\rho = 2 + 2 \sum_{n=1}^{\infty} [J_0(k_n\rho_\pm)/J_0^2(k_n)]J_o(k_n\rho). \tag{3.32}$$

In addition to Equations (3.28)-(3.31), $f_n(\zeta)$ and $g_n(\zeta)$ have to satisfy also the coupled Equations (3.23) and (3.24). With

$$\omega_{1n} = \omega_n^+ \ , \quad \omega_{2n} = \omega_n^- \ , \quad \omega_{3n} = -\omega_n^+, \quad \omega_{4n} = -\omega_n^- \ , \tag{3.33}$$

where

$$\omega_n^\pm \equiv \left[\frac{1}{2}\{[k_n^2(M^2 + N^2) + N^2H_\perp^2] \pm \{[k_n^2(M^2 + N^2) + N^2H_\perp^2]^2 - 4k_n^4M^2N^2\}^{\frac{1}{2}}\}\right]^{\frac{1}{2}} \ , \tag{3.34}$$

the general solutions for $f_n(\zeta) \propto e^{\omega_n^\pm\zeta}$ and $g_n(\zeta) \propto e^{\omega_n^\pm\zeta}$ of Equations (3.28) and (3.29), can be written as

$$f_n(\zeta) = A_n^+ \frac{\sinh \omega_n^+\zeta}{\sinh \omega_n^+} + B_n^+ \frac{\cosh \omega_n^+\zeta}{\cosh \omega_n^+} + A_n^- \frac{\sinh \omega_n^-\zeta}{\sinh \omega_n^-} + B_n^- \frac{\cosh \omega_n^-\zeta}{\cosh \omega_n^-} \ , \tag{3.35}$$

$$g_n(\zeta) = C_n^+ \frac{\sinh \omega_n^+ \zeta}{\sinh \omega_n^+} + D_n^+ \frac{\cosh \omega_n^+ \zeta}{\cosh \omega_n^+}$$

$$+ C_n^- \frac{\sinh \omega_n^- \zeta}{\sinh \omega_n^-} + D_n^- \frac{\cosh \omega_n^- \zeta}{\cosh \omega_n^-} . \tag{3.36}$$

Only four of the eight integration constants $A_n^\pm, \ldots, D_n^\pm$ for any $n \geq 1$ are independent; by Equations (3.23) and (3.24),

$$[(\omega_n^\pm)^2 - k_n^2 M^2] C_n^\pm = k_n M^2 A_n^\pm \quad ,$$

$$[(\omega_n^\pm)^2 - k_n^2 M^2] D_n^\pm = k_n M^2 B_n^\pm \quad , \tag{3.37}$$

and

$$[(\omega_n^\pm)^2 - (k_n^2 + H_\perp^2) N^2] A_n^\pm = k_n N^2 H_\perp^2 C_n^\pm \ ,$$

$$[(\omega_n^\pm)^2 - (k_n^2 + H_\perp^2) N^2] B_n^\pm = k_n N^2 H_\perp^2 D_n^\pm \ , \tag{3.38}$$

where the coefficient determinants of the pairs of corresponding equations in Equations (3.37) and (3.38) vanish owing to Equations (3.33) and (3.34).

Upon application of the four relations in Equation (3.38), which are equivalent to Equation (3.37) by Equations (3.33) and (3.34), and the boundary conditions (3.30), which give

$$-A_n^- = +A_n^+ \equiv A_n \ , \quad -B_n^- = +B_n^+ \equiv B_n \ . \tag{3.39}$$

Equations (3.35) and (3.36) become

$$f_n(\zeta) = A_n\left(\frac{\sinh \omega_n^+\zeta}{\sinh \omega_n^+} - \frac{\sinh \omega_n^-\zeta}{\sinh \omega_n^-}\right) + B_n\left(\frac{\cosh \omega_n^+\zeta}{\cosh \omega_n^+} - \frac{\cosh \omega_n^-\zeta}{\cosh \omega_n^-}\right), \tag{3.40}$$

$$g_n(\zeta) = \frac{A_n}{k_n N^2 H_\perp^2}\left(\Omega_n^+ \frac{\sinh \omega_n^+\zeta}{\sinh \omega_n^+} - \Omega_n^- \frac{\sinh \omega_n^-\zeta}{\sinh \omega_n^-}\right) + \frac{B_n}{k_n N^2 H_\perp^2}\left(\Omega_n^+ \frac{\cosh \omega_n^+\zeta}{\cosh \omega_n^+} - \Omega_n^- \frac{\cosh \omega_n^-\zeta}{\cosh \omega_n^-}\right), \tag{3.41}$$

where

$$\Omega_n^\pm \equiv (\omega_n^\pm)^2 - (k_n^2 + H_\perp^2)N^2 . \tag{3.42}$$

The boundary conditions (3.31) applied to Equation (3.41) yield

$$A_n = -\frac{k_n N^2 H_\perp^2}{J_0^2(k_n)} \frac{J_0(k_n\rho_-) + J_0(k_n\rho_+)}{\omega_n^+ \Omega_n^+ \operatorname{cth}\omega_n^+ - \omega_n^- \Omega_n^- \operatorname{cth}\omega_n^-} , \tag{3.43}$$

$$B_n = +\frac{k_n N^2 H_\perp^2}{J_0^2(k_n)} \frac{J_0(k_n\rho_-) - J_0(k_n\rho_+)}{\omega_n^+ \Omega_n^+ \operatorname{tgh}\omega_n^+ - \omega_n^- \Omega_n^- \operatorname{thh}\omega_n^-} . \tag{3.44}$$

Substitution of Equations (3.43) and (3.44) into Equations (3.40) and (3.41) gives as solutions for $f_n(\zeta)$ and $g_n(\zeta)$:

$$f_n(\zeta)\,\frac{J_0^2(k_n)}{k_n N_\perp^2 H_\perp^2} = -\frac{J_0(k_n\rho_-)+J_0(k_n\rho_+)}{\omega_n^+\Omega_n^+\,\mathrm{cgh}\omega_n^+ - \omega_n^-\Omega_n^-\,\mathrm{cth}\omega_n^-}\left(\frac{\sinh\omega_n^+\zeta}{\sinh\omega_n^+} - \frac{\sinh\omega_n^+\zeta}{\sinh\omega_n^-}\right)$$

$$+\frac{J_0(k_n\rho_-)-J_0(k_n\rho_+)}{\omega_n^+\Omega_n^+\,\mathrm{tgh}\omega_n^+ - \omega_n^-\Omega_n^-\,\mathrm{tgh}\omega_n^-}\left(\frac{\cosh\omega_n^+\zeta}{\cosh\omega_n^+} - \frac{\cosh\omega_n^+\zeta}{\cosh\omega_n^-}\right), \tag{3.45}$$

$$g_n(\zeta)\,J_0^2(k_n) = -\frac{J_0(k_n\rho_-)+J_0(k_n\rho_+)}{\omega_n^+\Omega_n^+\,\mathrm{cth}\omega_n^+ - \omega_n^-\Omega_n^-\,\mathrm{cth}\omega_n^-}\left(\Omega_n^+\frac{\sinh\omega_n^+\zeta}{\sinh\omega_n^+} - \Omega_n^-\frac{\sinh\omega_n^-\zeta}{\sinh\omega_n^-}\right)$$

$$+\frac{J_0(k_n\rho_-)-J_0(k_n\rho_+)}{\omega_n^+\Omega_n^+\,\mathrm{tgh}\omega_n^+ - \omega_n^-\Omega_n^-\,\mathrm{tgh}\omega_n^-}\left(\Omega_n^+\frac{\cosh\omega_n^+\zeta}{\cosh\omega_n^+} - \Omega_n^-\frac{\cosh\omega_n^-\zeta}{\cosh\omega_n^-}\right). \tag{3.46}$$

Equations (3.45) and (3.46) form, together with Equations (3.26) and (3.27), the closed form solution of the problem of the plasma centrifuge in an axial magnetic field $\vec{B}_o$:

$$V(\rho,\zeta) = -N_\perp^2 H_\perp^2 \sum_{n=1}^{\infty} \frac{k_n J_1(k_n\rho)}{J_0^2(k_n)}\left[\frac{J_0(k_n\rho_-)+J_0(k_n\rho_+)}{\omega_n^+\Omega_n^+\,\mathrm{cth}\omega_n^+ - \omega_n^-\Omega_n^-\,\mathrm{cth}\omega_n^-}\times\right.$$

$$\left(\frac{\sinh\omega_n^+\zeta}{\sinh\omega_n^+} - \frac{\sinh\omega_n^-\zeta}{\sinh\omega_n^-}\right)$$

$$\left. - \frac{J_0(k_n\rho_-)-J_0(k_n\rho_+)}{\omega_n^+\Omega_n^+\,\mathrm{tgh}\omega_n^+ - \omega_n^-\Omega_n^-\,\mathrm{tgh}\omega_n^-}\left(\frac{\cosh\omega_n^+\zeta}{\cosh\omega_n^+} - \frac{\cosh\omega_n^-\zeta}{\cosh\omega_n^-}\right)\right], \tag{3.47}$$

and

$$\Phi(\rho,\zeta) = -2\zeta - \sum_{n=1}^{\infty} \frac{J_0(k_n\rho)}{J_0^2(k_n)} \left[\frac{J_0(k_n\rho_-)+J_0(k_n\rho_+)}{\omega_n^+\Omega_n^+ \operatorname{cth}\omega_n^+ - \omega_n^-\Omega_n^- \operatorname{cth}\omega_n^-} \times \right.$$

$$\left(\Omega_n^+ \frac{\sinh \omega_n^+\zeta}{\sinh \omega_n^+} - \Omega_n^- \frac{\sinh \omega_n^-\zeta}{\sinh \omega_n^-} \right)$$

$$\left. - \frac{J_0(k_n\rho_-)-J_0(k_n\rho_+)}{\omega_n^+\Omega_n^+ \operatorname{tgh}\omega_n^+ - \omega_n^-\Omega_n^- \operatorname{tgh}\omega_n^-} \left(\Omega_n^+ \frac{\cosh \omega_n^+\zeta}{\cosh \omega_n^+} - \Omega_n^- \frac{\cosh \omega_n^-\zeta}{\cosh \omega_n^-} \right) \right] . \tag{3.48}$$

The remaining dimensionless centrifuge fields $\vec{E} = -\nabla\phi/E_o$ and $\vec{J} = \vec{J}/J_o$ are given in terms of the solutions for $\Phi(\rho,\zeta)$ and $V(\rho,\zeta)$:

$$E_\rho = -\partial\Phi/\partial\rho \ , \quad E_\theta = 0 \ , \quad E_\zeta = -N^{-1}\partial\Phi/\partial\zeta \ , \tag{3.49}$$

$$J_\rho = \frac{1}{1+\omega^2\tau^2}\left(-\frac{\partial\Phi}{\partial\rho} + V\right), \quad J_\theta = \frac{\omega\tau}{1+\omega^2\tau^2}\left(-\frac{\partial\Phi}{\partial\rho} + V\right), \quad J_\zeta = -\frac{1}{N}\frac{\partial\Phi}{\partial\zeta} \tag{3.50}$$

where $E_o \equiv \dot{\Phi}_o/R_o$ and $J_o \equiv \sigma\Phi_o/R_o$ [Eq. (3.13)].

If the cathode is in the plane $z = -c(\zeta = -1)$ and the anode is in the plane $z = +c(\zeta = +1)$, then the reference fields V_o and Φ_o [Eq. (3.13)] are negative, since $I < 0$. The results are also applicable to the case where the anode is in the plane $z = -c(\zeta = -1)$ and the cathode is in the plane $z = +c(\zeta + +1)$. In the latter situation, the reference fields V_o and Φ_o are positive, since $I > 0$. These explanations hold for magnetic fields pointing in the positive z-direction, $B_o > 0$; V_o changes its sign if $B_o < 0$ [Eq. (3.13)].

3.4. Numerical Illustrations and Results

As an illustration the radial (ρ) dependence of the dimensionless centrifuge fields $V(\rho,\zeta)$, $\Phi(\rho,\zeta)$, $E_\rho(\rho,\zeta)$, $E_\zeta(\rho,\zeta)$, and $J_\rho(\rho,\zeta)$ has been calculated for $I < 0$ in the cross-sectional planes $\zeta = -0.99$ (cathode region), $\zeta = 0$ (central region), and $\zeta = +0.99$ (anode region) based on Equations (3.47)-(3.50). The remaining fields $J_\theta(\rho,\zeta)$ and $J_\zeta(\rho,\zeta)$ are proportional to $J_\rho(\rho,\zeta)$ and $E_\zeta(\rho,\zeta)$, respectively [Eq. (3.50)]. The characteristic dimensionless magnetic interaction numbers are treated as parameters:

$$\omega\tau = 1,\ 10;\quad H = 1,\ 10,\ 100.$$

The geometry parameter N is taken to be $N = 1$ so that $M = (1 + \omega^2\tau^2)^{-\frac{1}{2}}$ corresponding to $R_o = c$ [Eq. (3.20)]. The radial positions of the cathode and anode are assumed to be

$$\rho_- = 0.01\ (R_- = 0.01\ R_o)\quad ;\quad \rho_+ = 0.9\ (R_+ = 0.9\ R_o).$$

The dimensional fields are negative everywhere where the dimensionless fields are positive, and vice-versa [Eq. (3.12)] since $V_o < 0$ and $\Phi_o < 0$ for $I < 0$ [Eq. (3.13)].

i) *Central Region*, $\zeta = 0$: In the Figures 3.2-3.6, the aximuthal velocity field $V(\rho,0)$, the electric potential $\Phi(\rho,0)$, the radial and axial electric fields $E_\rho(\rho,0)$ and $E_\zeta(\rho,0) \approx J_\zeta(\rho,0)$, and the radial current density $J_\rho(\rho,0)$ are represented versus ρ, with $(\omega\tau,H) = (1,1)$, $(1,10)$, $(1,100)$, $(10,1)$, $(10,10)$, $(10,100)$ as parameters. It is seen that $|V|$ increases considerably at any point $0 < \rho < 1$ if either H or $\omega\tau$ are increased. In the region $\rho \gtrsim 0$ sufficiently close to the axis, $|\Phi|$, $|E_\rho|$, $|E_\zeta - 2N^{-1}|$, and $|J_\rho|$ increase with increasing H or $\omega\tau$. The field distributions move towards the axis $\rho = 0$ as $\omega\tau$ becomes larger. The

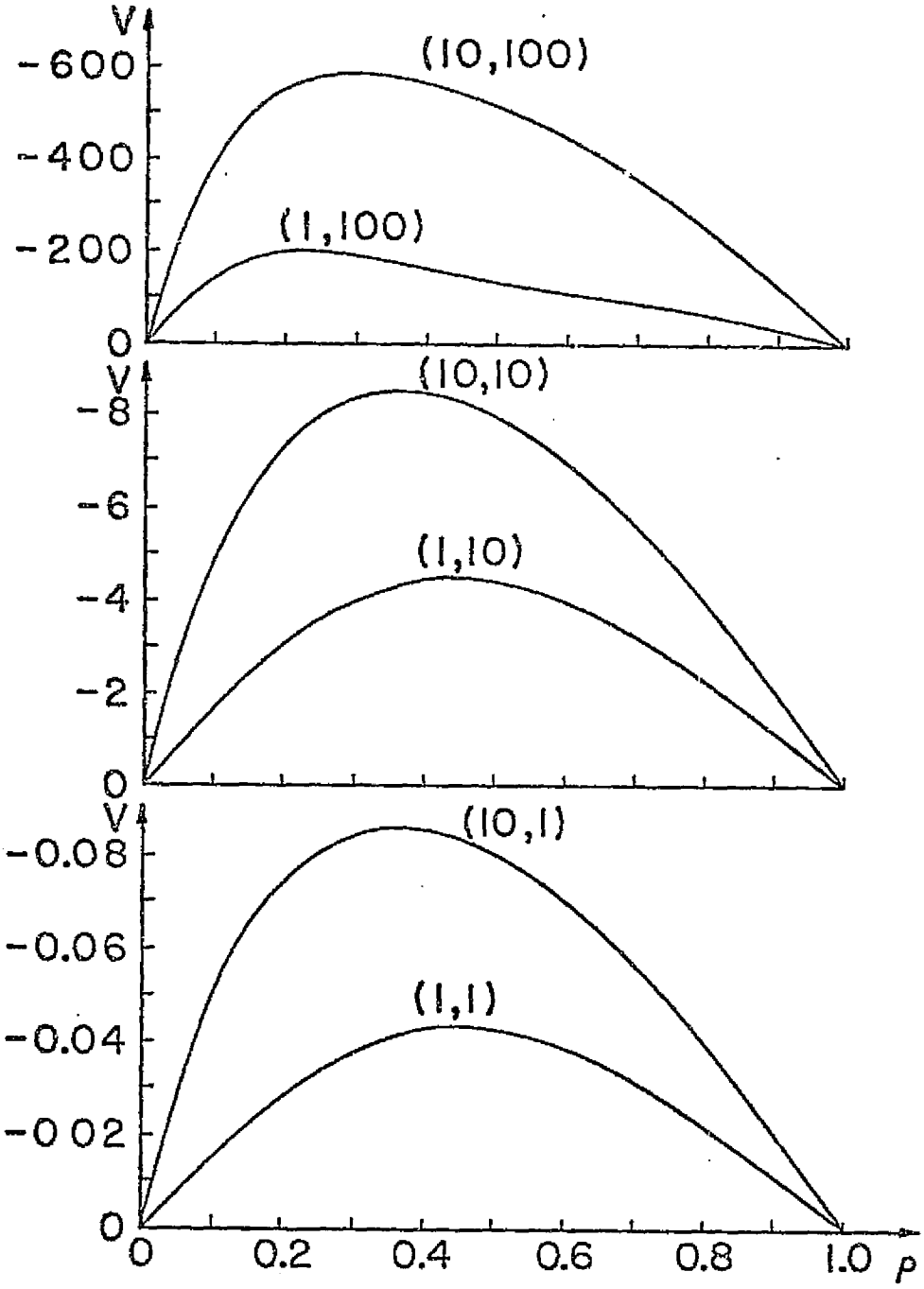

Fig. 3.2. $V(\rho,\zeta)$ versus ρ for $\zeta = 0$, and $(\omega\tau,H) = (1,1)$ to $(10,100)$.

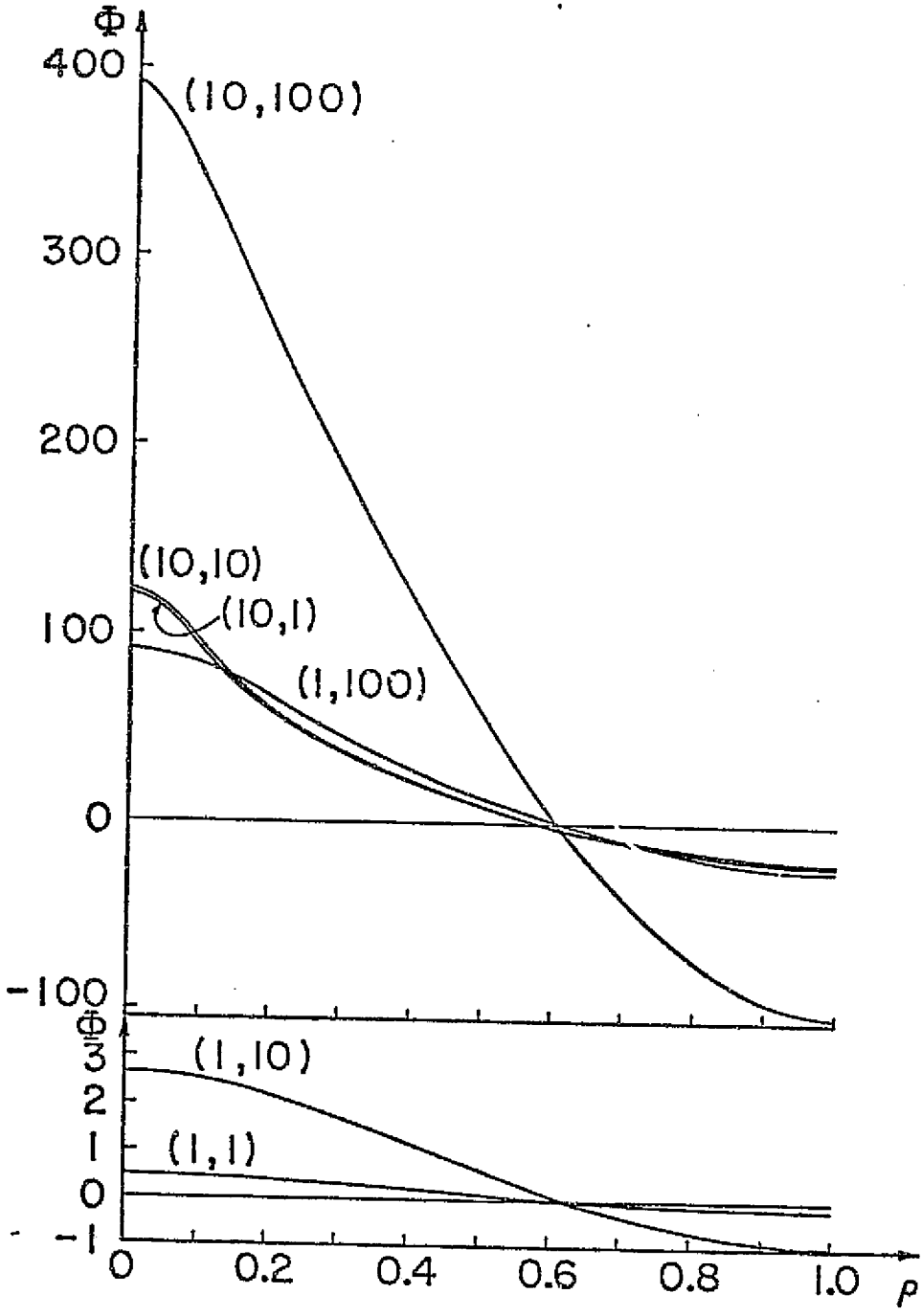

Fig. 3.3. $\Phi(\rho,\zeta)$ versus ρ for $\zeta = 0$, and $(\omega\tau,H) = (1,1)$ to $(10,100)$.

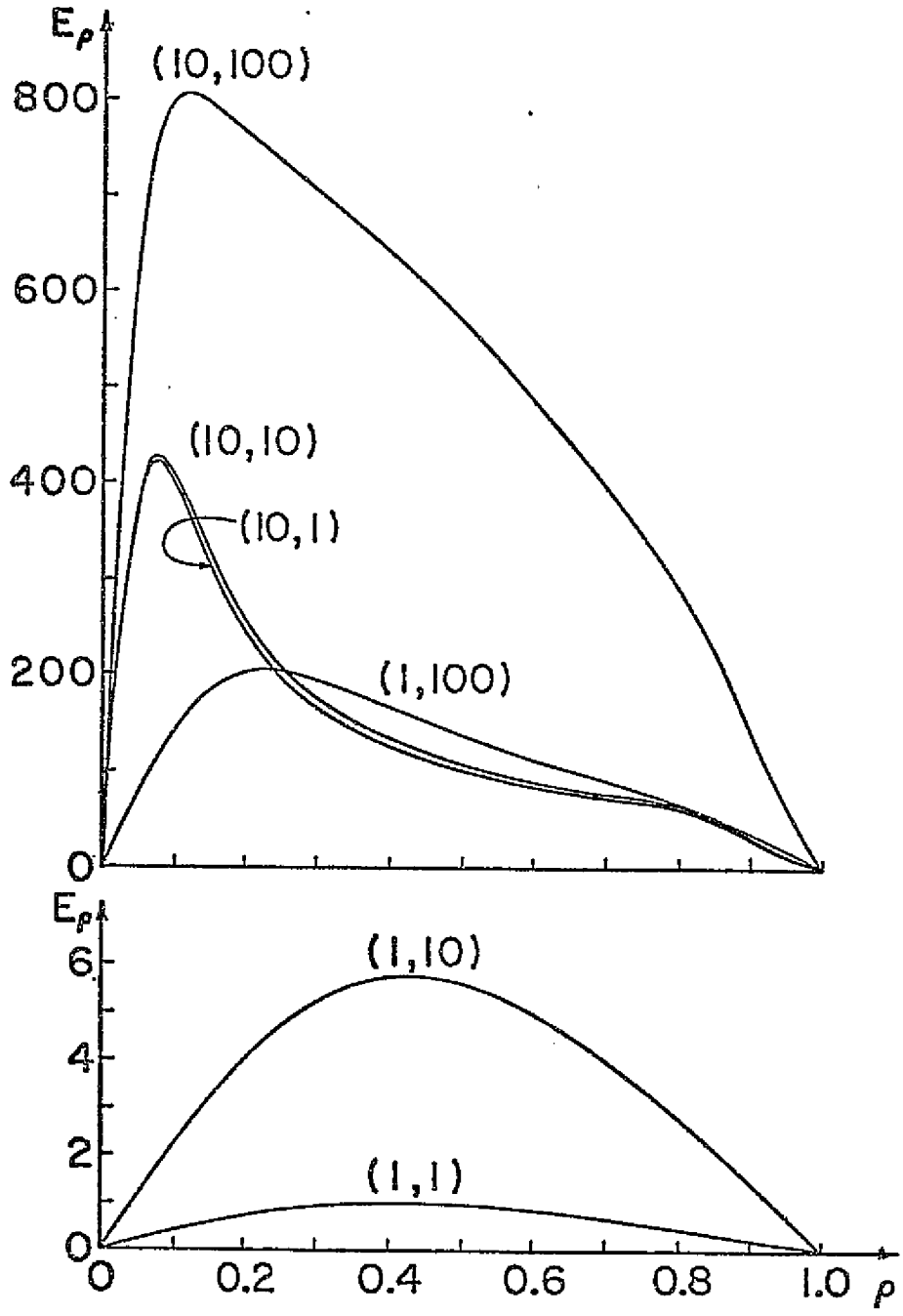

Fig. 3.4. $E_\rho(\rho,\zeta)$ versus ρ for $\zeta = 0$, and $(\omega\tau,H) = (1,1)$ to $(10,100)$.

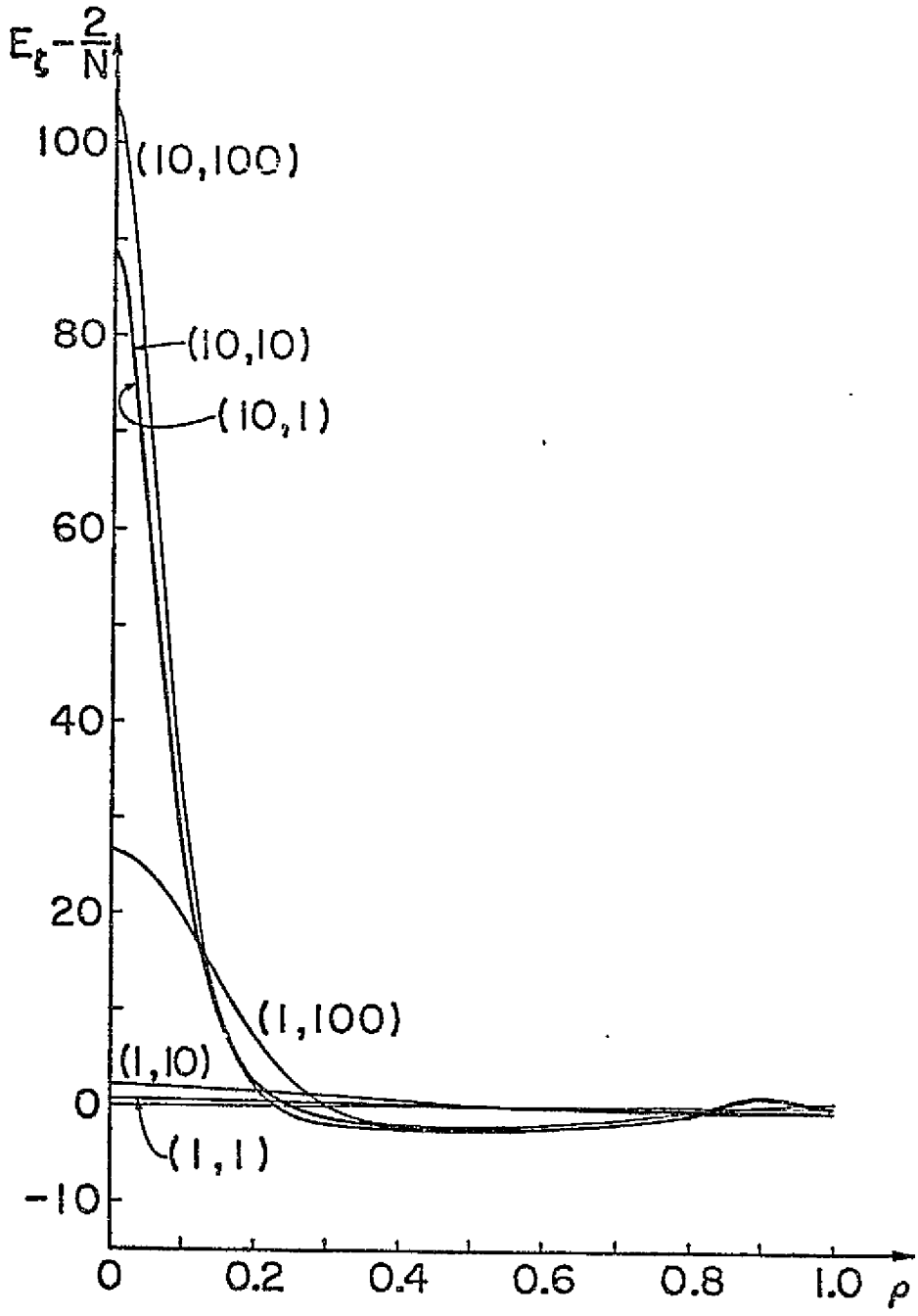

Fig. 3.5. $E_\zeta(\rho,\zeta)$ versus ρ for $\zeta = 0$, and $(\omega\tau,H) = (1,1)$ to $(10,100)$.

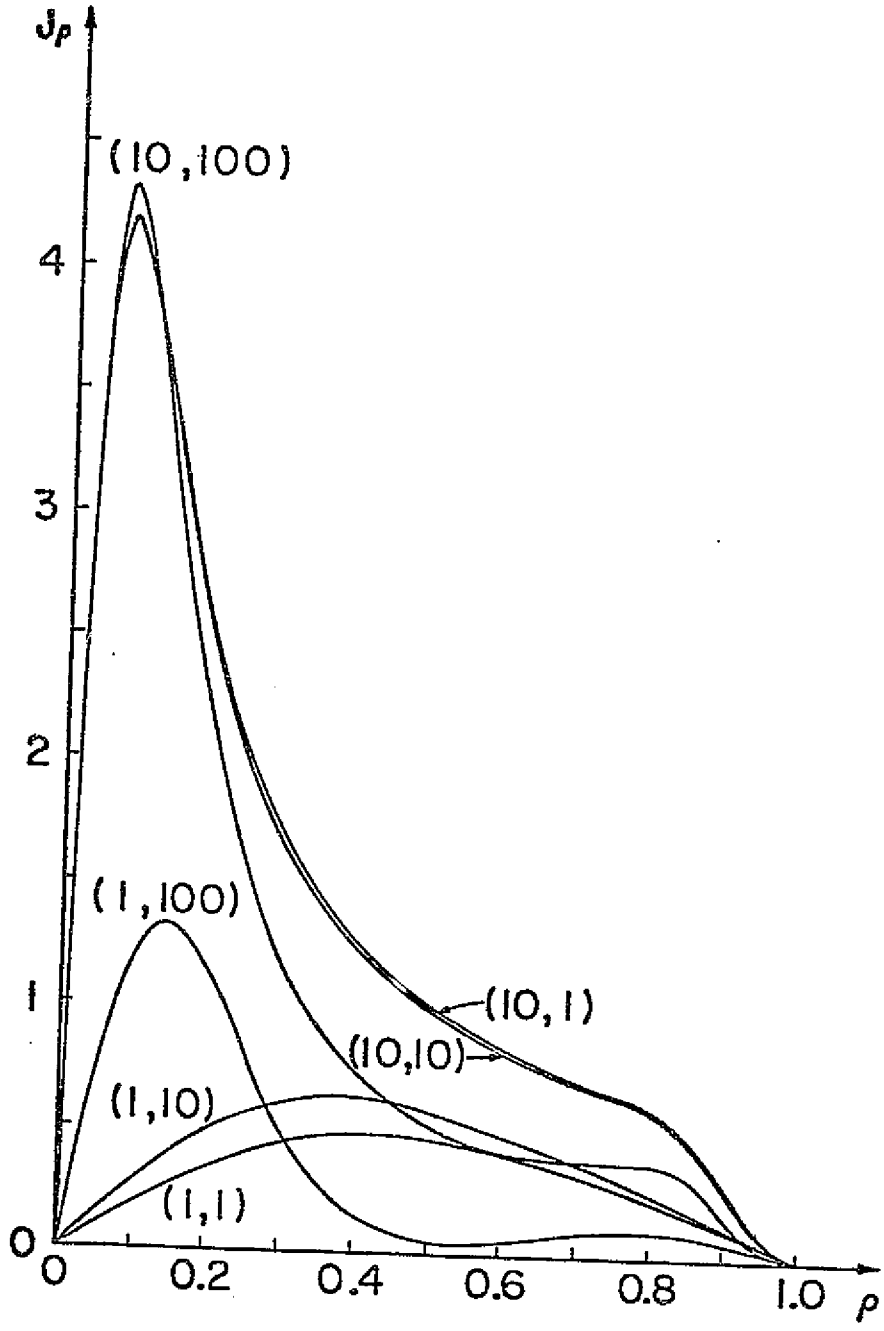

Fig. 3.6. $J_\rho(\rho,\zeta)$ versus ρ for $\zeta = 0$, and $(\omega\tau,H) = (1,1)$ to $(10,100)$.

"hump" developing at $\rho \approx 0.9$ (Figs. 3.4-3.6) with increasing $\omega\tau$ shows the influence of the ring anode ($\rho = 0.9$, $\zeta = +1$) in the plane $\zeta = 0$.

ii) *Cathode Region*, $\zeta = -0.99$: The Figures 3.7-3.11 show $V(\rho, -0.99)$, $\Phi(\rho, -0.99)$, $E_\rho(\rho, -0.99)$, $E_\zeta(\rho, -0.99) \propto J_\zeta(\rho, -0.99)$, and $J_\rho(\rho, -0.99)$ versus ρ with $(\omega\tau, H) = (1,1), \ldots (10,100)$ as parameters. These fields increase in intensity at any point $0 < \rho < 1$ if H or $\omega\tau$ is increased. Since the ring cathode is at $\rho_- = 0.01$ ($\zeta = -1$), the field distributions are closer concentrated at the axis $\rho = 0$ than those in the plane $\zeta = 0$ (Figs. 3.2-3.6). Note that the plasma rotates only in the region $\rho \approx 0.1$ with a significant velocity, since the Lorentz force $-J_\rho B_o$ decreases rapidly with increasing $\rho \to 1$. A comparison of the corresponding fields in Figures 3.2-3.6 and Figures 3.7-3.11 indicates that the discharge spreads slightly in radial direction with increasing $-1 < \zeta \leq 0$. In particular, an increasing radial section of the plasma rotates with a significant speed as $-1 < \zeta \leq 0$ increases.

iii) *Anode Region*, $\zeta = +0.99$: In the Figures 3.12-3.16, $V(\rho, +0.99)$, $\Phi(\rho, +0.99)$, $E_\rho(\rho, +0.99)$, $E_\zeta(\rho, +0.99) \propto J_\zeta(\rho, +0.99)$, and $J_\rho(\rho, +0.99)$ are plotted versus ρ with $(\omega\tau, H) = (1,1), \ldots (10,100)$ as parameters. The dependence of these fields on H and $\omega\tau$ is as in the previous cases for $\zeta = 0$ and $\zeta = -0.99$. The velocity distributions are fully developed nearly through the entire chamber across section $0 < \rho \leq 0.9$, since the Lorentz force $-J_\rho B_o$ is strongest in the vicinity $\rho \approx 0.9$ of the ring anode, $\rho_+ = 0.9 (\zeta = +1)$. As a result, a thin and steep boundary layer exists close to the cylinder wall ($\rho = 1$) with backflows at sufficiently small $\omega\tau$-values (Fig. 3.12). The radial distributions of Φ, E_ρ, $E_\zeta \propto J_\zeta$ and J_ρ (Figs. 3.13-3.16) clearly indicate

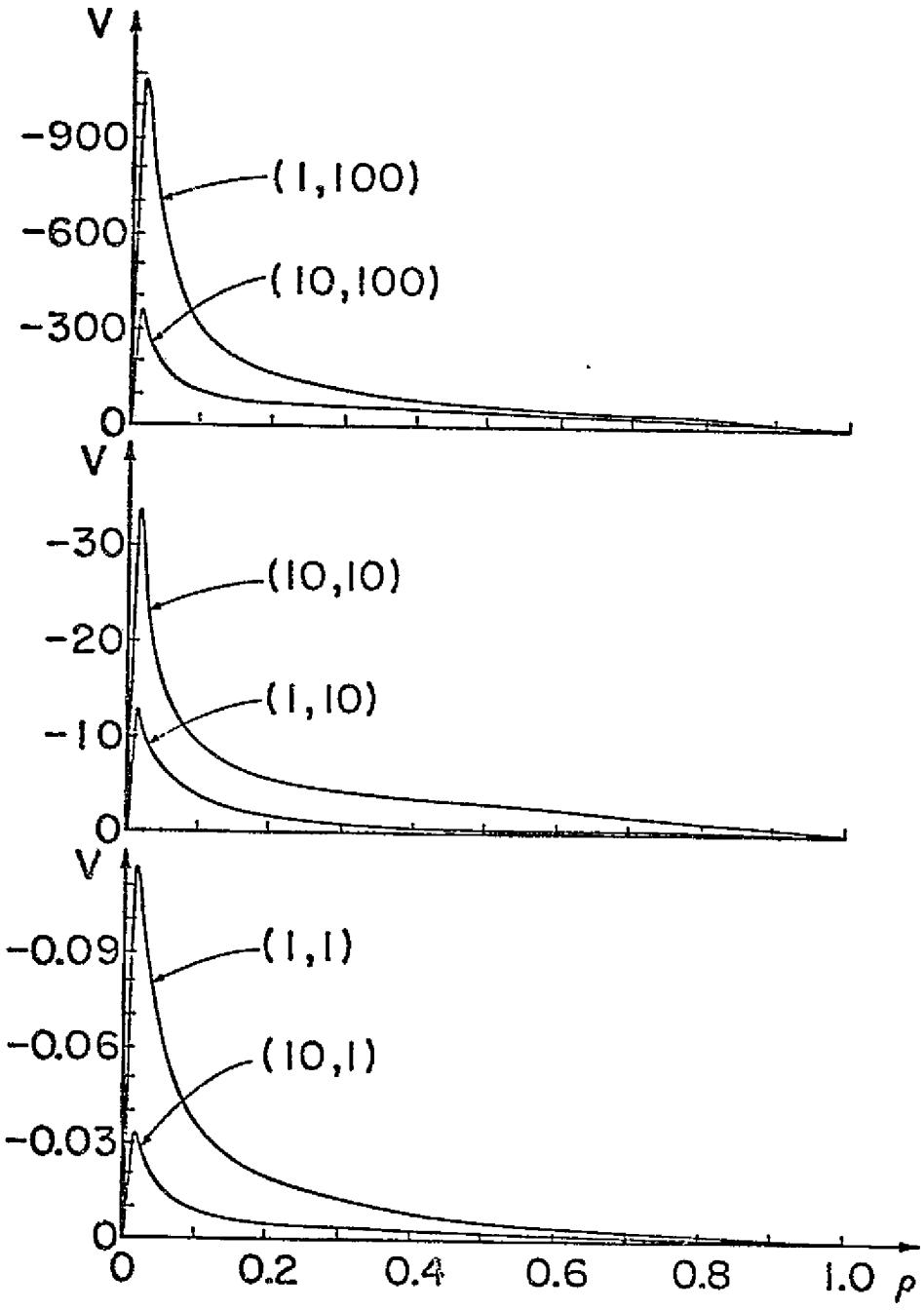

Fig. 3.7. $V(\rho,\zeta)$ versus ρ for $\zeta = -0.99$, and $(\omega\tau,H) = (1,1)$ to $(10,100)$.

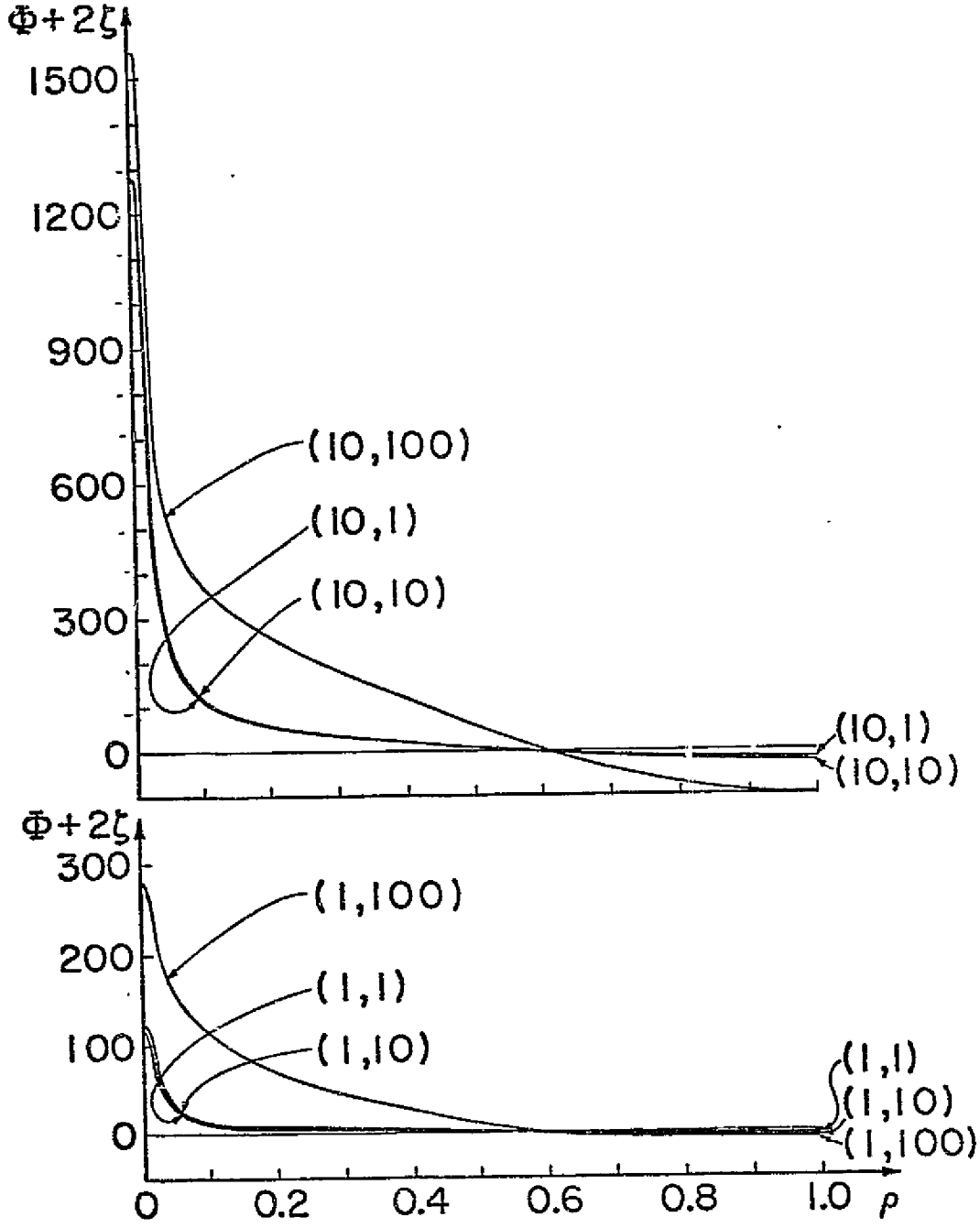

Fig. 3.8. $\Phi(\rho,\zeta)$ versus ρ for $\zeta = -0.99$, and $(\omega\tau,H) = (1,1)$ to $(10,100)$.

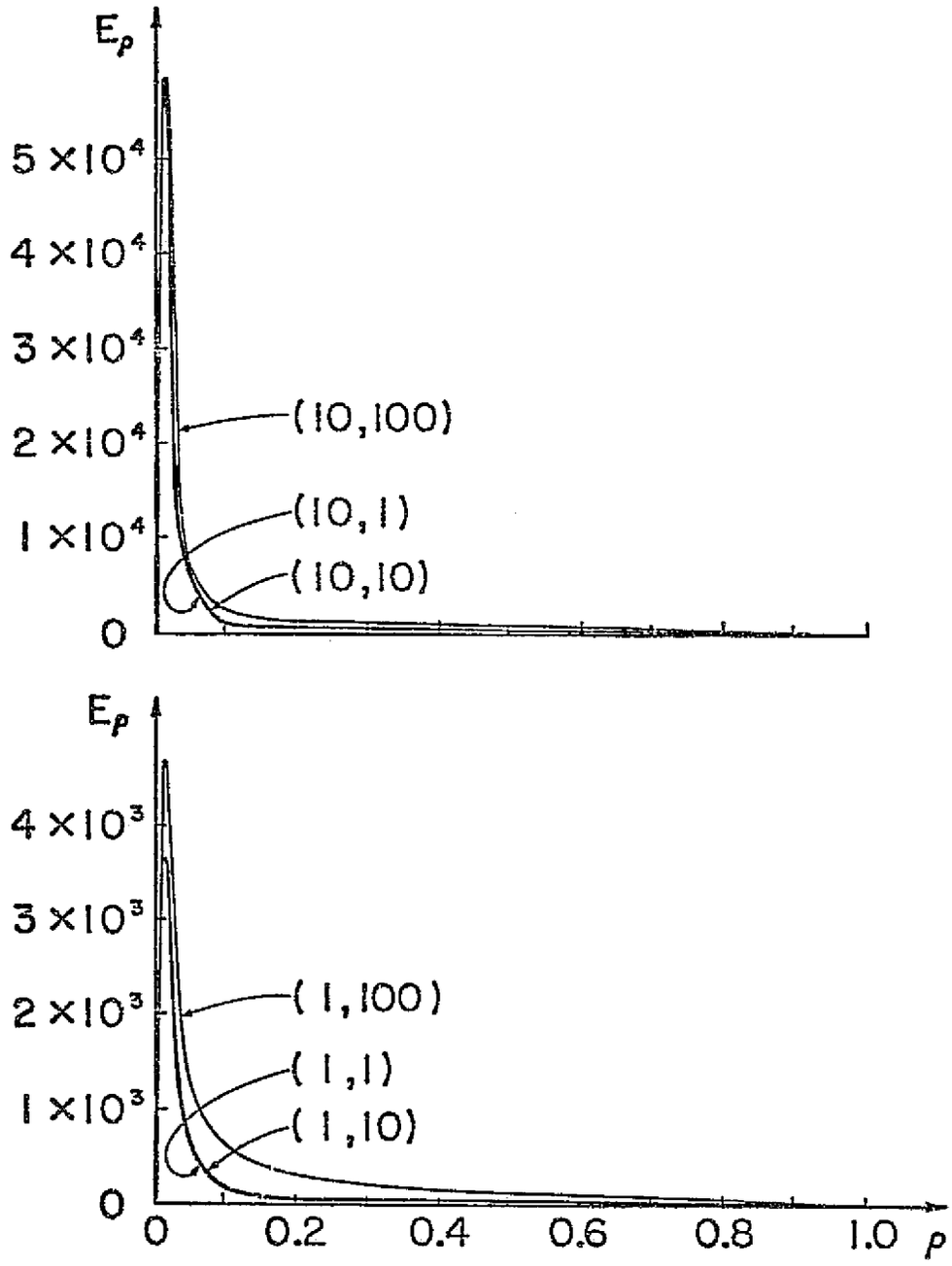

Fig. 3.9. $E_\rho(\rho,\zeta)$ versus ρ for $\zeta = -0.99$, and $(\omega\tau,H) = (1,1)$ to $(10,100)$.

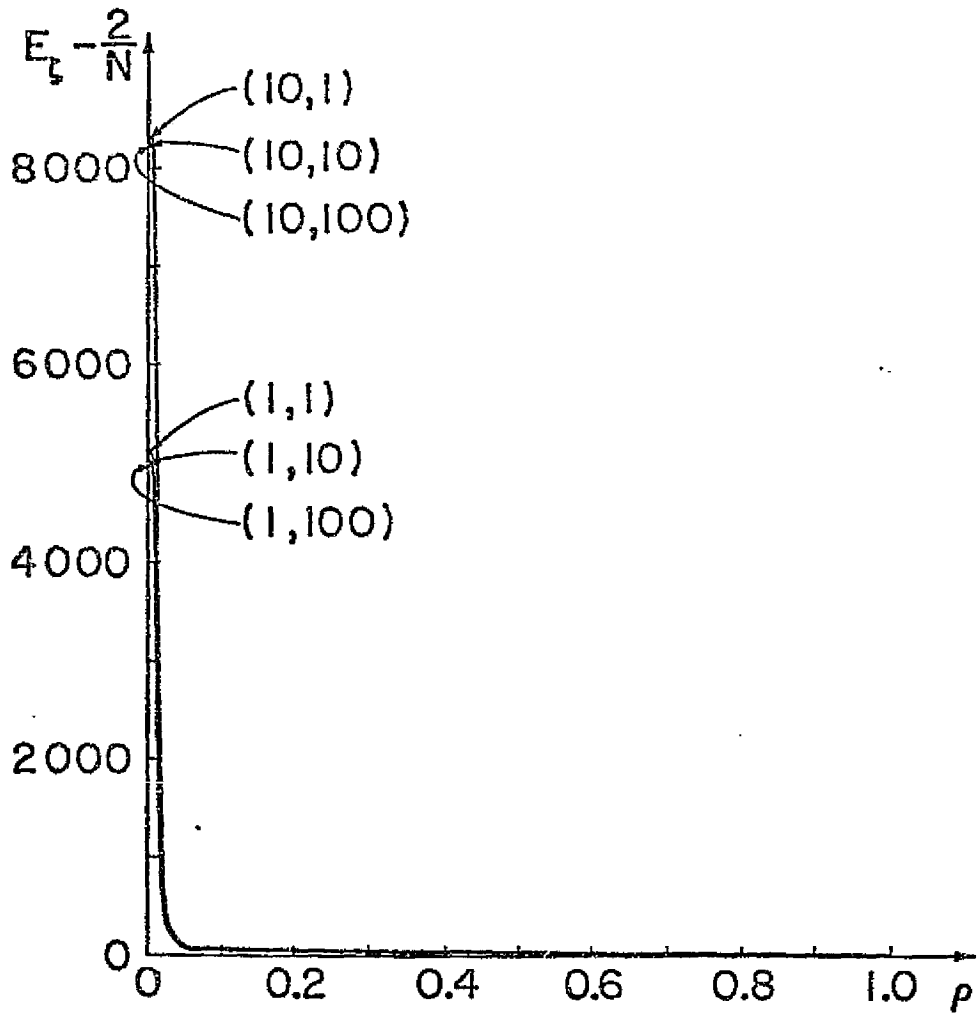

Fig. 3.10. $E_\zeta(\rho,\zeta)$ versus ρ for $\zeta = -0.99$, and $(\omega\tau,H) = (1,1)$ to $(10,100)$.

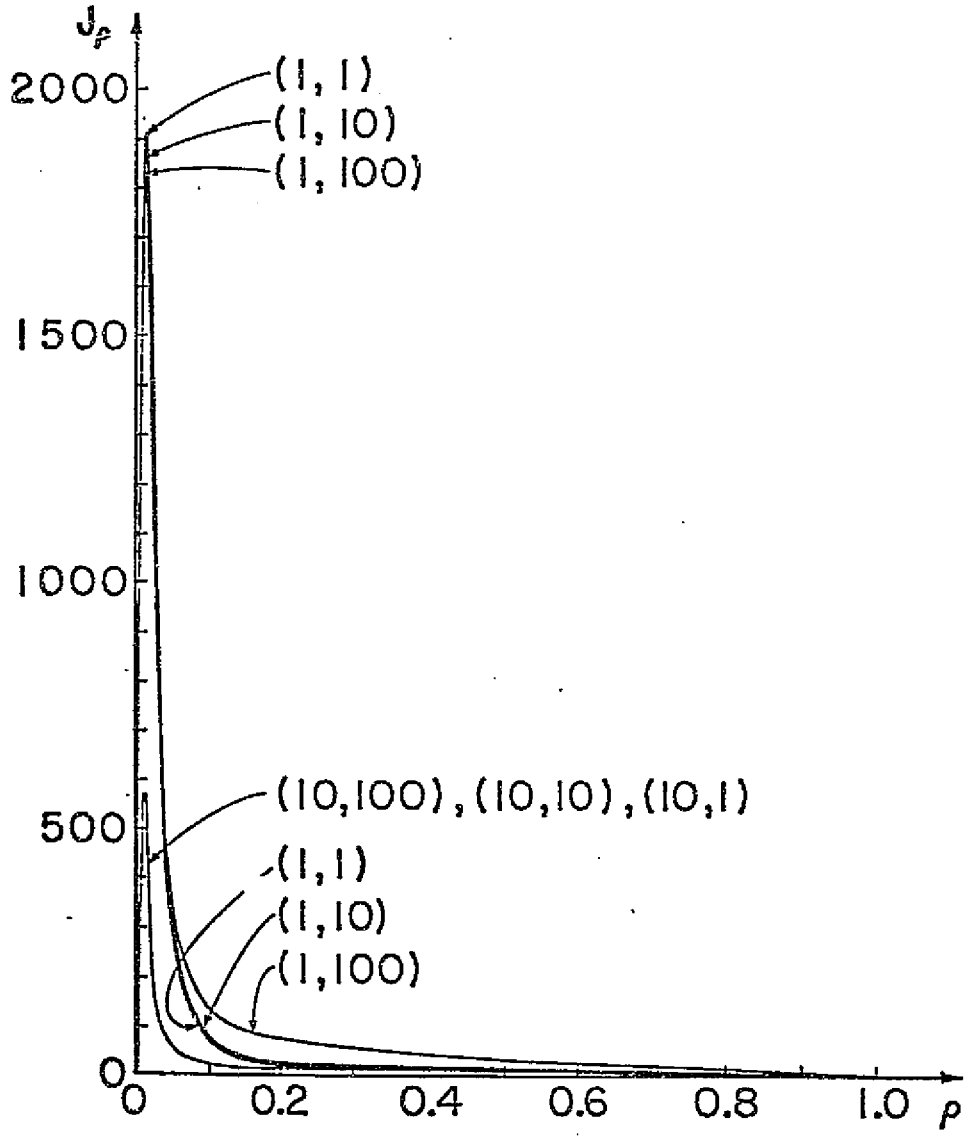

Fig. 3.11. $J_\rho(\rho,\zeta)$ versus ρ for $\zeta = -0.99$, and $(\omega\tau,H) = (1,1)$ to $(10,100)$.

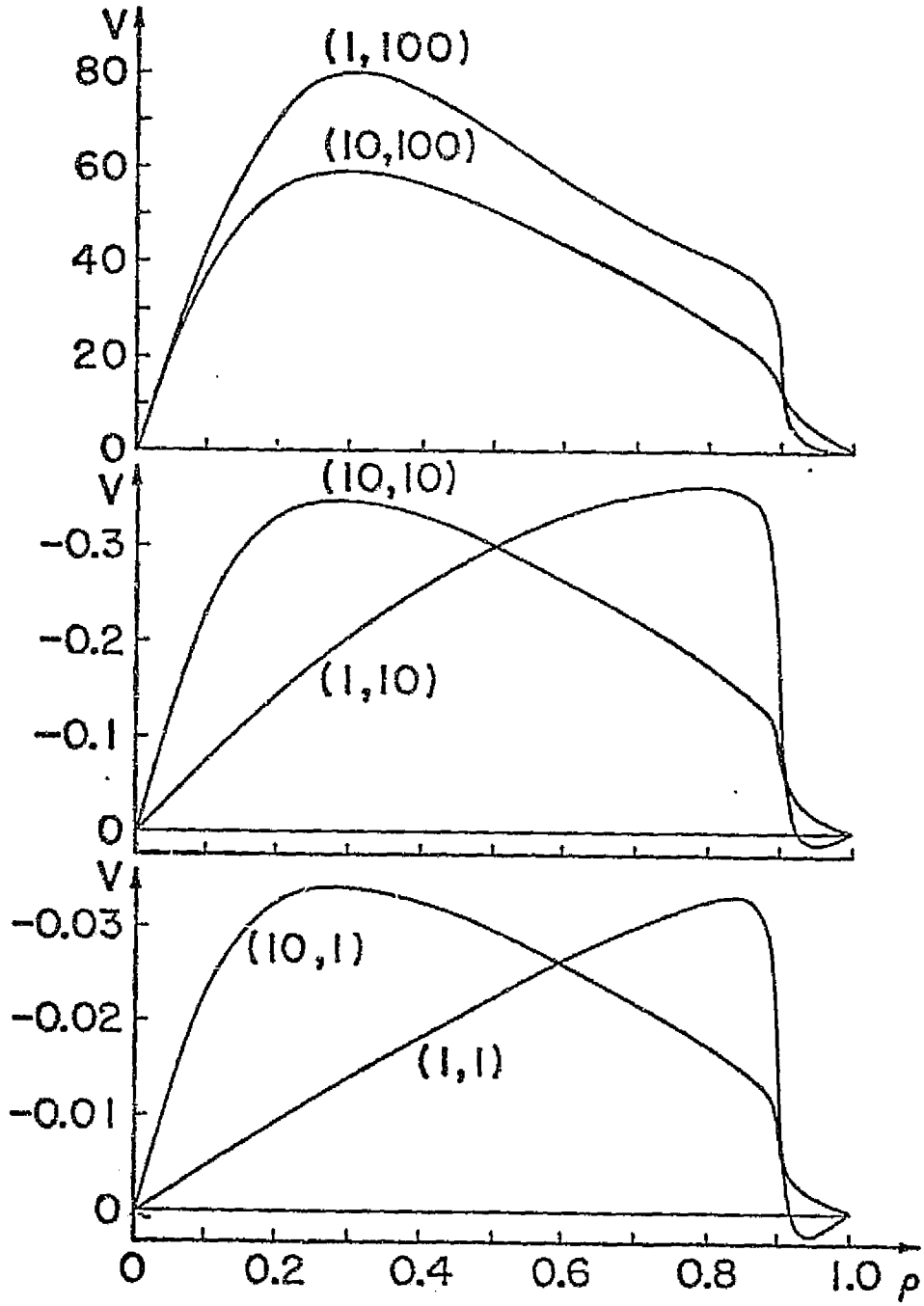

Fig. 3.12. $V(\rho,\zeta)$ versus ρ for $\zeta = +0.99$, and $(\omega\tau,H) = (1,1)$ to $(10,100)$.

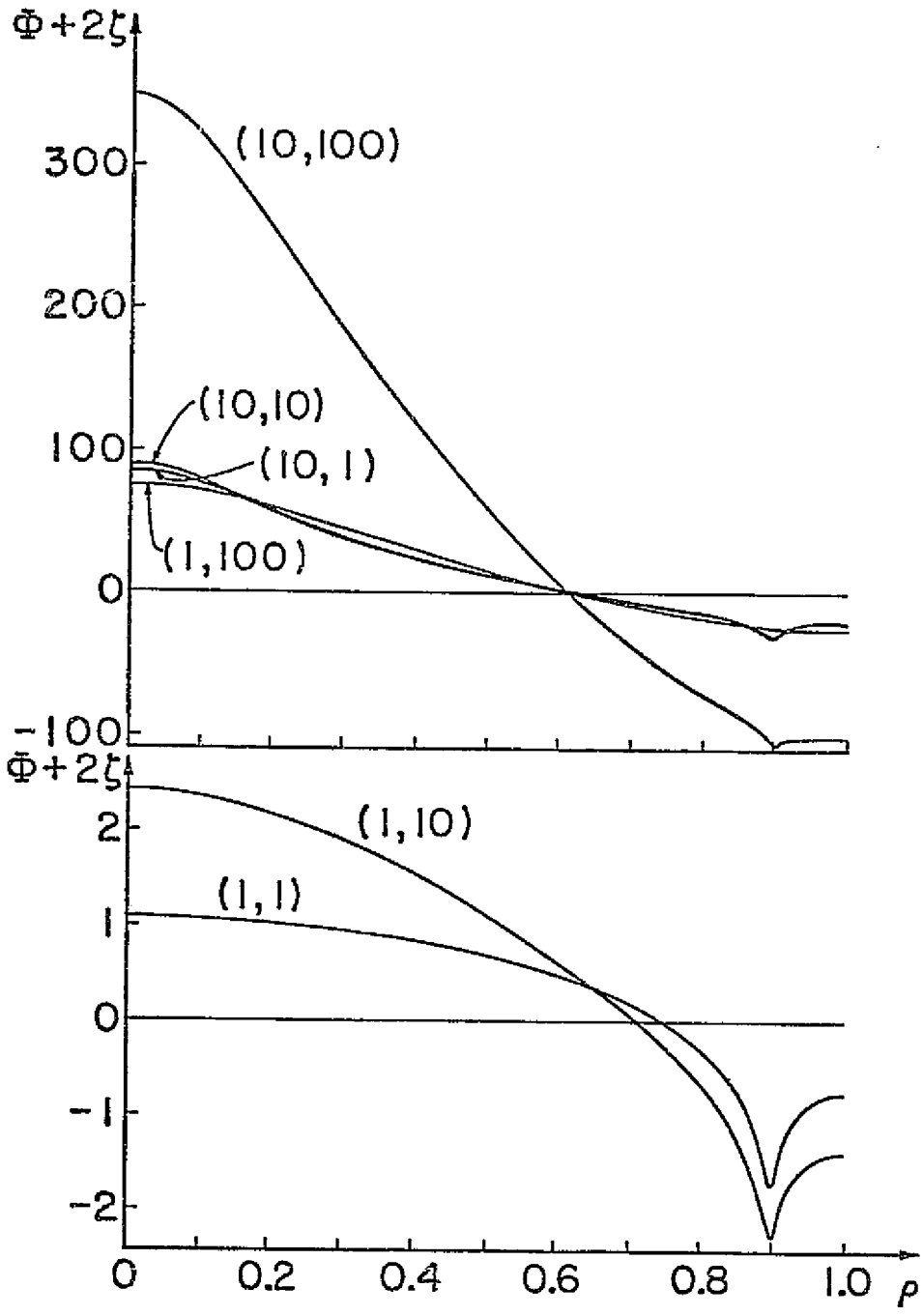

Fig. 3.13. $\Phi(\rho,\zeta)$ versus ρ for $\zeta = +0.99$, and $(\omega\tau,H) = (1,1)$ to $(10,100)$.

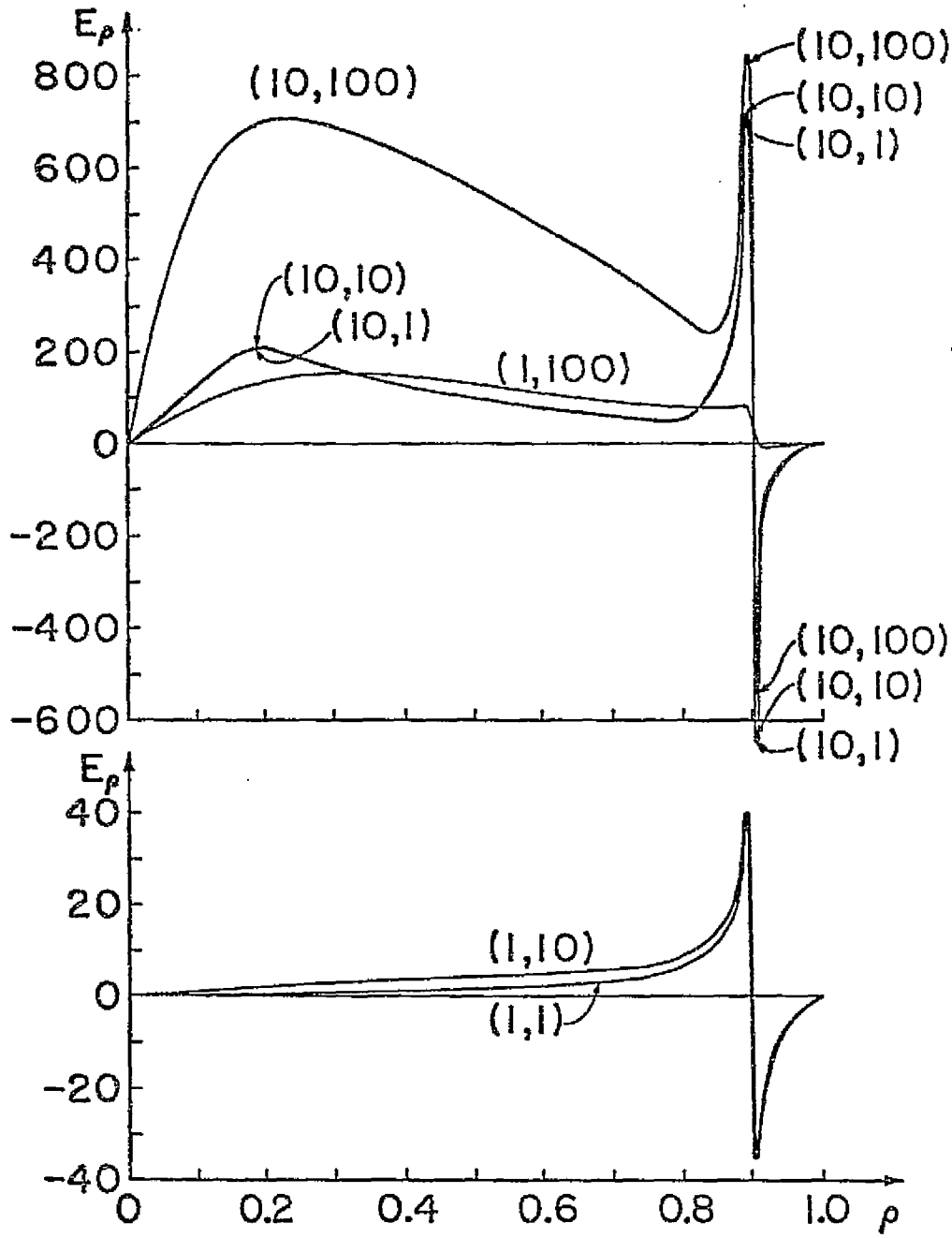

Fig. 3.14. $E_\rho(\rho,\zeta)$ versus ρ for $\zeta = +0.99$, and $(\omega\tau,H) = (1,1)$ to $(10,100)$.

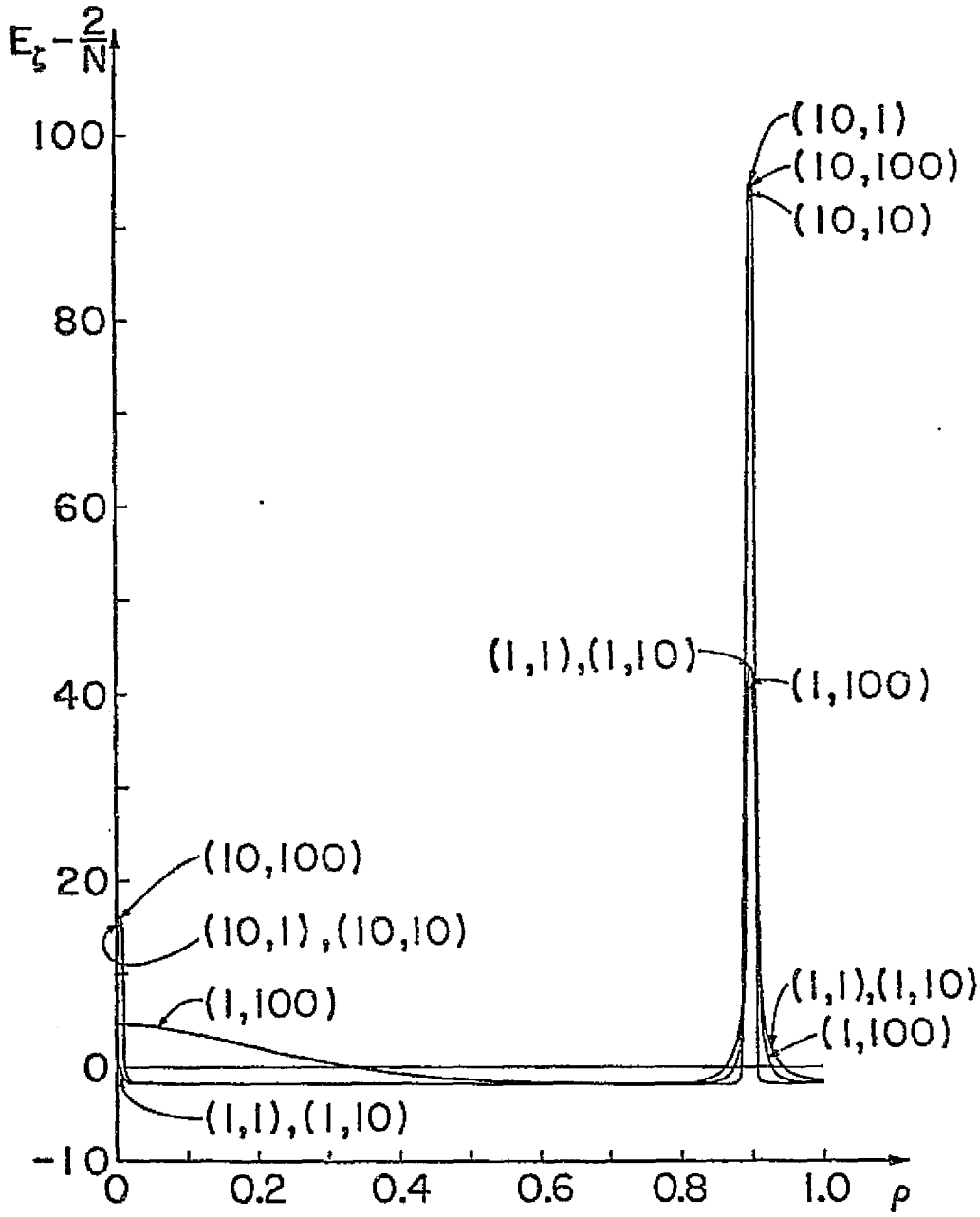

Fig. 3.15. $E_\zeta(\rho,\zeta)$ versus ρ for $\zeta = +0.99$, and $(\omega\tau,H) = (1,1)$ to $(10,100)$.

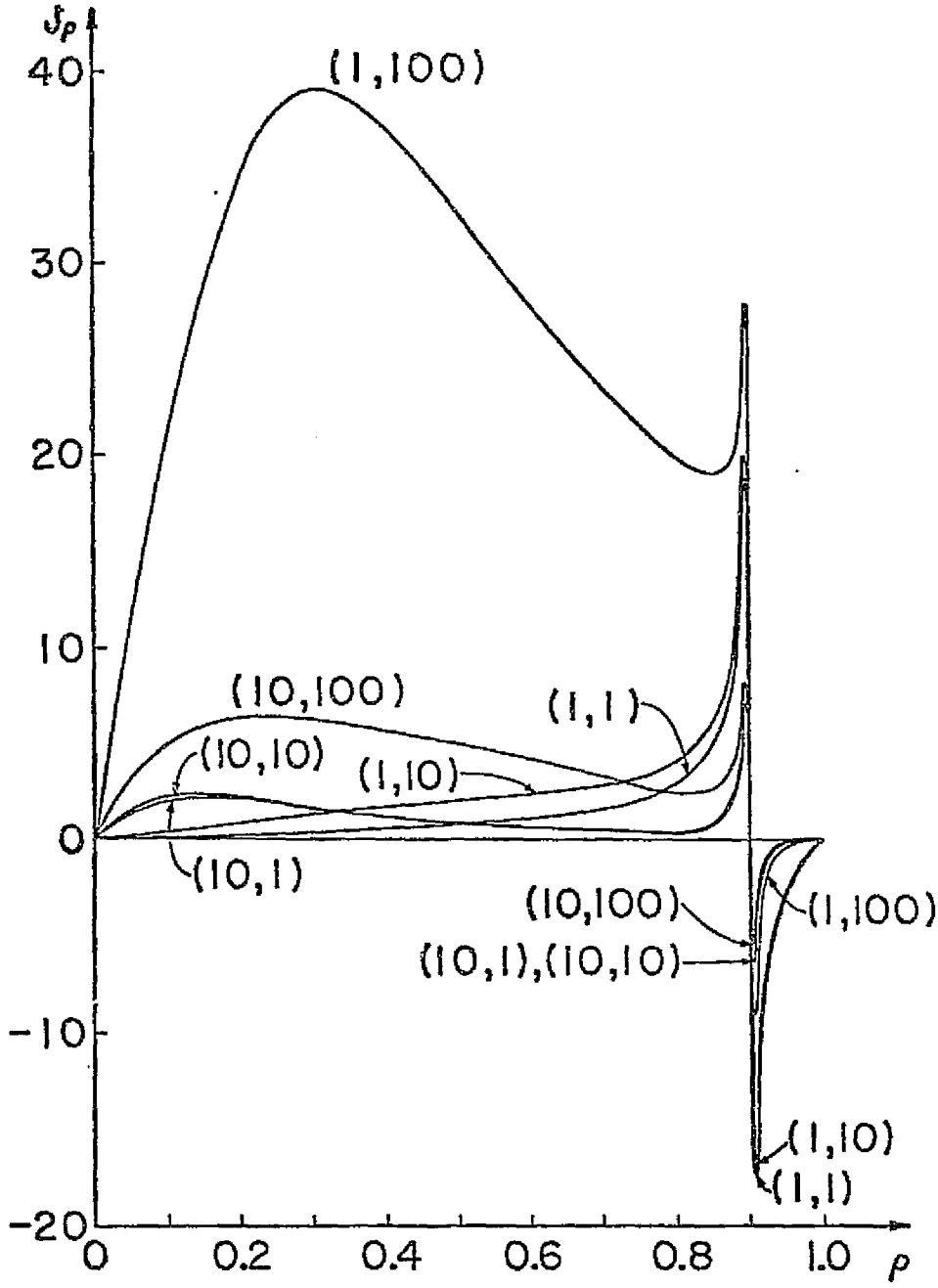

Fig. 3.16. $J_\rho(\rho,\zeta)$ versus ρ for $\zeta = +0.99$, and $(\omega\tau,H) = (1,1)$ to $(10,100)$.

that, in the plane $\zeta = +0.99$, the electrical discharge has shifted to the region $\rho \approx 0.9$ due to the influence of the nearby ring anode, $\rho_+ = 0.9(\zeta = +1)$. This shift occurs first slowly in the region $-1 < \zeta < +1 - \Delta\zeta$, and then rapidly in a relatively thin layer $\Delta\zeta << 1$ close to the anode plane $\zeta = +1$.

It is remarkable that the discharge remains concentrated in a radial region close to the cylinder axis with little radial spreading of the current density $\vec{J}$, except in a layer $\Delta\zeta$ close to the ring electrode of large radius ($R_+ >> R_-$) in which the radial current component J_ρ dominates the axial current component J_ζ. This spatial concentration of the discharge is the more pronounced the larger H and $\omega\tau$. The speed of plasma rotation $V(\rho,\zeta)$ increases with increasing magnetic induction B_o by orders of magnitude over the reference speed V_o as the Figures 3.2, 3.7 and 3.12 indicate which show $V(\rho,\zeta)$ for increasing $\omega\tau$ and H. The theoretical electric field and current density distributions are in qualitative agreement with experiments (Schwenn 1970).

The graphs in Figures 3.2-3.16 are based on the Fourier-series solutions, in which the first 100 terms were considered and the eigenvalues k_n were calculated up to the 10th decimal point. An even larger number of terms in the Fourier series solutions has to be taken into account if one wishes to compute (approximately) the centrifuge fields extremely close to the ring cathode ($\rho_- = 0.01$, $\zeta = -1$) and ring anode ($\rho_+ = 0.9$, $\zeta = +1$) where $\partial\Phi(\rho,\zeta)/\partial\zeta$ changes discontinuously with ρ due to the electrode boundary conditions. The Fourier-series representation may be highly unreliable for precise numerical work in the vicinity of a discontinuity due to Gibbs phenomenon, i.e., the overshoot

at a discontinuity. The Gibbs phenomenon could be suppressed drastically by the use of Lanczos convergence factors, which also accelerate convergence and are used as a means of data smoothing.

The system analysis presented indicates that extremely high speeds of plasma rotation are obtainable already at moderate discharge currents I and magnetic inductions B_o, presuming the magnetic interaction numbers are not small, $H > 1$, $\omega\tau > 1$. As an example, consider a plasma centrifuge with

$$|I| = 10^2 \text{ amp} \quad , \quad |B_o| = 10^0 \text{ Tesla},$$

$$\sigma = 10^2 \text{ mho/m} \quad , \quad R_o = c = 10^{-1}\text{m}.$$

Hence, by Equation (3.13)

$$V_o = Ic/2\pi\sigma B_o R_o^3 = (5/\pi) \times 10^1 \text{ m/sec},$$

and, by Figure 3.2,

$$O[V_\theta] = O[V_o V] = 10^4 \text{ m/sec} \quad , \text{ for } \omega\tau = 10,\ H = 100.$$

Speeds of plasma rotation V_θ, which are by orders of magnitude larger than 10^4 m/sec, can be produced if the order of magnitude of the parameters $\omega\tau$ and H is increased. The viscous forces reduce, however, the speed of plasma rotation always in the layers close to the walls ($z = \pm c$; $r = R_o$).

CHAPTER IV

EFFECT OF INDUCED MAGNETIC FIELD ON DIVERGING PLASMA CENTRIFUGE AT ARBITRARY MAGNETIC REYNOLDS NUMBERS

This chapter deals with the boundary-value problem for the partial differential equations, which describe the (azimuthal) rotation velocity and induced magnetic fields in the diverging plasma centrifuge with ring electrodes of different radii and an external, axial magnetic field. The closed-form solutions of the Fourier-Bessel series are obtained based on the magnetogasdynamic approximation for dense isotope plasma with negligible Hall effect. The electric field, current density, and velocity distributions are discussed in terms of the Hartmann number H and the magnetic Reynolds number R. For small Hall-coefficients, $\omega\tau \ll 1$, the induced magnetic field does not affect the plasma rotation. The rotating plasma with speeds as high as 10^3 m/sec is obtainable at typical conditions that can be realized in the practical application to the isotope separation.

4.1. Boundary-value Problem for Velocity and Induced Magnetic Field

The plasma centrifuge model under consideration is the same as depicted schematically in Figure 3.1 of Chapter III. The plasma is sustained by a discharge current I, which enters the centrifuge chamber of radius R_o through a ring anode of radius R_+ in the anode plane

$z = +c$ and leaves it through a ring cathode of radius R_- in the cathode plane $z = -c$. Accordingly, $2\pi \int_0^{R_o} J_z(r,z)\, r dr = I \int_0^{R_o} \delta(r-R_\pm)\, dr = I$ for the axial current density J_z in any plane $-c \leq z \leq +c$. The external magnetic field is axial and homogeneous $\vec{B}_o = \{0, 0, B_o\}$. In view of the symmetry of the system with respect to the axis $r = 0$, the plasma flow field is azimuthal, $\vec{V} = \{0, V_\theta(r,z), 0\}$, so that $\nabla \cdot \vec{V} = 0$, i.e., the plasma behaves incompressible. For negligible Hall-effect ($\omega\tau \ll 1$), $J_\theta = 0$ and $\nabla \times \vec{B} = \mu_o\{J_r, 0, J_z\}$ in accordance with Maxwell's equation for the magnetic induction $\vec{B}$. Hence, $B_r = 0$ and $B_z = 0$ because of the homogeneous boundary conditions for B_r and B_z. However, $B_\theta(r,z) \neq 0$, since

$$B_\theta(r,z)_{r=R_o} = \mu_o I/2\pi R_o \ , \ -c \leq z \leq +c \ ,$$

$$\frac{1}{r}\frac{\partial}{\partial r}\left[rB_\theta(r,z)\right]_{z=\pm c} = \mu_o I\ \delta(r-R_\pm)/2\pi r \ , \quad 0 \leq r \leq R_o \ .$$

Since the induced magnetic field (B_θ) is azimuthal, the induced electric field (E_r) is due to the rotation (V_θ) of the plasma across the external magnetic field (B_o). The pressure distribution $P(r,z)$ in the rotating plasma is determined by the r- and z-components of the magnetogasdynamic equation of motion [Eq. (2.1)],

$$-\rho_p \frac{V_\theta^2}{r} = -\frac{\partial P}{\partial r} - J_z B_\theta, \quad 0 = -\frac{\partial P}{\partial z} + J_r B_\theta \ , \tag{4.1}$$

where

$$\frac{1}{r}\frac{\partial}{\partial r}(rB_\theta) = \mu_o J_z, \quad -\frac{\partial B_\theta}{\partial z} = \mu_o J_r \ . \tag{4.2}$$

The current density, $\vec{J}(r,z)$, and pressure, $P(r,z)$, fields are readily determined from the magnetic field $\vec{B} = \{0, B_\theta, B_o\}$ and the

velocity field $\vec{V} = \{0, V_\theta, 0\}$, whereas the electric field is given by Ohm's law, $\vec{E} = -\vec{V} \times \vec{B} + \vec{J}/\sigma$. In accordance with the equation of motion, Maxwell's equations and Ohm's law (Section 2.1), the plasma in the centrifuge with homogeneous magnetic field $\vec{B}_o$ (Fig. 3.1) is described by the boundary-value problem for azimuthal velocity $V_\theta(r,z)$ and azimuthal induction $B_\theta(r,z)$ fields:

$$\frac{\partial}{\partial r}\left[\frac{1}{r}\frac{\partial}{\partial r}(rV_\theta)\right] + \frac{\partial^2 V}{\partial z^2} = -\frac{B_o}{\mu\mu_o}\frac{\partial B_\theta}{\partial z}, \tag{4.3}$$

$$\frac{\partial}{\partial r}\left[\frac{1}{r}\frac{\partial}{\partial r}(rB_\theta)\right] + \frac{\partial^2 B_\theta}{\partial z^2} = -\mu_o\sigma B_o\frac{\partial V_\theta}{\partial z}, \tag{4.4}$$

where

$$V_\theta(r,z)_{r=R_o} = 0, \quad -c \le z \le +c, \tag{4.5}$$

$$V_\theta(r,z)_{z=\pm c} = 0, \quad 0 \le r \le R_o, \tag{4.6}$$

and

$$B_\theta(r,z)_{r=R_o} = \mu_o I/2\pi R_o, \quad -c \le z \le +c, \tag{4.7}$$

$$\frac{1}{r}\frac{\partial}{\partial r}[rB_\theta(r,z)]_{z=\pm c} = \mu_o I\,\delta(r-R_\pm)/2\pi r, \quad 0 \le r \le R_o. \tag{4.8}$$

Equations (4.3) and (4.4) are the azimuthal components of the equations of plasma motion and magnetic induction $[\nabla^2\vec{B} = -\mu_o\sigma\nabla\times(\vec{V}\times\vec{B})]$. The boundary conditions (4.5) and (4.6) consider that the plasma does not slip at the walls $r = R_o$ and $z = \pm c$. The boundary conditions (4.7) and (4.8) follow from Maxwell's equations for a total discharge current of $|I|$ amps flowing from the ring anode ($r=R_+$) to the ring cathode ($r=R_-$) of vanishing radial width if $I < 0$ (Fig. 3.1).

4.2. Analytical Solutions in Terms of Fourier-Bessel Series

For physical and mathematical reasons (Section 1.3), it is suitable to formulate the boundary-value problem for the coupled plasma fields $V_\theta(r,z)$ and $B_\theta(r,z)$ in dimensionless form by introducing the dimensionless independent and dependent variables,

$$\rho = r/R_o \ , \quad 0 \leq \rho \leq 1 \ , \tag{4.9}$$

$$\zeta = z/c, \quad -1 \leq \zeta \leq +1 \ , \tag{4.10}$$

and

$$V(\rho,\zeta) = V_\theta(r,z)/V_o, \quad B(\rho,\zeta) = B_\theta(r,z)/B_o \ , \tag{4.11}$$

where the reference values V_o and B_o are defined as ($B_o \equiv$ external induction),

$$V_o \equiv I/2\pi R_o B_o \sigma c, \quad B_o \equiv B_o \ . \tag{4.12}$$

In the dimensionless formulation, the boundary-value problem for the azimuthal velocity, $V(\rho,\zeta)$, and azimuthal induction, $B(\rho,\zeta)$, fields assumes the form

$$\frac{\partial}{\partial\rho}\left[\frac{1}{\rho}\frac{\partial}{\partial\rho}(\rho V)\right] + N^{-2}\frac{\partial^2 V}{\partial\zeta^2} = -\frac{H^2}{R}\frac{\partial B}{\partial\zeta} \ , \tag{4.13}$$

$$\frac{\partial}{\partial\rho}\left[\frac{1}{\rho}\frac{\partial}{\partial\rho}(\rho B)\right] + N^{-2}\frac{\partial^2 B}{\partial\zeta^2} = -\frac{R}{N^2}\frac{\partial V}{\partial\zeta} \ , \tag{4.14}$$

where

$$V(\rho,\zeta)_{\rho=1} = 0, \quad -1 \leq \zeta \leq +1 \ , \tag{4.15}$$

$$V(\rho,\zeta)_{\zeta=\pm1} = 0, \quad 0 \leq \rho \leq 1 \ , \tag{4.16}$$

and

$$B(\rho,\zeta)_{\rho=1} = R, \quad -1 \leq \zeta \leq +1 \quad , \tag{4.17}$$

$$\frac{1}{\rho}\frac{\partial}{\partial\rho}\,[\rho B(\rho,\zeta)]_{\zeta=\pm 1} = R\,\delta(\rho-\rho_{\pm})/\rho, \quad 0 \leq \rho \leq 1 \quad , \tag{4.18}$$

with

$$H \equiv (\sigma/\mu)^{\frac{1}{2}} B_o R_o \ , \quad N \equiv c/R_o, \quad R \equiv \mu_o I/2\pi R_o B_o = \mu_o \sigma V_o c \gtrless 0. \tag{4.19}$$

The Hartmann number H, N, and the magnetic Reynolds number R characterize the ratio of Lorentz to viscous forces, the geometry of the centrifuge, and the intensity ratio of the induced and external magnetic fields, respectively. Equations (4.15), (4.16) and (4.17), (4.18) are the homogeneous and inhomogeneous boundary conditions for the fields $V(\rho,\zeta)$ and $B(\rho,\zeta)$, respectively. The linear statement,

$$B(\rho,\zeta) = R[\rho + \Psi(\rho,\zeta)] \quad , \tag{4.20}$$

reduces the Equations (4.14), (4.17) and (4.18) for $B(\rho,\zeta)$ to equations with a homogeneous boundary condition (4.22) for $\Psi(\rho,\zeta)$

$$\frac{\partial}{\partial\rho}\,[\frac{1}{\rho}\frac{\partial}{\partial\rho}\,(\rho\Psi)] + N^{-2}\,\frac{\partial^2\Psi}{\partial\zeta^2} = -\,N^{-2}\,\frac{\partial V}{\partial\zeta} \quad , \tag{4.21}$$

where

$$\Psi(\rho,\zeta)_{\rho=1} = 0, \quad -1 \leq \zeta \leq +1 \quad , \tag{4.22}$$

$$\frac{1}{\rho}\frac{\partial}{\partial\rho}\,[\rho\Psi(\rho,\zeta)]_{\zeta=\pm 1} = \frac{\delta(\rho-\rho_{\pm})}{\rho} - 2 \ , \quad 0 \leq \rho \leq 1 \quad . \tag{4.23}$$

Introducing Bessel's function $J_1(k_n\rho)$ of first order, partial solutions of the coupled inhomogeneous Equations (4.13) and (4.21) are in the form,

$$V_n(\rho,\zeta) = J_1(k_n\rho)\ f_n(\zeta) \quad , \tag{4.24}$$

$$\Psi_n(\rho,\zeta) = J_1(k_n\rho)\ g_n(\zeta) \quad , \tag{4.25}$$

where the eigenvalues $k_n > 0$ are determined by the homogeneous boundary conditions (4.15) and (4.22) as the real roots of the transcendental equation,

$$J_1(k_n) = 0 \ , \ n = 1,2,3,\ldots \quad . \tag{4.26}$$

Thus, the general solution of the coupled Equations (4.13) and (4.21) obtains by linear superposition as the Fourier-Bessel series,

$$V(\rho,\zeta) = \sum_{n=1}^{\infty} J_1(k_n\rho)\ f_n(\zeta) \ , \tag{4.27}$$

$$\Psi(\rho,\zeta) = \sum_{n=1}^{\infty} J_1(k_n\rho)\ g_n(\zeta) \ . \tag{4.28}$$

Substitution of Equations (4.24) and (4.25) into Equations (4.13) and (4.21) yields ordinary coupled differential equations of second order for $f_n(\zeta)$ and $g_n(\zeta)$:

$$f_n'' - k_n^2 N^2 f_n = -H^2N^2 g_n' \quad , \tag{4.29}$$

$$g_n'' - k_n^2 N^2 g_n = -f_n' \quad . \tag{4.30}$$

By elimination, Equations (4.29) and (4.30) are reduced to decoupled differential equations of fourth order,

$$f_n'''' - (2k_n^2 + H^2)N^2 f_n'' + k_n^4 N^4 f_n = 0 \quad , \tag{4.31}$$

$$g_n'''' - (2k_n^2 + H^2)N^2 g_n'' + k_n^4 N^4 g_n = 0 \quad , \tag{4.32}$$

with

$$f_n(\zeta)_{\zeta=\pm 1} = 0 \ , \tag{4.33}$$

$$g_n(\zeta)_{\zeta=\pm 1} = 2k_n^{-1} J_0(k_n \rho_\pm)/J_0^2(k_n) \ , \tag{4.34}$$

as boundary conditions, by Equations (4.16) and (4.23), respectively. In deriving Equation (4.34), the Fourier-Dini series representation of the Dirac function [Eq. (3.32)] has been used. In addition to Equations (4.33) and (4.34), $f_n(\zeta)$ and $g_n(\zeta)$ have to satisfy also the coupled Equations (4.29) and (4.30). With the four real roots of Equations (4.31) and (4.32) $[f_n, g_n \propto \exp(\omega_n^{\pm}\zeta)]$,

$$\omega_{1n} \equiv \omega_n^+ \ , \quad \omega_{2n} \equiv \omega_n^- \ , \quad \omega_{3n} \equiv -\omega_n^+ \ , \quad \omega_{4n} \equiv -\omega_n^- \quad , \tag{4.35}$$

where

$$\omega_n^{\pm} \equiv 2^{-\frac{1}{2}} N\{(2k_n^2 + H^2) \pm [(2k_n^2 + H^2)^2 - 4k_n^4]^{\frac{1}{2}}\}^{\frac{1}{2}} \quad , \tag{4.36}$$

the general solutions for $f_n(\zeta)$ and $g_n(\zeta)$ of Equations (4.31) and (4.32) can be written as

$$\begin{aligned} f_n(\zeta) = {} & A_n^+ \frac{\sinh \omega_n^+ \zeta}{\sinh \omega_n^+} + B_n^+ \frac{\cosh \omega_n^+ \zeta}{\cosh \omega_n^+} \\ & + A_n^- \frac{\sinh \omega_n^- \zeta}{\sinh \omega_n^-} + B_n^- \frac{\cosh \omega_n^- \zeta}{\cosh \omega_n^-} \quad , \end{aligned} \tag{4.37}$$

$$g_n(\zeta) = C_n^+ \frac{\sinh \omega_n^+ \zeta}{\sinh \omega_n^+} + D_n^+ \frac{\cosh \omega_n^+ \zeta}{\cosh \omega_n^+}$$

$$+ C_n^- \frac{\sinh \omega_n^- \zeta}{\sinh \omega_n^-} + D_n^- \frac{\cosh \omega_n^- \zeta}{\cosh \omega_n^-} \quad . \tag{4.38}$$

Only four of the eight integration constants $A_n^\pm$, ... $D_n^\pm$ are independent. Substitution of Equations (4.37) and (4.38) into Equation (4.29) and Equation (4.30) yields

$$A_n^\pm \, [(\omega_n^\pm)^2 - k_n^2 N^2]/\omega_n^\pm = -H^2 N^2 \, \mathrm{tgh}\omega_n^\pm \, D_n^\pm \, , \tag{4.39}$$

$$B_n^\pm \, [(\omega_n^\pm)^2 - k_n^2 N^2]/\omega_n^\pm = -H^2 N^2 \, \mathrm{cth}\omega_n^\pm \, C_n^\pm \, , \tag{4.40}$$

and

$$C_n^\pm \, [(\omega_n^\pm)^2 - k_n^2 N^2]/\omega_n^\pm = - \, \mathrm{tgh}\omega_n^\pm \, B_n^\pm \, , \tag{4.41}$$

$$D_n^\pm \, [(\omega_n^\pm)^2 - k_n^2 N^2]/\omega_n^\pm = - \, \mathrm{cth}\omega_n^\pm \, A_n^\pm \, , \tag{4.42}$$

respectively. The coefficient determinant of Equations (4.39) and (4.42) or Equations (4.40) and (4.41) vanishes (condition for existence of nontrivial solution),

$$\Delta^\pm \equiv [(\omega_n^\pm)^2 - k_n^2 N^2]^2 - H^2 N^2 (\omega_n^\pm)^2 = 0 \, , \tag{4.43}$$

in agreement with Equation (4.36). From the latter or Equation (4.43) one deduces the relations,

$$[(\omega_n^\pm)^2 - k_n^2 N^2]/\omega_n^\pm = \pm NH \, , \tag{4.44}$$

which simplify the left-hand sides of Equations (4.39)-(4.42).

Application of the boundary conditions (4.33) to Equation (4.37) shows that

$$-A_n^- = +A_n^+ \equiv A_n \ , \quad -B_n^- = +B_n^+ \equiv B_n \ . \tag{4.45}$$

Substitution of Equation (4.45) into Equations (4.37) and (4.38) gives

$$\begin{aligned} f_n(\zeta) &= A_n\left(\frac{\sinh \omega_n^+\zeta}{\sinh \omega_n^+} - \frac{\sinh \omega_n^-\zeta}{\sinh \omega_n^-}\right) \\ &\quad + B_n\left(\frac{\cosh \omega_n^+\zeta}{\cosh \omega_n^+} - \frac{\cosh \omega_n^-\zeta}{\cosh \omega_n^-}\right), \end{aligned} \tag{4.46}$$

and

$$\begin{aligned} g_n(\zeta) &= -A_n \frac{1}{NH}\left(\frac{\cosh \omega_n^+\zeta}{\sinh \omega_n^+} + \frac{\cosh \omega_n^-\zeta}{\sinh \omega_n^-}\right) \\ &\quad -B_n \frac{1}{NH}\left(\frac{\sinh \omega_n^+\zeta}{\cosh \omega_n^+} + \frac{\sinh \omega_n^-\zeta}{\cosh \omega_n^-}\right), \end{aligned} \tag{4.47}$$

the latter under consideration of Equations (4.41), (4.42) and Equation (4.44). Application of the boundary conditions (4.34) to Equation (4.47) yields, upon elimination

$$A_n = -\frac{NH}{k_n}\frac{J_0(k_n\rho_-) + J_0(k_n\rho_+)}{(\mathrm{cth}\omega_n^+ + \mathrm{cth}\omega_n^-)\ J_0^2(k_n)} \ , \tag{4.48}$$

$$B_n = +\frac{NH}{k_n}\frac{J_0(k_n\rho_-) - J_0(k_n\rho_+)}{(\mathrm{tgh}\omega_n^+ + \mathrm{tgh}\omega_n^-)\ J_0^2(k_n)} \ . \tag{4.49}$$

By combining Equations (4.46)-(4.49) the solutions for $f_n(\zeta)$ and $g_n(\zeta)$ in final form are

$$f_n(\zeta)/NH = -\frac{J_0(k_n\rho_-) + J_0(k_n\rho_+)}{(\mathrm{cth}\omega_n^+ + \mathrm{cth}\omega_n^-)k_n\ J_0^2(k_n)}\left(\frac{\sinh\ \omega_n^+\zeta}{\sinh\ \omega_n^+} - \frac{\sinh\ \omega_n^-\zeta}{\sinh\ \omega_n^-}\right)$$

$$+\frac{J_0(k_n\rho_-) - J_0(k_n\rho_+)}{(\mathrm{tgh}\omega_n^+ + \mathrm{tgh}\omega_n^-)k_n\ J_0^2(k_n)}\left(\frac{\cosh\ \omega_n^+\zeta}{\cosh\ \omega_n^+} - \frac{\cosh\ \omega_n^-\zeta}{\cosh\ \omega_n^-}\right), \qquad (4.50)$$

$$g_n(\zeta) = +\frac{J_0(k_n\rho_-) + J_0(k_n\rho_+)}{(\mathrm{cth}\omega_n^+ + \mathrm{cth}\omega_n^-)k_n\ J_0^2(k_n)}\left(\frac{\cosh\ \omega_n^+\zeta}{\sinh\ \omega_n^+} + \frac{\cosh\ \omega_n^-\zeta}{\sinh\ \omega_n^-}\right)$$

$$-\frac{J_0(k_n\rho_-) - J_0(k_n\rho_+)}{(\mathrm{tgh}\omega_n^+ + \mathrm{tgh}\omega_n^-)k_n\ J_0^2(k_n)}\left(\frac{\sinh\ \omega_n^+\zeta}{\cosh\ \omega_n^+} + \frac{\sinh\ \omega_n^-\zeta}{\cosh\ \omega_n^-}\right) . \qquad (4.51)$$

Below, also the ζ-derivative of $g_n(\zeta)$ is required, which is given by

$$g_n'(\zeta) = +\frac{J_0(k_n\rho_-) + J_0(k_n\rho_+)}{(\mathrm{cth}\omega_n^+ + \mathrm{cth}\omega_n^-)k_n\ J_0^2(k_n)}\left(\omega_n^+\frac{\sinh\ \omega_n^+\zeta}{\sinh\ \omega_n^+} + \omega_n^-\frac{\sinh\ \omega_n^-\zeta}{\sinh\ \omega_n^-}\right)$$

$$-\frac{J_0(k_n\rho_-) - J_0(k_n\rho_+)}{(\mathrm{tgh}\omega_n^+ + \mathrm{tgh}\omega_n^-)k_n\ J_0^2(k_n)}\left(\omega_n^+\frac{\cosh\ \omega_n^+\zeta}{\cosh\ \omega_n^+} + \omega_n^-\frac{\cosh\ \omega_n^-\zeta}{\cosh\ \omega_n^-}\right). \qquad (4.52)$$

In terms of $f_n(\zeta)$, $g_n(\zeta)$, and $g_n'(\zeta)$, the solutions for the dimensionless fields $\vec{V} = \{0,V,0\}$, $\vec{B} = \{0,B,1\}$, $\vec{J} = \{J_\rho,0,J_\zeta\}$ and $\vec{E} = \{E_\rho,0,E_\zeta\}$ of the plasma centrifuge are by Equations (4.20), (4.27) and (4.28)

$$V(\rho,\zeta) = \sum_{n=1}^{\infty} J_1(k_n\rho)f_n(\zeta) \quad , \qquad (4.53)$$

$$B(\rho,\zeta) = R[\rho + \sum_{n=1}^{\infty} J_1(k_n\rho)g_n(\zeta)] \ , \qquad (4.54)$$

$$J_\rho(\rho,\zeta) = - N^{-1} \sum_{n=1}^{\infty} J_1(k_n\rho) g_n'(\zeta) \quad , \tag{4.55}$$

$$J_\zeta(\rho,\zeta) = 2 + \sum_{n=1}^{\infty} k_n J_0(k_n\rho) g_n(\zeta) \quad , \tag{4.56}$$

$$E_\rho(\rho,\zeta) = - V(\rho,\zeta) + N\, J_\rho(\rho,\zeta), \quad E_\zeta(\rho,\zeta) = NJ_\zeta(\rho,\zeta). \tag{4.57}$$

The reference values V_o and B_o for $V(\rho,\zeta)$ and $B(\rho,\zeta)$ are defined in Equation (4.12). The dimensionless fields $J_{\rho,\zeta}(\rho,\zeta)$ and $E_{\rho,\zeta}(\rho,\zeta)$ are normalized with respect to

$$J_o \equiv 1/2\pi R_o^2 \ , \quad E_o \equiv V_o B_o = 1/2\pi R_o\ c \ . \tag{4.58}$$

It can be proved that the solution $V(\rho,\zeta)$ derived here from the boundary-value problem with a significant induced magnetic field B_θ remains valid even for the boundary-value problem in Chapter III as long as the Hall effect is negligible. Let $V_{III}(\rho,\zeta)$ and $V_{IV}(\rho,\zeta)$ designate the solutions for the dimensionless azimuthal velocity in Chapter III for $\omega\tau << 1$ and the present chapter, respectively. The Ohm's law for $\omega\tau << 1$, $J_r = - \frac{\partial\phi}{\partial r} + V_\theta B_o$, and Faraday's law, $- \frac{\partial B_\theta}{\partial z} = \mu o J_r$, give the following relation in dimensionless form

$$- \frac{\partial\Phi}{\partial\rho} + V_{III} = - \frac{1}{R}\frac{\partial B}{\partial\zeta} \ . \tag{4.59}$$

Substitution of this relation into Equations (3.14), (4.13) and boundary conditions for V_{III} and V_{IV} yields a new boundary-value problem for $W(\rho,\zeta) \equiv V_{III}(\rho,\zeta) - V_{IV}(\rho,\zeta)$:

$$\frac{\partial}{\partial\rho}\left[\frac{1}{\rho}\frac{\partial}{\partial\rho}(\rho W)\right] + N^{-2}\frac{\partial^2 W}{\partial\zeta^2} = 0 \ , \tag{4.60}$$

where

$$W(\rho,\zeta)_{\rho=1} = 0 \ , \quad -1 \leq \zeta \leq +1 \ , \tag{4.61}$$

$$W(\rho,\zeta)_{\zeta=\pm 1} = 0 \ , \quad 0 \leq \rho \leq 1 \ . \tag{4.62}$$

The general solution of Equation (4.60) has the form

$$W(\rho,\zeta) = \sum_{n=1}^{\infty} J_1(k_n\rho) \ [A_n \cosh(Nk_n\zeta) + B_n \sinh(Nk_n\zeta)] \ , \tag{4.63}$$

where the integration constants A_n and B_n are determined by boundary conditions (4.62):

$$A_n \cosh(Nk_n) + B_n \sinh(Nk_n) = 0 \ , \tag{4.64}$$

$$A_n \cosh(Nk_n) - B_n \sinh(Nk_n) = 0 \ . \tag{4.65}$$

However, $W(\rho,\zeta)$ should have only trivial solution ($W \equiv V_{III} - V_{IV} = 0$) since the coefficient determinant for A_n and B_n of Equations (4.64) and (4.65) would not vanish, i.e.,

$$\begin{vmatrix} \cosh(Nk_n) & \sinh(Nk_n) \\ \cosh(Nk_n) & -\sinh(Nk_n) \end{vmatrix} \neq 0 \ . \tag{4.66}$$

This means that $V_{III}(\rho,\zeta)$ [Eq. (3.47)] for $\omega\tau = 0$ should be identical to $V_{IV}(\rho,\zeta)$ [Eq. (4.53)].

4.3. Numerical Illustrations and Results

As an illustration, the radial (ρ) dependence of the dimensionless discharge fields $V(\rho,\zeta)$, $B(\rho,\zeta)$, $E_\rho(\rho,\zeta)$, $J_\rho(\rho,\zeta)$, and $J_\zeta(\rho,\zeta)$ has been computed for $I < 0$ in the cross-sectional planes $\zeta = -0.99$ (cathode region), $\zeta = 0$ (central region), and $\zeta = +0.99$ (anode region) based on Equations (4.53)-(4.57). The remaining field $E_\zeta(\rho,\zeta)$ is proportional to $J_\zeta(\rho,\zeta)$ [Eq. (4.57)]. The characteristic dimensionless magnetic interaction number H is treated as a parameter: H = 1, 10, 100. The geometry parameter $N = c/R_o$ is taken to be N = 1 corresponding to $R_o = c$ [Eq. (4.19)]. The radial positions of the cathode and anode are assumed to be

$$\rho_- = 0.01 \ (R_- = 0.01 \ R_o) \ ; \ \ \rho_+ = 0.9 \ (R_+ = 0.9 \ R_o).$$

With the exception of $B_\theta = B_o B$, the dimensional fields are negative everywhere where the dimensionless fields are positive, and vice-versa since $V_o < 0$, $J_o < 0$ and $E_o < 0$ for $I < 0$ [Eqs. (4.12), (4.58)]. Note that the magnetic Reynolds R in Equation (4.19) is defined to change its sign with the sign of V_o.

The Equations (4.53)-(4.57) indicate that the velocity field $V(\rho,\zeta)$, the current density field $J_{\rho,\zeta}(\rho,\zeta)$, and the electric field $E_{\rho,\zeta}(\rho,\zeta)$ are independent of the magnetic Reynolds number R, whereas the induced magnetic field $B(\rho,\zeta)$ is proportional to R. This is due to the azimuthal direction of the induced magnetic field $B(\rho,\zeta)$, which is parallel to the velocity field $V(\rho,\zeta)$ of rotation. Accordingly, the plasma fields $V(\rho,\zeta)$, $B(\rho,\zeta)/R$, $J_{\rho,\zeta}(\rho,\zeta)$, and $E_{\rho,\zeta}(\rho,\zeta)$ depend only on the Hartmann number H, presuming that the Hall effect is negligible ($\omega\tau \ll 1$).

i) *Central Region*, $\zeta = 0$: In Figures 4.1-4.5, $V(\rho,0)$, $[B(\rho,0) - R\rho]/R$, $E_\rho(\rho,0)$, $J_\rho(\rho,0)$, and $J_\zeta(\rho,0) \propto E_\zeta(\rho,0)$ are shown versus $0 \leq \rho \leq 1$ with $H = 1, 10, 100$ as a parameter. It is seen that $|V|$ increases considerably at any point $0 < \rho < 1$ as H is increased. Similarly, $(B - R\rho)/R$ and the sources $J_{\rho,\zeta}$ of the magnetic induction increase in intensity within the main central region $0 < \rho < 1 - \Delta\rho$ as H is increased. For large values $H \gtrsim 10$, B and $J_{\rho,\zeta}$ decrease in the wall region $\Delta\rho = \Delta\rho(H)$, so that the electrical discharge becomes more concentrated in the center $0 < \rho < 1 - \Delta\rho$ of the centrifuge. The intensity of E_ρ increases uniformly in the region $0 < \rho < 1$ as H is increased, while $E_\zeta \propto J_\zeta$.

ii) *Cathode Region*, $\zeta = -0.99$: The Figures 4.6-4.10 show $V(\rho,-0.99)$, $[B(\rho,-0.99) - R\rho]/R$, $E_\rho(\rho,-0.99)$, $J_\rho(\rho,-0.99)$, and $J_\zeta(\rho,-0.99) \propto E_\zeta(\rho,-0.99)$ versus $0 \leq \rho \leq 1$ for $H = 1, 10, 100$. The fields V, $E_{\rho,\zeta}$, and $J_{\rho,\zeta}$ increase in intensity at any point $0 < \rho < 1$ with increasing H, whereas B/R decreases in $0 < \rho < 1$ with increasing H. Since the ring cathode is at $\rho_- = 0.01$ ($\zeta = -1$), the field distributions are more closely concentrated at the axis $\rho \cong 0$ than those in the plane $\zeta = 0$ (Figs. 4.1-4.5). Note that the plasma rotates only in the region $\rho \cong 0.1$ with a significant velocity, since the Lorentz force $-J_\rho B_o$ decreases rapidly with increasing $\rho \to 1$.

iii) *Anode Region*, $\zeta = +0.99$: The Figures 4.11-4.15 present $V(\rho,+0.99)$, $[B(\rho,+0.99) - R\rho]/R$, $E_\rho(\rho,+0.99)$, $J_\rho(\rho,+0.99)$, $J_\zeta(\rho,+0.99) \propto E_\zeta(\rho,+0.99)$ versus $0 \leq \rho \leq 1$ for $H = 1, 10, 100$. The velocity field is fully developed nearly through the entire centrifuge across section $0 < \rho \lesssim 0.9$, since the Lorentz force $-J_\rho B_o$ is strongest in the vicinity

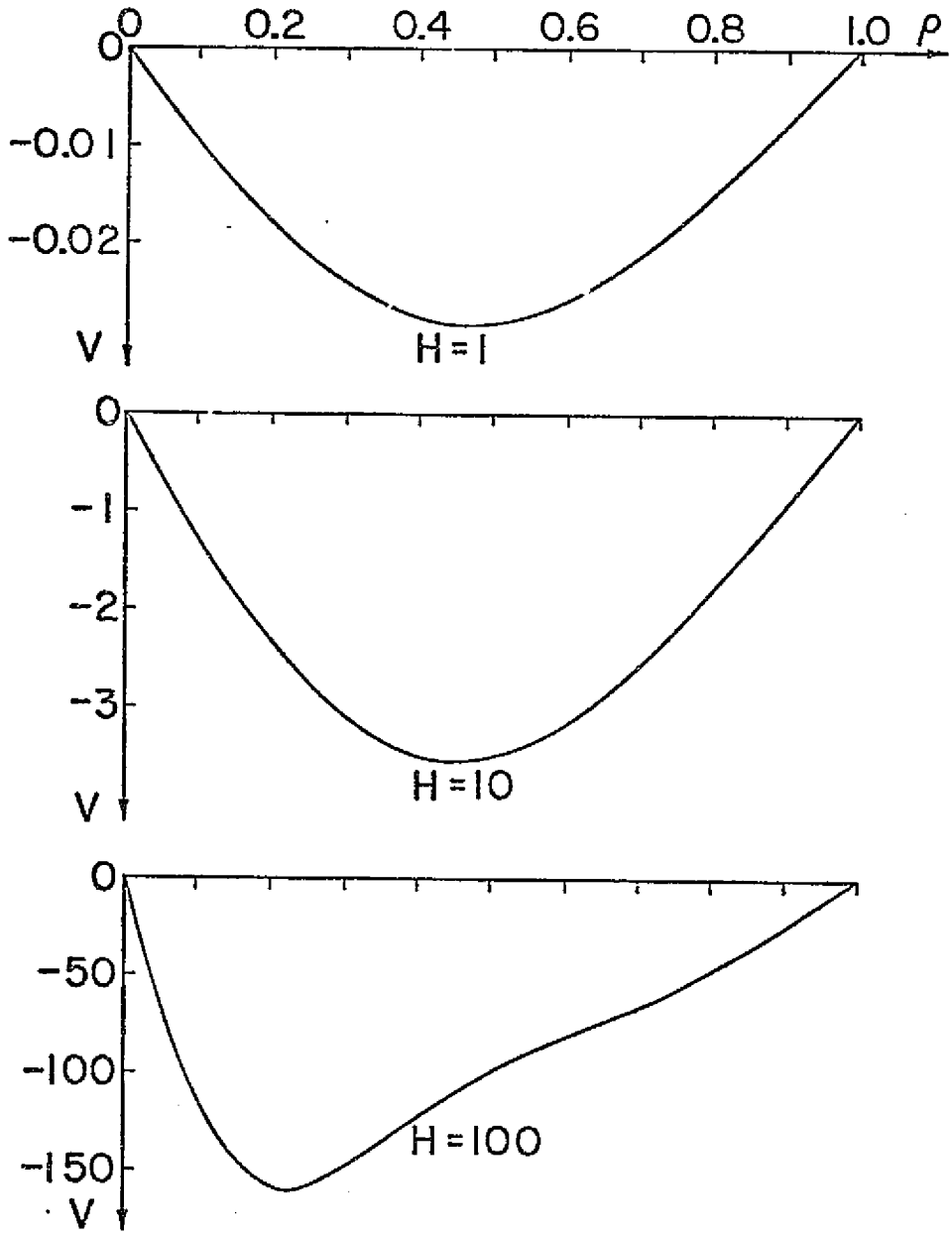

Fig. 4.1. $V(\rho,\zeta)$ versus ρ for $\zeta = 0$, and $H = 1, 10, 100$.

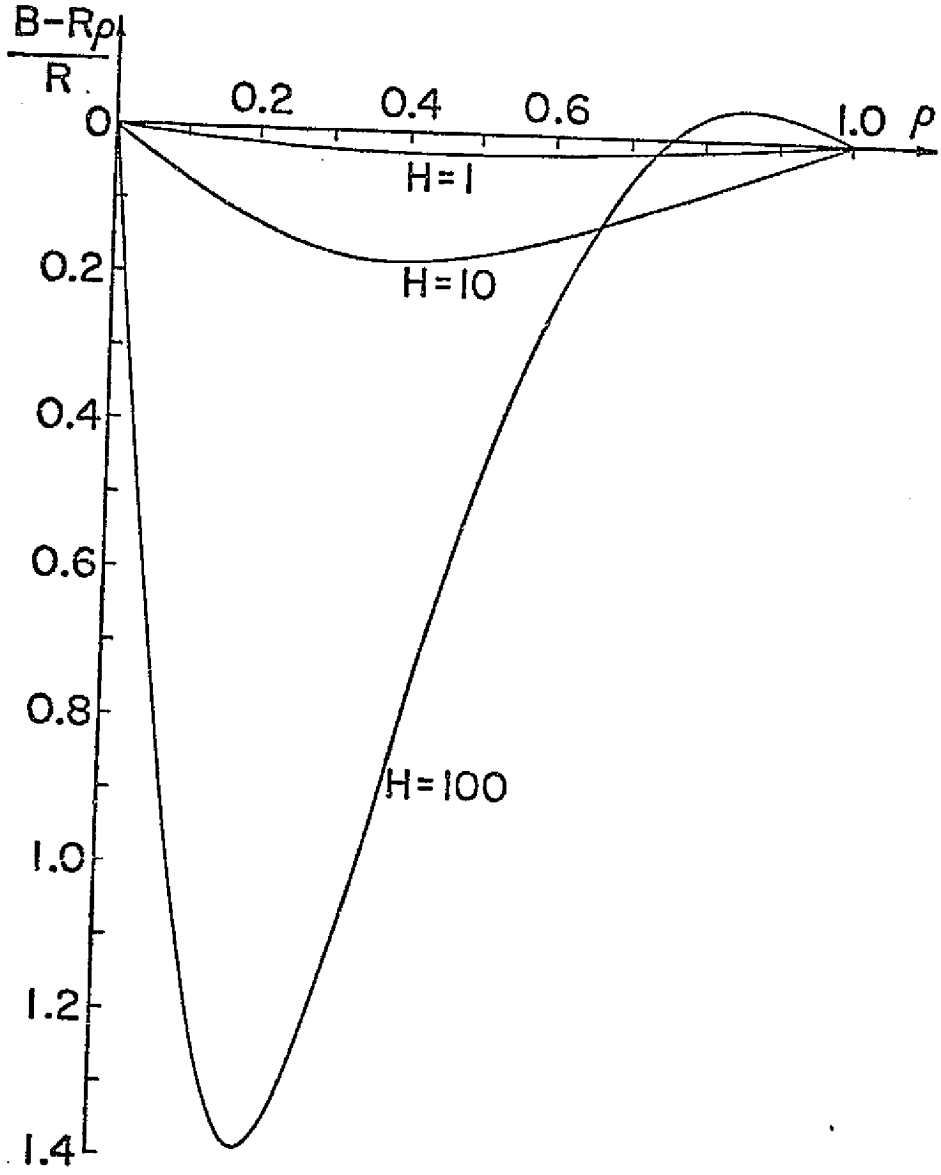

Fig. 4.2. $[B(\rho,\zeta)-R\rho]/R$ versus ρ for $\zeta = 0$, and $H = 1, 10, 100$.

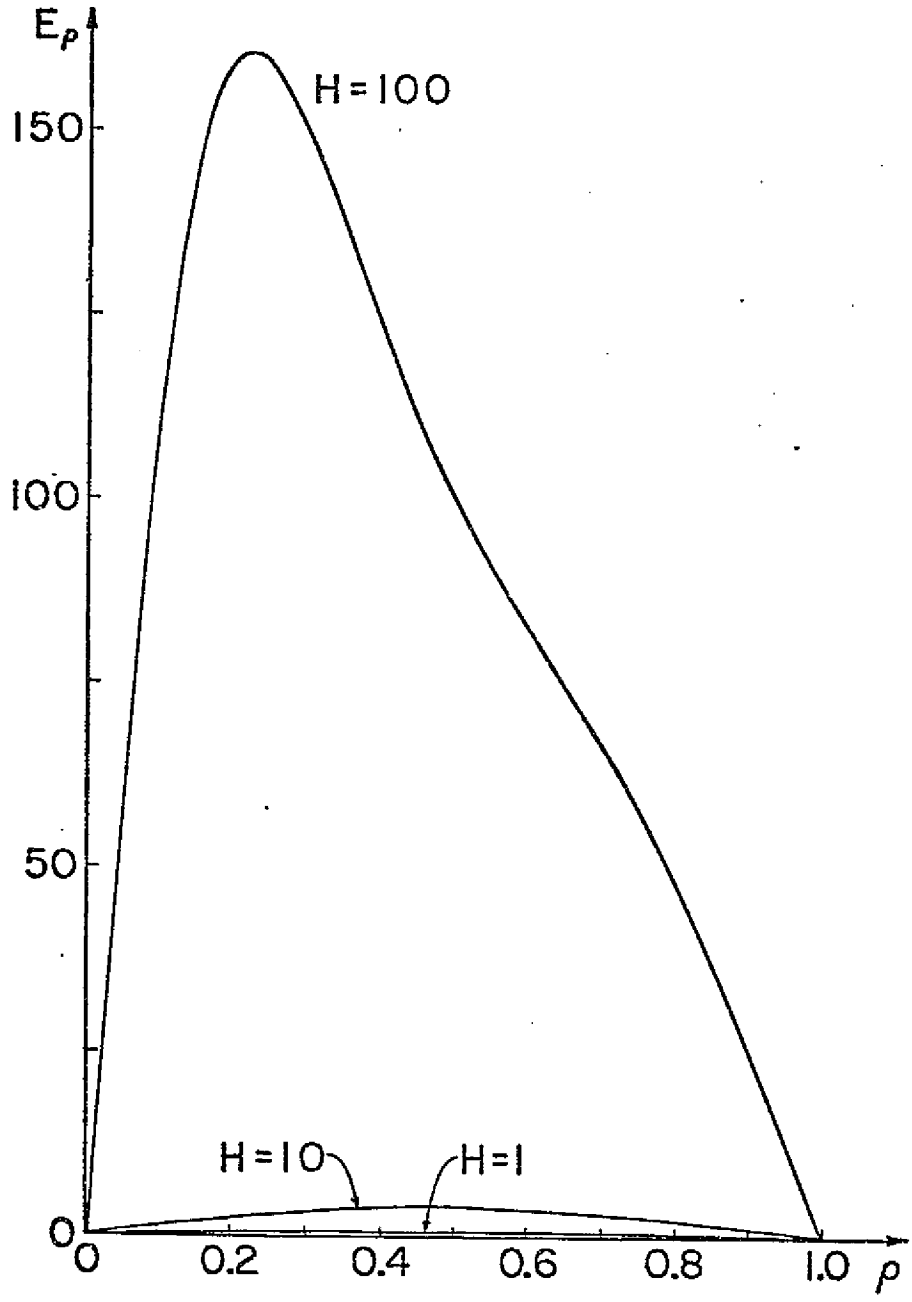

Fig. 4.3. $E_\rho(\rho,\zeta)$ versus ρ for $\zeta = 0$, and $H = 1, 10, 100$.

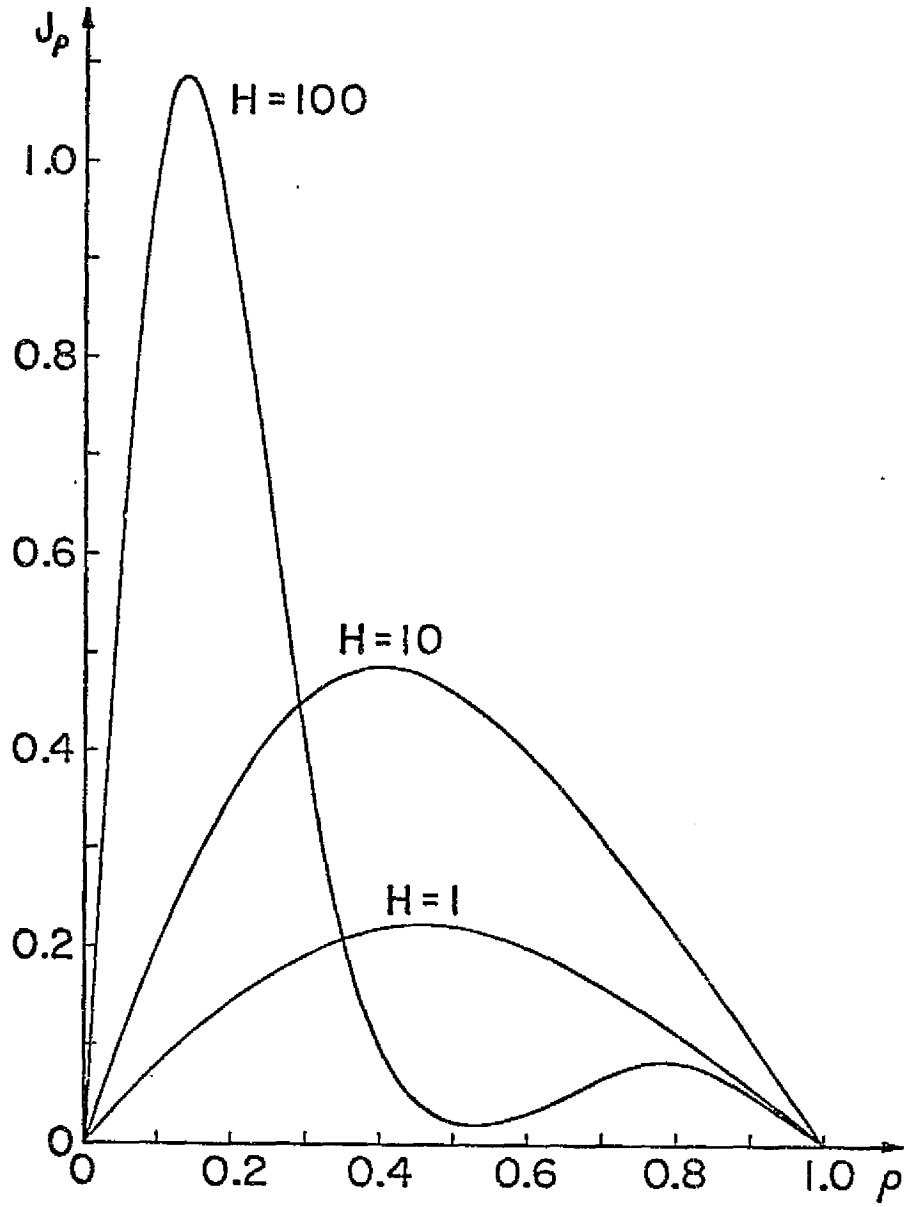

Fig. 4.4. $J_\rho(\rho,\zeta)$ versus ρ for $\zeta = 0$, and $H = 1, 10, 100$.

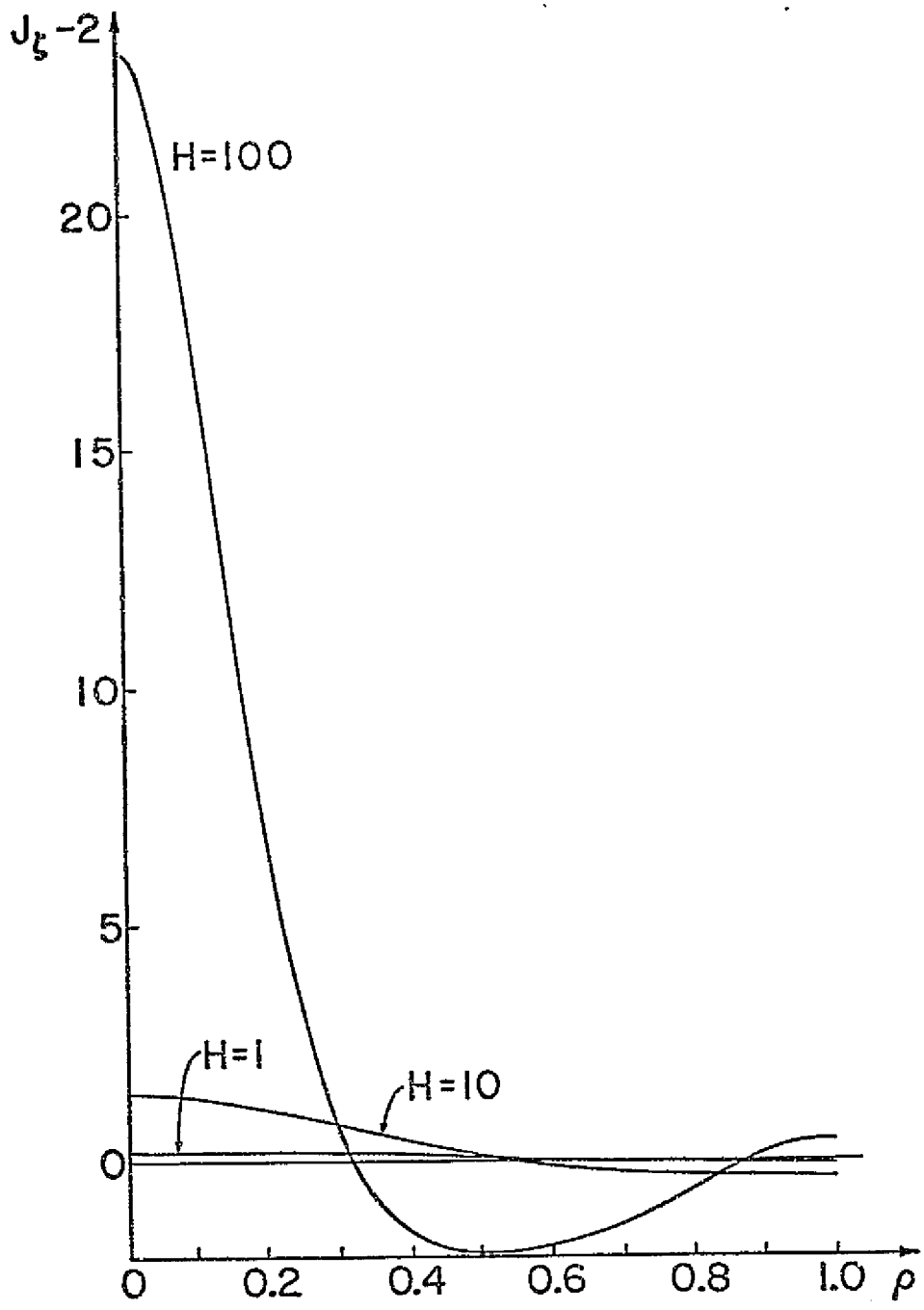

Fig. 4.5. $J_\zeta(\rho,\zeta)-2$ versus ρ for $\zeta = 0$, and $H = 1, 10, 100$.

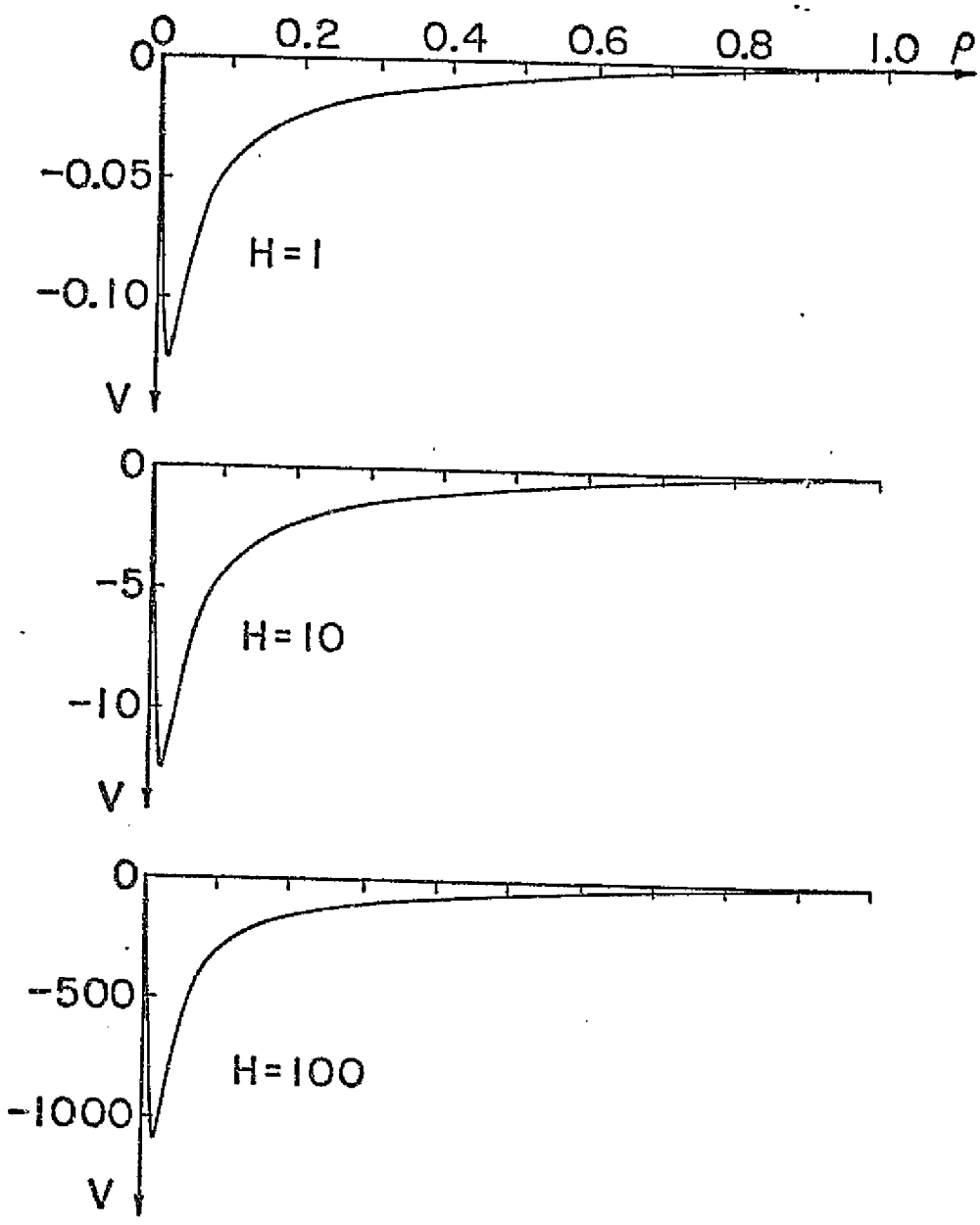

Fig. 4.6. $V(\rho,\zeta)$ versus ρ for $\zeta = -0.99$, and $H = 1, 10, 100$.

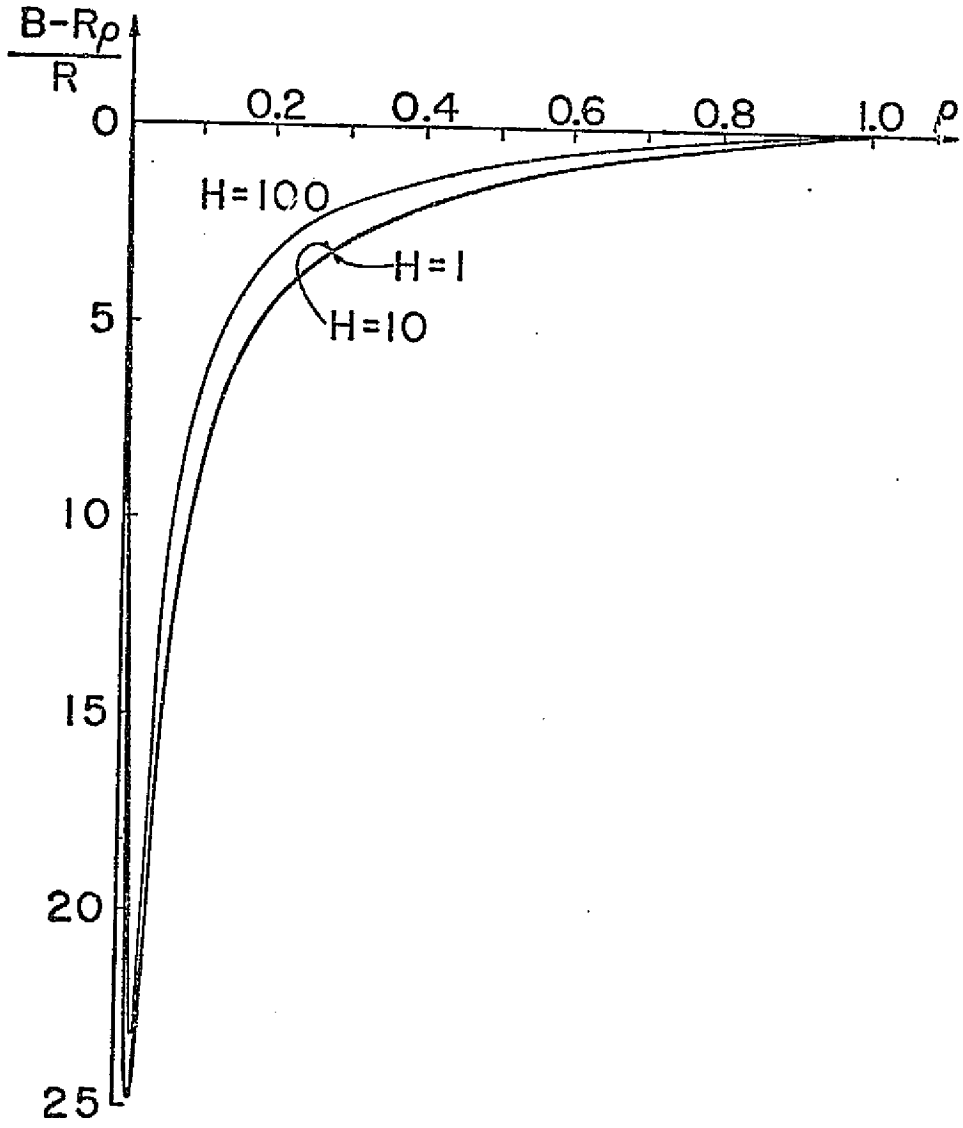

Fig. 4.7. $[B(\rho,\zeta)-R\rho]/R$ versus ρ for $\zeta = -0.99$, and $H = 1, 10, 100$.

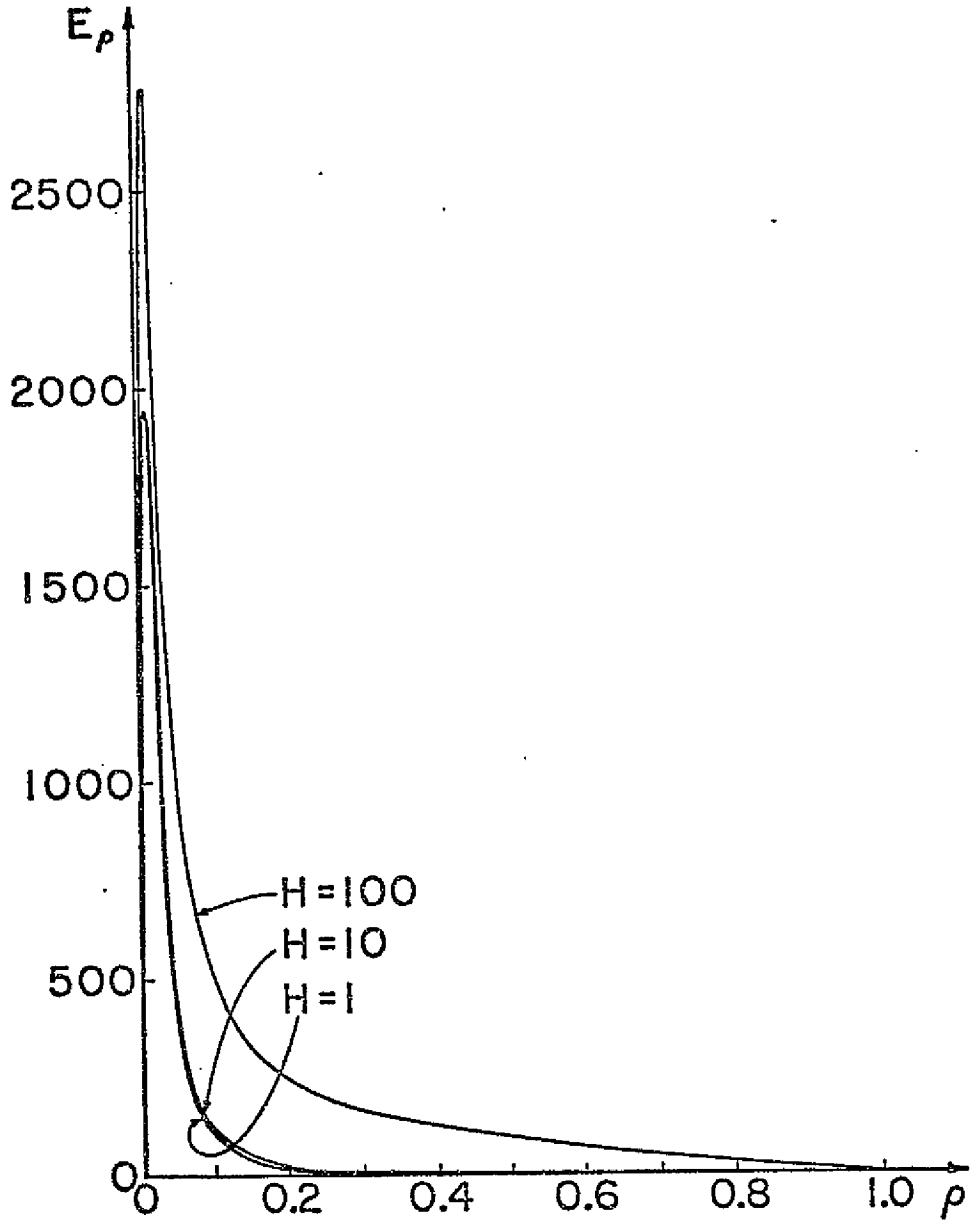

Fig. 4.8. $E_\rho(\rho,\zeta)$ versus ρ for $\zeta = -0.99$, and $H = 1, 10, 100$.

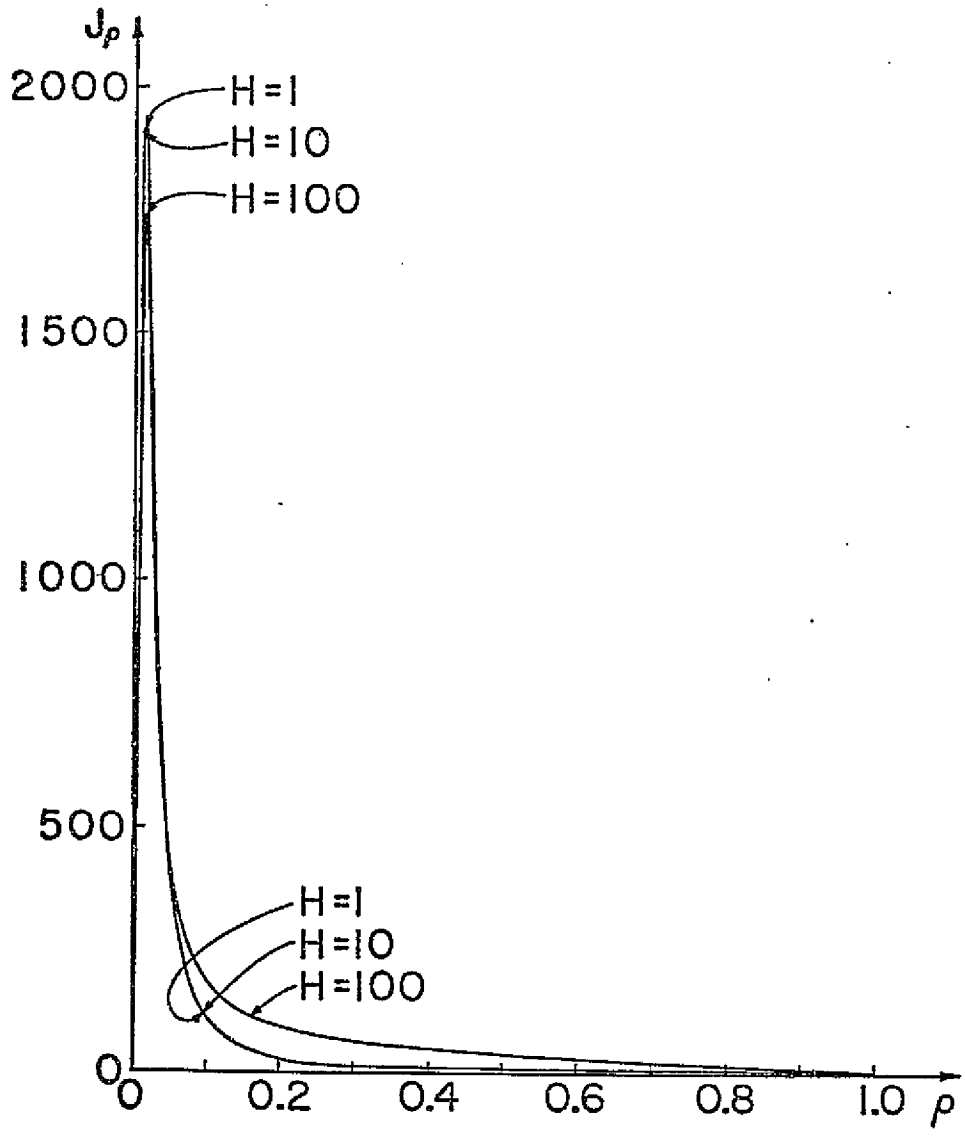

Fig. 4.9. $J_\rho(\rho,\zeta)$ versus ρ for $\zeta = -0.99$, and $H = 1, 10, 100$.

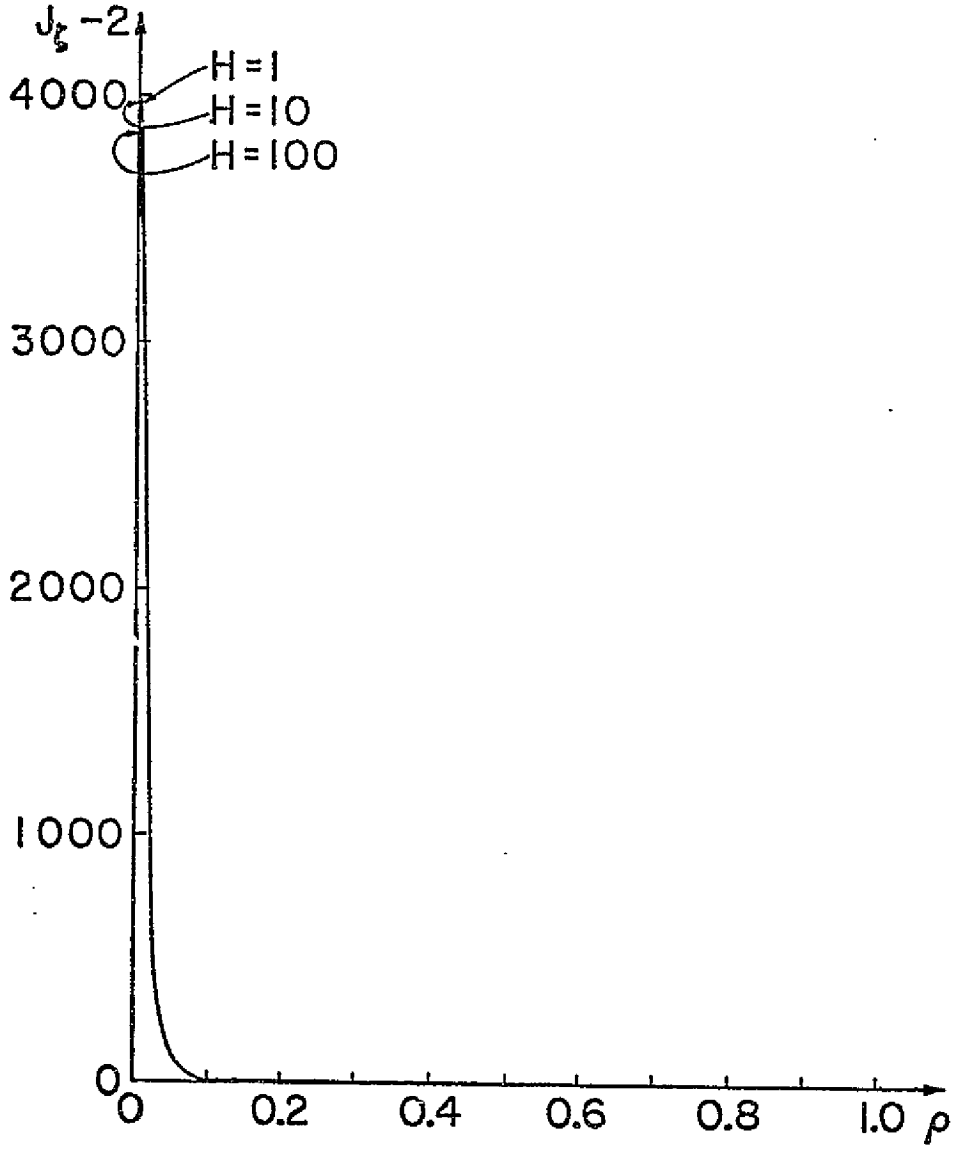

Fig. 4.10. $J_\zeta(\rho,\zeta)-2$ versus ρ for $\zeta = -0.99$, and $H = 1, 10, 100$.

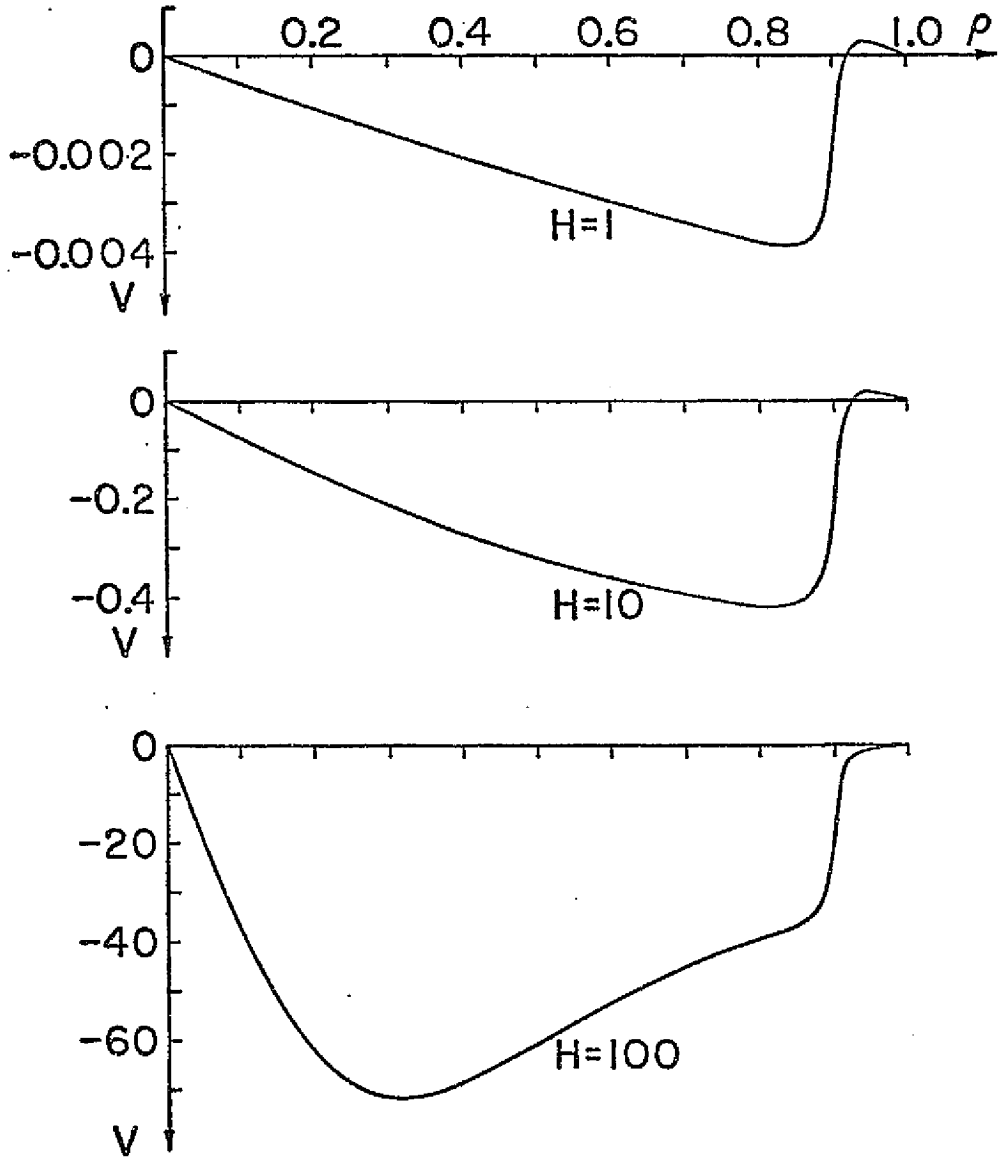

Fig. 4.11. $V(\rho,\zeta)$ versus ρ for $\zeta = +0.99$, and $H = 1, 10, 100$.

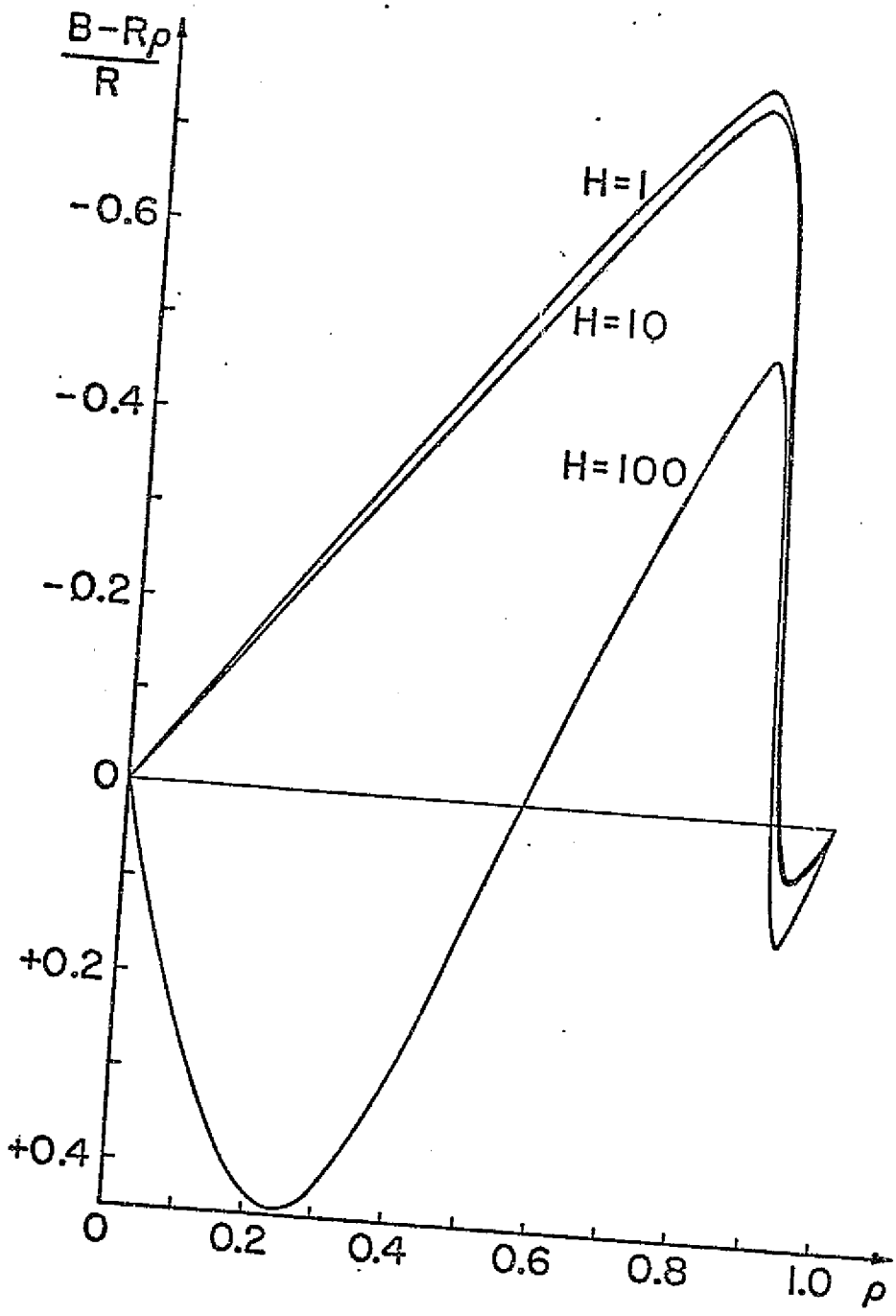

Fig. 4.12. $[B(\rho,\zeta)-R\rho]/R$ versus ρ for $\zeta = +0.99$, and $H = 1, 10, 100$.

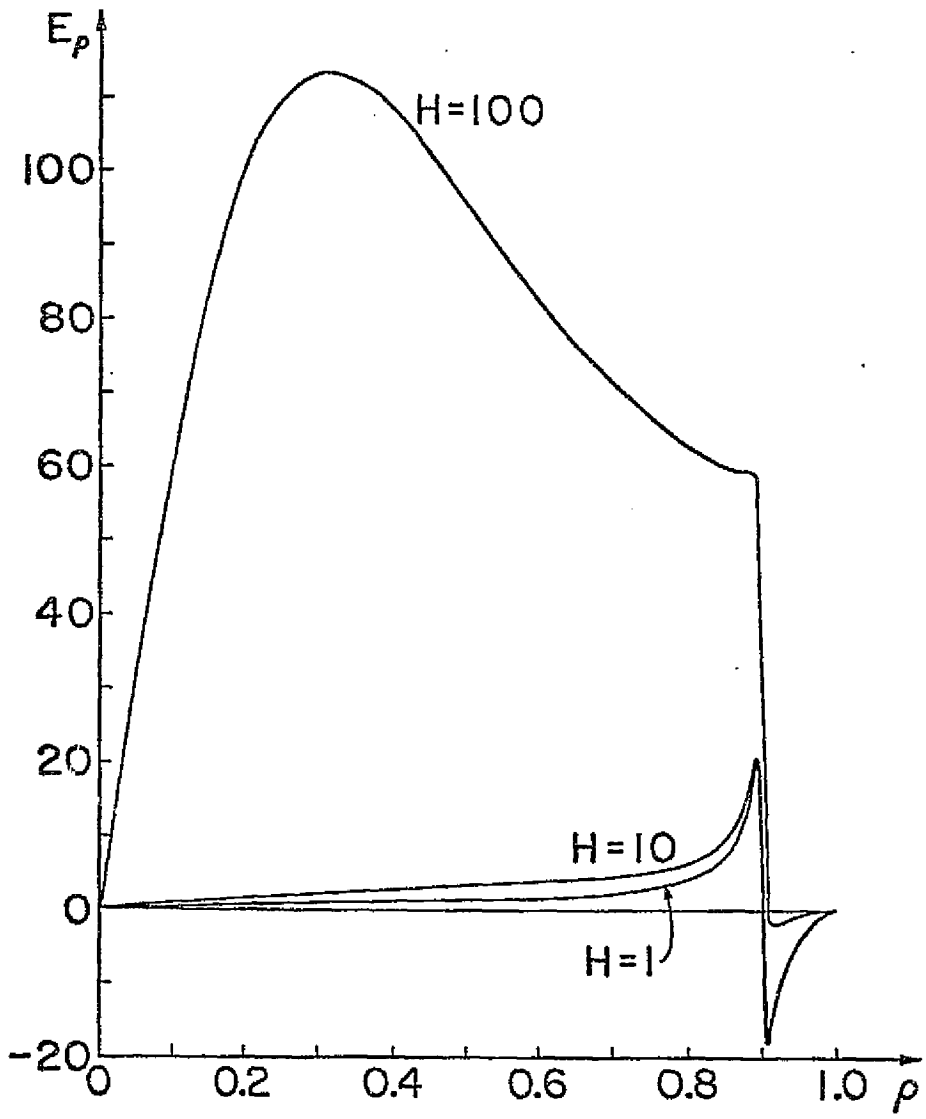

Fig. 4.13. $E_\rho(\rho,\zeta)$ versus ρ for $\zeta = +0.99$, and H = 1, 10, 100.

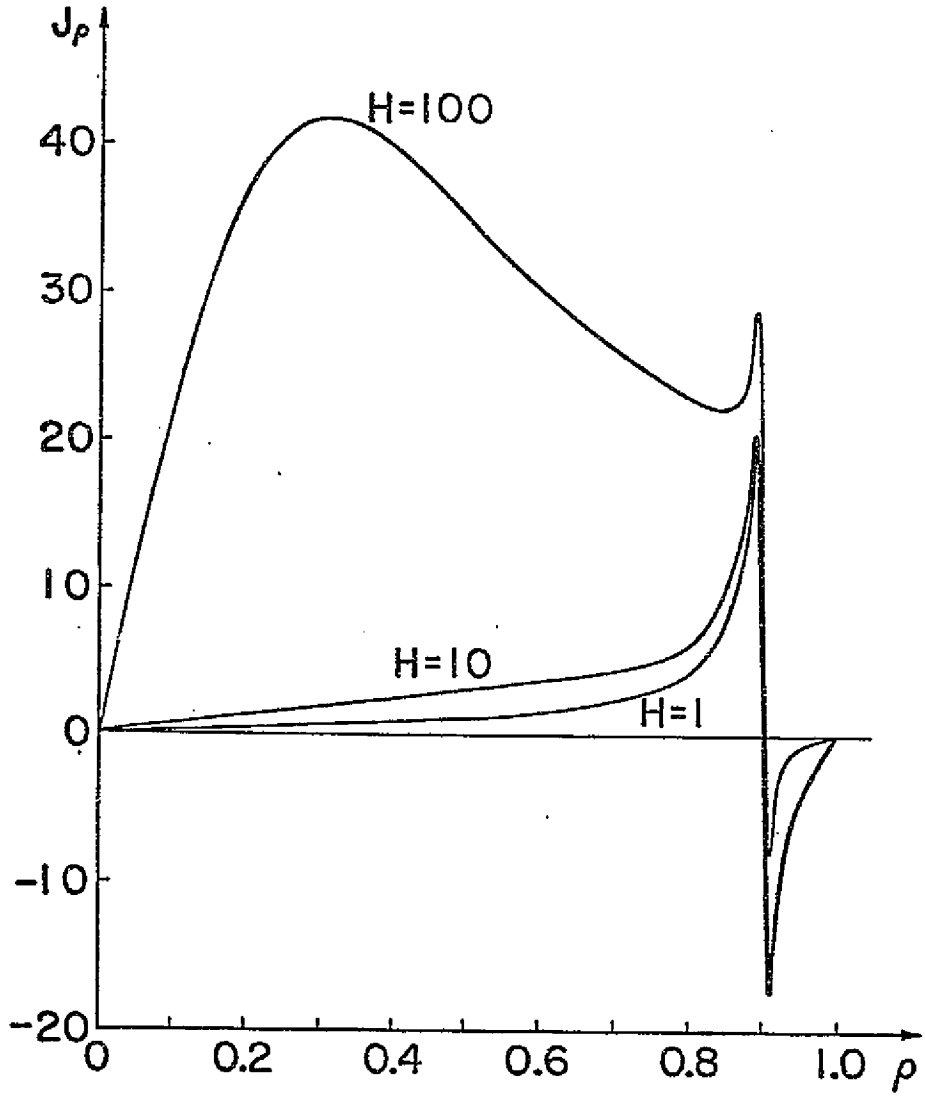

Fig. 4.14. $J_\rho(\rho,\zeta)$ versus ρ for $\zeta = +0.99$, and $H = 1, 10, 100$.

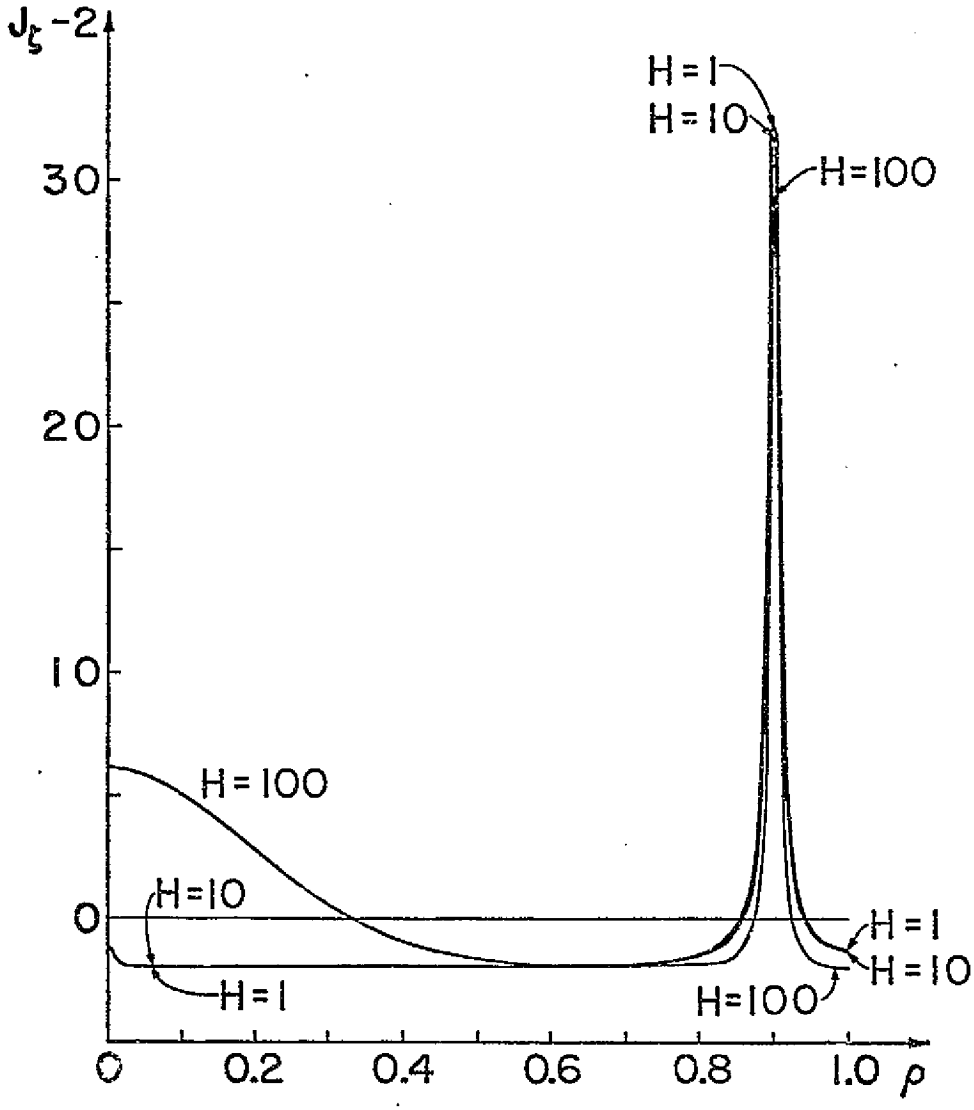

Fig. 4.15. $J_\zeta(\rho,\zeta)-2$ versus ρ for $\zeta = +0.99$, and $H = 1, 10, 100$.

$\rho \cong 0.9$ of the ring anode $\rho_+ = 0.9(\zeta = +1)$. As a result, a thin and steep boundary layer exists close to the cylinder wall ($\rho = 1$) with plasma counter-rotation at sufficiently small H-values. The radial distributions of B, $E_{\rho,\zeta}$, $J_{\rho,\zeta}$ clearly indicate that, in the plane $\zeta = +0.99$, the electrical discharge has shifted to the region $\rho \cong 0.9$ due to the influence of the (nearby) ring anode at $\rho_+ = 0.9(\zeta = +1)$.

In the graphical illustrations, the cathode radius R_- was chosen to be small compared to the anode radius R_+ to ensure a large angle between the current field lines $\vec{J}(\vec{r})$ and the external magnetic field $\vec{B}_o$, i.e., a significant Lorentz force. A comparison of the Figures 4.1 and 4.6 with Figure 4.11 indicates that this choice of electrode radii results in a radial boundary layer of large width and low velocity in the lower half $-c \leq z \leq 0$ of the centrifuge. Hence, $R_- << R_+$ (or $R_- >> R_+$) is not the best choice for a centrifuge of maximum efficiency. Figure 4.11 demonstrates that a velocity profile rising uniformly with radius r and decreasing rapidly in a steep boundary layer of narrow width Δr, is obtained by using a cathode and an anode of the same radius $R_- = R_+ \lesssim R_o$, which is nearly as large as the centrifuge radius R_o. Although $R_- = R_+$ in this case, the current field lines $\vec{J}(\vec{r})$ intersect with $\vec{B}_o$ at a sufficiently large angle $\measuredangle(\vec{J},\vec{B}_o) \neq 0$ due to the repulsion of the current filaments. As a result, a net Lorentz torque results for a centrifuge with $R_- = R_+$ which is still of the same order of magnitude as for a centrifuge with $R_- << R_+$ (presuming that I, and B_o, c, and R_o are the same).

The centrifuge analysis presented indicates that extremely high speeds of plasma rotation are obtainable as shown in Chapter III at moderate discharge currents I and magnetic inductions B_o, presuming the

Hartmann number H is not small, $H > 1$. As an example, consider an isotope centrifuge discharge with the same values of $|I|$, $|B_o|$, σ, R_o and c as those in Chapter III.

Hence, by Equation (4.12)

$$V_o = I/2\pi R_o B_o \sigma c = (5/\pi) \times 10^1 \text{ m/sec},$$

and, by Figure 4.1

$$O[V_\theta] = O[V_o V] = 10^3 \text{ m/sec, for } H = 100.$$

Based on these examples, one can assume with some confidence that high-power plasma centrifuges are technically realizable employing dense, collision-dominated isotope plasmas. The proposed high-density plasma centrifuge would use arc plasmas at pressures of about one atmosphere so that the isotope masses separated are increased by orders of magnitude. The large Hartmann numbers $H = (\sigma/\mu)^{\frac{1}{2}} B_o R_o$ required for high speeds of isotope rotation are achievable because of the (relative) small viscosity μ and large conductivity σ of gaseous plasmas. Speeds of plasma rotation, which are by an order-of-magnitude larger than those in the above examples, can be achieved at realistic Hartmann numbers H. Since $\omega = 1.76 \times 10^{11}$ B sec., the Hall-effect is insignificant in dense plasmas for B = 1 Tesla as long as $\tau < 10^{-12}$ sec. In general, the Hall-effect increases the speed of plasma rotation for $\omega\tau > 1$, i.e., in plasmas of lower density as shown in Chapter III. In developing a plasma centrifuge, therefore, apparently a trade-off between isotope density and rotation velocity has to be made.

CHAPTER V

PLASMA COUNTER-ROTATION IN MULTI-DISCHARGE CENTRIFUGE

This chapter is concerned with a plasma centrifuge between two ring electrodes embedded in the mantle of a cylindrical chamber, in which the plasma in the anode and cathode regions rotates in opposite directions under the influence of a spatially converging and diverging current density and an external axial magnetic field. The associated boundary-value problem for the coupled partial differential equations describing the azimuthal velocity and radial current density fields is solved in closed form. The difficulties associated with the complex, inhomogeneous boundary conditions are overcome by means of Fourier expansions for Bessel functions of complex argument. The velocity, current density, induced magnetic induction, and electric fields are presented for typical Hartmann numbers, magnetic Reynolds numbers, and geometry parameters. The discharge is shown to produce anodic and cathodic plasma sections rotating at speeds of the order 10^4 m/sec for conventional magnetic field intensities. Possible application of the magnetoactive discharge as a multi-discharge plasma centrifuge for isotope separation is discussed.

5.1. Model for Multi-discharge Centrifuge

The plasma centrifuge to be studied herein exhibits the interesting effect of plasma counter-rotation, i.e., the plasma in the anodic

and cathodic half-spaces rotates in opposite directions. As depicted schematically in Figure 5.1, the centrifuge system consists of an electrically insulating cylindrical chamber of radius R_o with end walls at $z=\pm L$. A perfectly conducting ring anode ($r=R_o$, $z=-c$) and ring cathode ($r=R_o$, $z=+c$) are embedded in the cylinder R_o (eventually in form of thin, "hollow" slit electrodes). The electrodes are placed far from the end walls ($c \ll L$) to reduce velocity losses due to the end plates. The plasma is produced in the space $-c \leq z \leq +c$, $0 \leq r \leq R_o$ through a gaseous discharge resulting in a curved current density distribution $\vec{J}(r,z)$ which intersects the axial, homogeneous magnetic field B_o applied from outside. The $\vec{J} \times \vec{B}_o$ force rotates the plasma counter-clockwise in the anode region $-c \leq z < 0$ and clockwise in the cathode region $0 < z \leq +c$ (Fig. 5.1), since the $\vec{J}$-lines converge for $z < 0$ and diverge for $z > 0$. In the central plane $z=0$, the plasma is at rest.

The purpose of the investigation is to evaluate theoretically the electromagnetogasdynamics of plasma counter-rotation as a contribution to the physics of plasma centrifuges. Furthermore, it appears that this type of centrifuge might be useful for isotope separation, in which the heavy isotope would be enriched in the anodic and cathodic "layers" $z = \pm c$ and the light isotope would be enriched in the central layer $z = 0$. The end spaces $-L \leq z < -c$ and $+c < z \leq +L$ would serve as reservoirs for the unseparated isotope mixture. For a proper choice of the geometry parameters, R_o, c, and L, well-developed azimuthal velocity distributions can be expected. In view of the circumferential electrode arrangement, a large number of such centrifuges can be set up in a long insulating cylinder to rotate large volumes of isotope mixtures, as

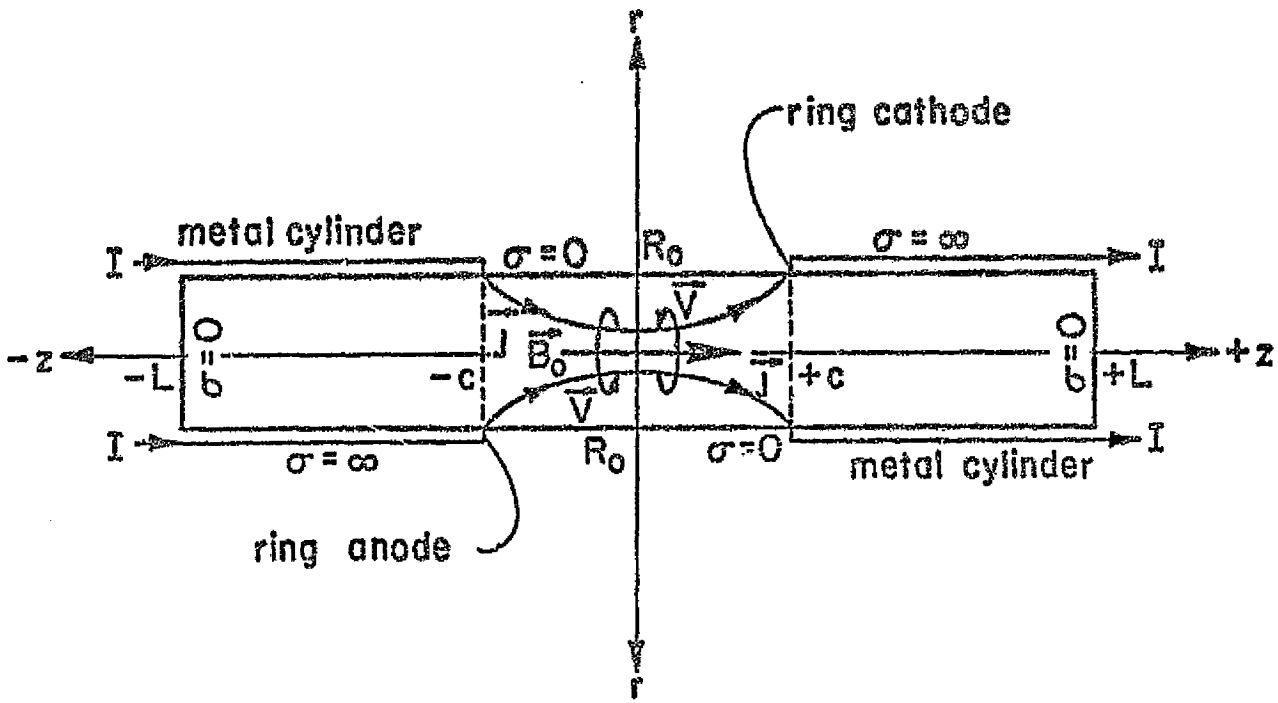

Fig. 5.1. Counter-rotating plasma centrifuge model of radius R_o and length 2L with ring anode ($r=R_o$, $z=-c$), ring cathode ($r=R_o$, $z=+c$), and axial magnetic field B_o ($c \ll L$).

shown schematically in Figure 5.2. Each circumferential cathode or anode serves as a common electrode for the adjacent discharges. It is seen that the volume of rotating plasma is nearly doubled in each electrode region, compared to the single discharge centrifuge.

ORIGINAL PAGE IS
OF POOR QUALITY

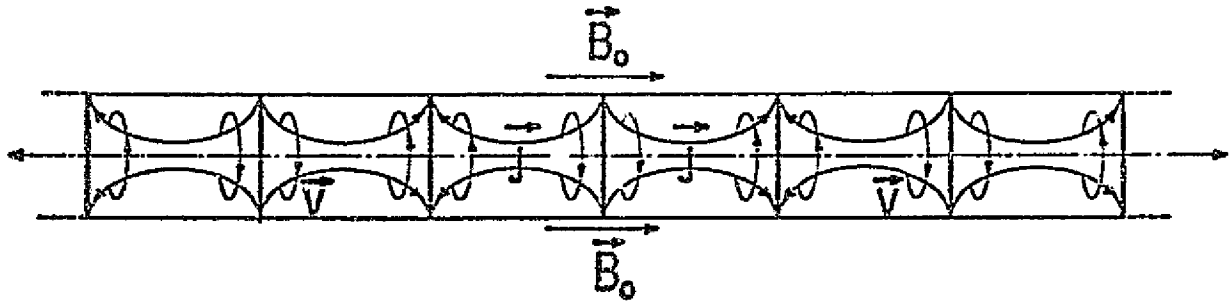

Fig. 5.2. Scheme of multi-discharge centrifuge.

5.2. Boundary-value Problem for Velocity and Radial Current Density

The steady-state rotation of the plasma centrifuge shown in Figure 5.1 is theoretically investigated based on the magnetogasdynamic equations (Section 2.1) for dense plasmas. Laminar flow is assumed and (conceivable) secondary flows superimposed on the main rotational flow are disregarded. Experiments indicate secondary flows in the motion of incompressible fluids between rotating cylinders (Chandrasekhar 1961), but secondary flows have not been observed in plasmas which rotate under the influence of electromagnetic forces. In view of the symmetry of the centrifuge configuration with respect to z-axis, the plasma flow field is then azimuthal, $\vec{V} = \{0, V_\theta(r,z), 0\}$, so that the plasma behaves

incompressible ($\nabla\cdot\vec{V}=0$). It is assumed that the gyration frequency ω of the electrons is much smaller than the collision frequency τ^{-1} between electrons and plasma particles ($\omega\tau<<1$). In this case, the current density is of the form $\vec{J} = \{J_r(r,z), 0, J_z(r,z)\}$, and the Hall-effect is negligible (dense plasmas of low ionization degrees). The magnetic induction is of the form $\vec{B} = \{0, B_\theta(r,z), B_o\}$ in accordance with Maxwell's equations and the homogeneous boundary conditions for B_r and B_z.

The counter-rotating plasma centrifuge is described by the boundary-value problem for the azimuthal velocity $V_\theta(r,z)$ and radial current density $J_r(r,z)$ fields:

$$\frac{\partial}{\partial r}[\frac{1}{r}\frac{\partial}{\partial r}(rV_\theta)] + \frac{\partial^2 V_\theta}{\partial z^2} = \frac{B_o}{\mu} J_r \quad , \tag{5.1}$$

$$\frac{\partial}{\partial r}[\frac{1}{r}\frac{\partial}{\partial r}(rJ_j)] + \frac{\partial^2 J_r}{\partial z^2} = \sigma B_o \frac{\partial^2 V}{\partial z^2} \quad , \tag{5.2}$$

where

$$V_\theta(r,z)_{r=R_o} = 0, \quad -L \leq z \leq +L \quad , \tag{5.3}$$

$$V_\theta(r,z)_{z=\pm L} = 0, \quad 0 \leq r \leq R_o \quad , \tag{5.4}$$

and

$$J_r(r,z)_{r=R_o} = \frac{I}{2\pi R_o}[\delta(z-c) - \delta(z+c)], \quad -L \leq z \leq +L \quad , \tag{5.5}$$

$$J_r(r,z)_{z=\pm L} = 0, \quad 0 \leq r \leq R_o \quad . \tag{5.6}$$

Equations (5.1) and (5.2) are the azimuthal component of the equation of plasma motion and the induction equation combined with

$\nabla \times \vec{B} = \mu_o \vec{J}$ and $\nabla \cdot \vec{J} = 0$, respectively. The boundary conditions (5.3) and (5.4) specify that the plasma does not slip at the chamber walls $r = R_o$ and $z = \pm L$. The boundary conditions (5.5) imply that a total discharge current I flows from the ring anode ($z = -c$) to the ring cathode ($z = +c$) of vanishing axial width, $\Delta z \to 0$. The boundary conditions (5.6) consider that no radial current flows at the end plates at $z = \pm L$ according to Ohm's law, $J_r = \sigma(E_r + V_\theta B_o)$, since $V_\theta(r,z)_{z=\pm L} = 0$ and $E_r(r,z)_{z=\pm L} = 0$ by $\vec{n} \times [\vec{E}] = \vec{0}$.

The remaining centrifuge fields are consecutively determined by using the solutions for $V_\theta(r,z)$ and $J_r(r,z)$. The axial current density $J_z(r,z)$ is obtained by the conservation equation for the electric charge density ($\nabla \cdot \vec{J} = 0$):

$$J_z(r,z) = -\int^z [\frac{1}{r}\frac{\partial}{\partial r}(rJ_r)]dz + c_1(r) \ , \tag{5.7}$$

where the integration constant $c_1(r)$ is determined by the boundary conditions (no axial current flows into end walls),

$$J_z(r,z)_{z=\pm L} = 0, \quad 0 \le r \le R_o \ . \tag{5.8}$$

The induced magnetic field $B_\theta(r,z)$ is obtained from the z-component of Maxwell's equation, $\nabla \times \vec{B} = \mu_o \vec{J}$:

$$B_\theta(r,z) = \frac{1}{r}[\mu_o \int^r J_z r dr + c_2(z)], \tag{5.9}$$

where the integration constant $c_2(z)$ is determined by the boundary conditions [equivalent to the boundary conditions (5.5) since $-\partial B_\theta/\partial z = \mu_o J_r$, $H(c-|z|)$ = Heaviside step function],

$$B_\theta(r,z)_{r=R_o} = \frac{\mu_o I}{2\pi R_o} H(c-|z|), \qquad -L \le z \le +L \ . \tag{5.10}$$

The electric field $\vec{E}(r,z)$ is given by Ohm's law:

$$\vec{E}(r,z) = \{J_r/\sigma - B_o V_\theta,\ 0,\ J_z/\sigma\} \quad . \tag{5.11}$$

Finally, the pressure distribution can be calculated from the r- and z-component of the equation of motion [Eq. (2.1)] of the plasma if desired.

5.3. Fourier Series Solutions in Terms of Bessel Functions of Complex Arguments

In order to solve analytically the boundary-value problem for the coupled plasma fields $V_\theta(r,z)$ and $J_r(r,z)$, it is convenient to formulate Equations (5.1)-(5.6) in dimensionless form by introducing dimensionless independent and dependent variables,

$$\rho = r/R_o, \quad 0 \leq \rho \leq 1 \ , \tag{5.12}$$

$$\zeta = z/c, \quad -L \leq \zeta \leq +L, \qquad L \equiv L/c \ , \tag{5.13}$$

and

$$V(\rho,\zeta) = V_\theta(r,z)/V_o, \quad J_\rho(\rho,\zeta) = J_r(r,z)/J_o \ , \tag{5.14}$$

where the reference values V_o and J_o are defined as

$$V_o \equiv I/2\pi R_o c B_o \sigma, \quad J_o \equiv \sigma v_o B_o = I/2\pi R_o c \quad . \tag{5.15}$$

Thus, the boundary-value problem defined in Equations (5.1)-(5.6) becomes for $V(\rho,\zeta)$ and $J_\rho(\rho,\zeta)$:

$$\frac{\partial}{\partial\rho}\left[\frac{1}{\rho}\frac{\partial}{\partial\rho}(\rho V)\right] + N^{-2}\frac{\partial^2 V}{\partial\zeta^2} = H^2 J_\rho \ , \tag{5.16}$$

$$\frac{\partial}{\partial\rho}\left[\frac{1}{\rho}\frac{\partial}{\partial\rho}(\rho J_\rho)\right] + N^{-2}\frac{\partial^2 J_\rho}{\partial\zeta^2} = N^{-2}\frac{\partial^2 V}{\partial\zeta^2} \ , \tag{5.17}$$

where

$$V(\rho,\zeta)_{\rho=1} = 0, \quad -L \leq \zeta \leq +L \ , \tag{5.18}$$

$$V(\rho,\zeta)_{\zeta=\pm L} = 0, \quad 0 \leq \rho \leq 1 \ , \tag{5.19}$$

$$J_\rho(\rho,\zeta)_{\rho=1} = -\delta(\zeta+1) + \delta(\zeta-1), \quad -L \leq \zeta \leq +L \ , \tag{5.20}$$

$$J_\rho(\rho,\zeta)_{\zeta=\pm L} = 0, \quad 0 \leq \rho \leq 1. \tag{5.21}$$

The dimensionless parameters N and H are defined by

$$N \equiv c/R_o, \quad H \equiv (\sigma/\mu)^{\frac{1}{2}} B_o R_o \ . \tag{5.22}$$

In view of symmetric geometry of the centrifuge configuration and asymmetric boundary conditions (5.20) and (5.21), $J_\rho(\rho,\zeta)$ is asymmetric about $\zeta = 0$, i.e., $J_\rho(\rho,\zeta) = -J_\rho(\rho,-\zeta)$. Accordingly, the radial current densities at $(r, \pm z)$ have opposite directions, but same magnitudes. Consequently, as a result of the radial current densities normal to an axially applied magnetic field, the Lorentz forces set the plasma in rotation with an azimuthal velocity field which is also asymmetric, i.e., $V(\rho,\zeta) = -V(\rho,-\zeta)$.

In accordance with the above conclusions and the boundary conditions (5.18)-(5.21), the general solutions of the coupled partial differential equations (5.16) and (5.17) are sought in the form of the Fourier series:

$$V(\rho,\zeta) = \sum_{n=1}^{\infty} f_n(\rho)\sin\lambda_n\zeta, \tag{5.23}$$

$$J_\rho(\rho,\zeta) = \sum_{n=1}^{\infty} g_n(\rho)\sin\lambda_n\zeta, \tag{5.24}$$

where

$$\lambda_n = n\pi/L. \tag{5.25}$$

The ρ-dependent functions $f_n(\rho)$ and $g_n(\rho)$ are determined by the following coupled ordinary differential equations and boundary conditions:

$$\frac{d}{d\rho}\left[\frac{1}{\rho}\frac{d}{d\rho}(\rho f_n)\right] - \left(\frac{\lambda_n}{N}\right)^2 f_n = H^2 g_n, \tag{5.26}$$

$$\frac{d}{d\rho}\left[\frac{1}{\rho}\frac{d}{d\rho}(\rho g_n)\right] - \left(\frac{\lambda_n}{N}\right)^2 g_n = -\left(\frac{\lambda_n}{N}\right)^2 f_n, \tag{5.27}$$

[illegible] a Fourier sine series in the interval $-L \leq \zeta \leq +L$.

$$-\delta(\zeta+1) + \delta(\zeta-1) = (2/L) \sum_{n=1}^{\infty} \sin\lambda_n \sin\lambda_n\zeta. \tag{5.30}$$

By elimination, Equations (5.26) and (5.27) are reduced to decoupled differential equations of fourth order,

$$\left\{\frac{d}{d\rho}\left[\frac{1}{\rho}\frac{d}{d\rho}(\rho)\right] - \left(\frac{\lambda_n}{N}\right)^2\right\}^2 f_n = -\left(\frac{H\lambda_n}{N}\right)^2 f_n , \tag{5.31}$$

$$\left\{\frac{d}{d\rho}\left[\frac{1}{\rho}\frac{d}{d\rho}(\rho)\right] - \left(\frac{\lambda_n}{N}\right)^2\right\}^2 g_n = -\left(\frac{H\lambda_n}{N}\right)^2 g_n . \tag{5.32}$$

The general solutions for $f_n(\rho)$ and $g_n(\rho)$ of the identical biharmonic equations (5.31) and (5.32) are

$$f_n(\rho) = A_n J_1(\kappa_n\rho) + B_n J_1(\kappa_n^*\rho) , \tag{5.33}$$

$$g_n(\rho) = C_n J_1(\kappa_n\rho) + D_n J_1(\kappa_n^*\rho) , \tag{5.34}$$

where A_n, B_n, C_n and D_n are integration constants. $J_1(\kappa_n\rho)$ and $J_1(\kappa_n^*\rho)$ are complex conjugate Bessel functions of the first kind of order 1, since κ_n and κ_n^* are complex conjugate eigenvalues given by

$$\begin{aligned} \kappa_n &= \left[\frac{\lambda_n}{N}\left(-\frac{\lambda_n}{N} + iH\right)\right]^{\frac{1}{2}} = \xi e^{+i\phi} , \\ \kappa_n^* &= \left[\frac{\lambda_n}{N}\left(-\frac{\lambda_n}{N} - iH\right)\right]^{\frac{1}{2}} = \xi e^{-i\phi} , \end{aligned} \tag{5.35}$$

ORIGINAL PAGE IS
OF POOR QUALITY

where

$$\xi = [\frac{\lambda_n}{N}(\frac{\lambda_n}{N^2} + H^2)^{\frac{1}{2}}]^{\frac{1}{2}} \quad , \tag{5.36}$$

$$\phi = \tfrac{1}{2} \arccos[\frac{-\lambda_n}{N(\lambda_n^2/N^2+H^2)^{\frac{1}{2}}}] = \tfrac{1}{2} \arcsin[\frac{H}{(\lambda_n^2/N^2+H^2)^{\frac{1}{2}}}] \quad .$$

Furthermore, the solutions (5.33) and (5.34) have also to satisfy original coupled equations (5.26) and (5.27) and boundary conditions (5.28) and (5.29), i.e., the integration constants are interrelated by

$$A_n = i\frac{NH}{L\lambda_n}\frac{\sin\lambda_n}{J_1(\kappa_n)} = B_n^* \quad ,$$

$$C_n = \frac{\sin\lambda_n}{LJ_1(\kappa_n)} = D_n^* \quad . \tag{5.37}$$

By combining Equations (5.23) and (5.24), Equations (5.33), (5.34) and (5.37) and noticing that $J_1(\kappa_n^*\rho) = J_1^*(\kappa_n\rho)$, the solution for $V(\rho,\zeta)$ and $J_\zeta(\rho,\zeta)$ are obtained in the final form

$$V(\rho,\zeta) = -2NHL^{-1} \sum_{n=1}^{\infty} \lambda_n^{-1}\sin\lambda_n\sin\lambda_n\zeta \; Im[J_1(\kappa_n\rho)/J_1(\kappa_n)] \quad , \tag{5.38}$$

$$J_\rho(\rho,\zeta) = 2L^{-1} \sum_{n=1}^{\infty} \sin\lambda_n\sin\lambda_n\zeta \, Re[J_1(\kappa_n\rho)/J_1(\kappa_n)] \quad , \tag{5.39}$$

where $Re[J_1(\kappa_n\rho)/J_1(\kappa_n)]$ and $Im[J_1(\kappa_n\rho)/J_1(\kappa_n)]$ refer to real and imaginary parts of $J_1(\kappa_n\rho)/J_1(\kappa_n)$, respectively.

The dimensionless expressions of Equations (5.7)-(5.11) together with the solutions (5.38) and (5.39) for $V(\rho,\zeta)$ and $J_\rho(\rho,\zeta)$ yield the remaining dimensionless discharge fields $J_\zeta(\rho,\zeta)$, $B(\rho,\zeta)$ and $E_{\rho,\zeta}(\rho,\zeta)$ which are normalized with respect to $J_o \equiv \sigma V_o B_o$ and $E_o \equiv V_o B_o$, respectively:

$$J_\zeta(\rho,\zeta) = 2NL^{-1} \sum_{n=1}^{\infty} \lambda_n^{-1}\sin\lambda_n[\cos\lambda_n\zeta-(-1)^n]\ Re[\kappa_n J_0(\kappa_n\rho)/J_1(\kappa_n)], \quad (5.40)$$

$$B(\rho,\zeta) = 2RL^{-1} \sum_{n=1}^{\infty} \lambda_n^{-1}\sin\lambda_n[\cos\lambda_n\zeta-(-1)^n]\ Re[J_1(\kappa_n\rho)/J_1(\kappa_n)] , \quad (5.41)$$

$$E_\rho(\rho,\zeta) = J_\rho(\rho,\zeta) - V(\rho,\zeta) , \quad (5.42)$$

$$E_\zeta(\rho,\zeta) = J_\zeta(\rho,\zeta) . \quad (5.43)$$

$J_0(\kappa_n\rho)$ is a Bessel function of the first kind of order 0 with complex argument, and R is the magnetic Reynolds number,

$$R \equiv \mu_o\sigma V_o c = \mu_o I/2\pi R_o B_o . \quad (5.44)$$

From all plasma fields, only the induced magnetic field $B(\rho,\zeta)$ depends on the magnetic Reynolds number. It is also noticed that Equation (5.40) satisfies the integral condition,

$$\int_0^1 J_\zeta(\rho,\zeta)\rho d\rho = NH(1-|\zeta|) , \quad (5.45)$$

which is proved with the help of the following Fourier series expansions in the interval, $-L \leq \zeta \leq +L$,

$$\zeta = -2 \sum_{n=1}^{\infty} (-1)^n \lambda_n^{-1}\sin\lambda_n\zeta ,$$
$$H(1-|\zeta|) = L^{-1}(1 + 2 \sum_{n=1}^{\infty} \lambda_n^{-1}\sin\lambda_n\cos\lambda_n\zeta) . \quad (5.46)$$

Equation (5.45) is rewritten in dimensional form as a non-vanishing integral for any cross section $-c < z < +c$,

$$2\pi\int_0^{R_o} J_z(r,z)rdr = IH(c- |z|) , \quad (5.47)$$

which shows that the plasma is sustained by the total discharge current I.

5.4. Numerical Illustrations and Results

As numerical illustrations, the axial (ζ) and radial (ρ) dependence of the dimensionless centrifuge fields $V(\rho,\zeta)$, $J_\rho(\rho,\zeta)$, $J_\zeta(\rho,\zeta)$, $B(\rho,\zeta)$, and $E_\rho(\rho,\zeta)$ has been calculated in some (interesting) cylindrical regions (ρ = 0, 0.7, 1) and cross-sectional planes (ζ = 0, 0.9, 1, 1.1), respectively. The remaining field $E_\zeta(\rho,\zeta)$ is proportional to $J_\zeta(\rho,\zeta)$. Since the centrifuge fields $V(\rho,\zeta)$, $J_{\rho,\zeta}(\rho,\zeta)$, $B(\rho,\zeta)/R$, and $E_{\rho,\zeta}(\rho,\zeta)$ depend only on H, L and N, the Hartmann numbers are treated as parameters, H = 1, 10, 100, and the geometry parameters are taken as $L = L/c = 10$ and $N = c/R_o = 1, 5, 10$. The axial positions of the anode and cathode are at $\zeta = -1$ and $\zeta = +1$, respectively. The solutions in Equations (5.38)-(5.43) indicate that $V(\rho,\zeta)$, $J_\rho(\rho,\zeta)$, and $E_\rho(\rho,\zeta)$ are asymmetric, $J_\zeta(\rho,\zeta)$, $B(\rho,\zeta)$ and $E_\zeta(\rho,\zeta)$ are symmetric with respect to the central planes ($\zeta = 0$).

i) *Velocity field* $V(\rho,\zeta)$ [Figs. 5.3 and 5.4]: The oppositely directed azimuthal velocity fields are asymmetric about $\zeta = 0$ and are distributed over the entire system, $0 < \rho < 1$, $|\zeta|<L$, with zero velocity at the central plane ($\zeta = 0$) and end walls ($\zeta = L = 10$). The maxima of $|V|$ are at the electrode planes ($\zeta = \pm 1$), and move toward the cylinder wall ($\rho = 1$) as either H is increased or N is decreased. It is seen that $|V|$ spreads more widely along the ζ-axis and grows considerably at any point $0 < \rho < 1$ and $0 < |\zeta| < L$ as H is raised. It is also observed that $|V|$ stretches along ζ and dwindles at any point $0 < \rho < 1$ as N is reduced.

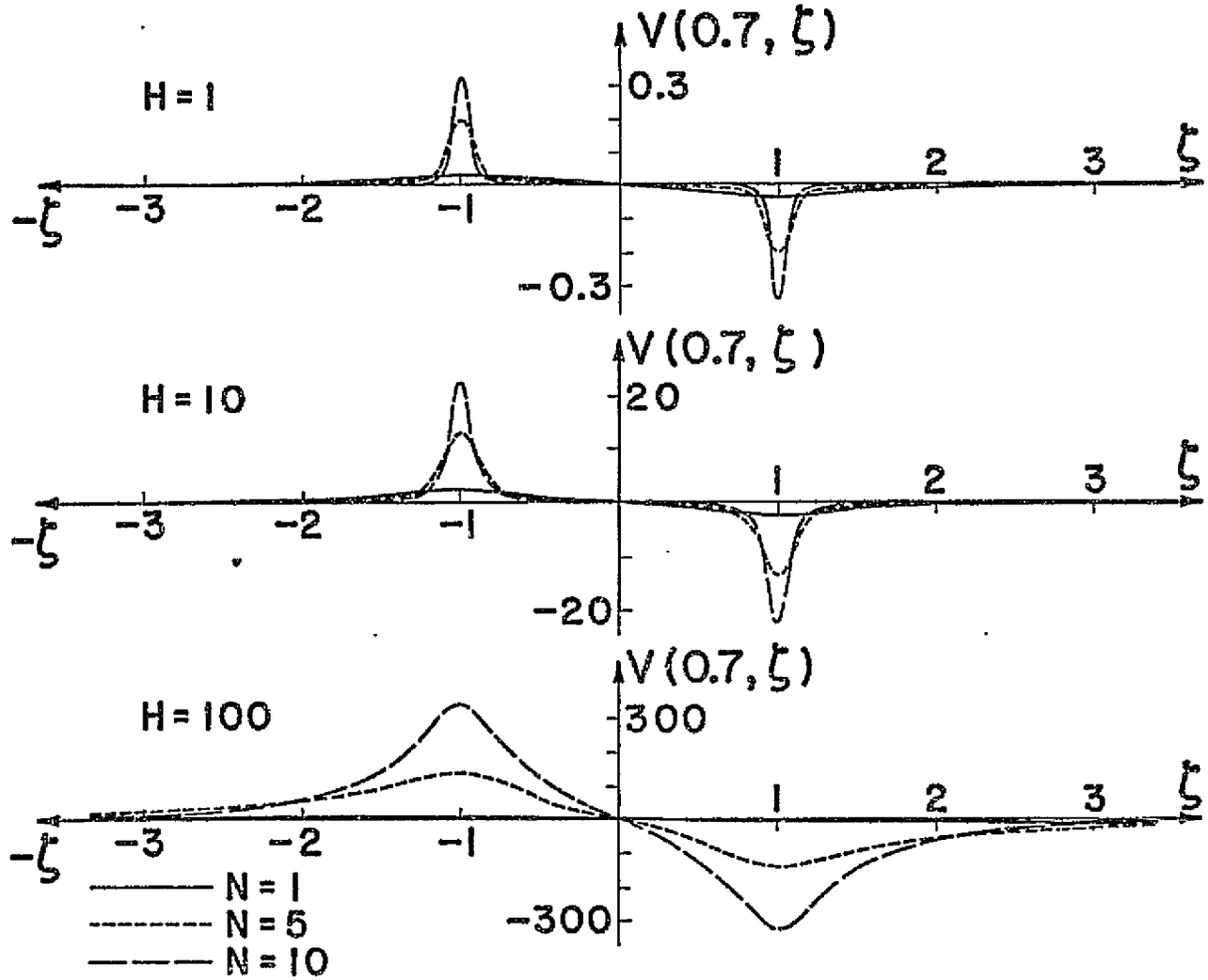

Fig. 5.3. $V(\rho,\zeta)$ versus ζ for $\rho = 0.7$, $N = 1, 5, 10$ and $H = 1, 10, 100$.

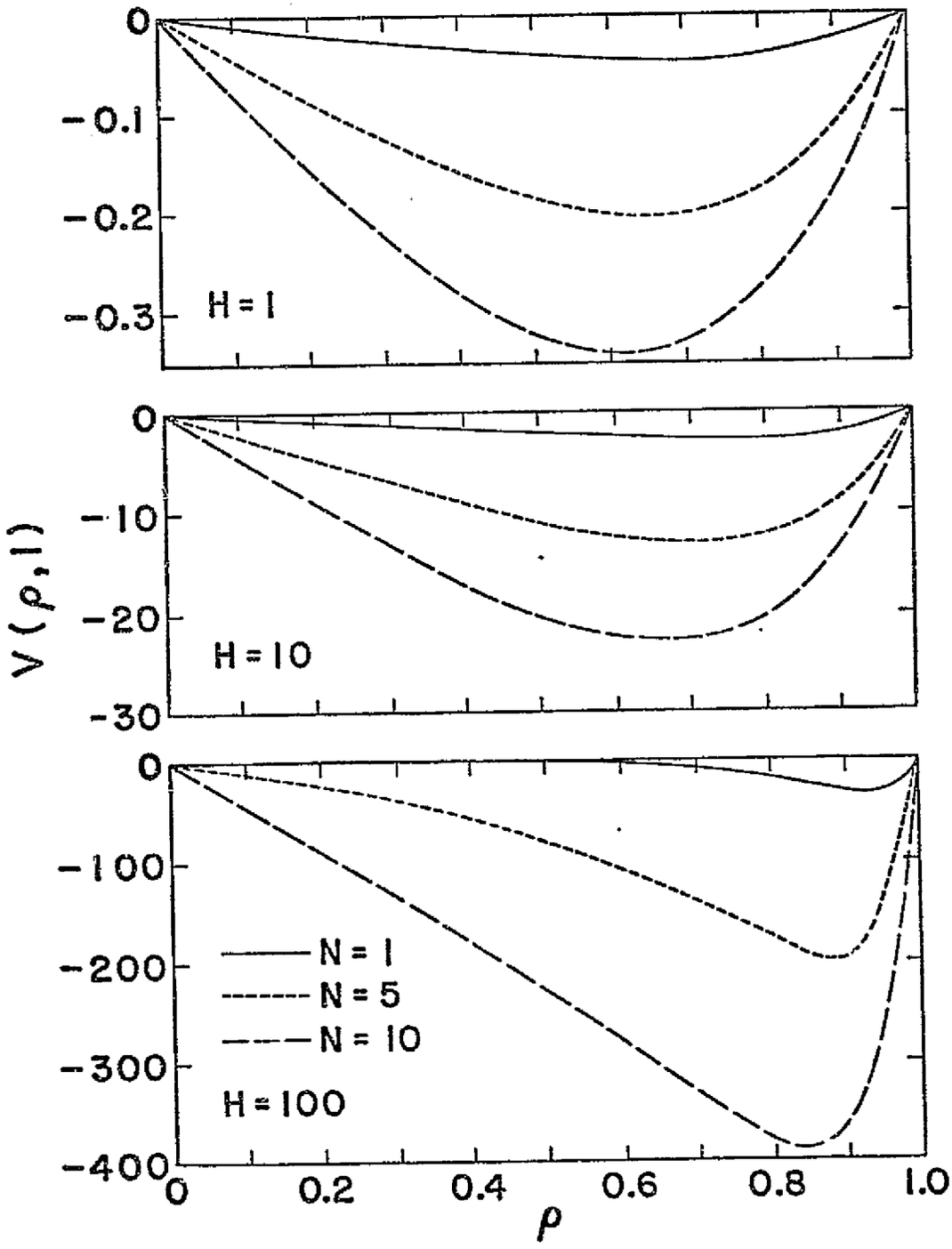

Fig. 5.4. $V(\rho,\zeta)$ versus ρ for $\zeta = 1$, $N = 1, 5, 10$ and $H = 1, 10, 100$.

ii) *Current density fields* $J_{\rho,\zeta}(\rho,\zeta)$ [Figs. 5.5-5.8]: The electric discharge becomes more closely concentrated near the cylinder wall as H is increased. Backward current density ($J_\zeta < 0$) appears to be abundant near the cylinder wall for $|\zeta| > 1$ as either H or N is increased.

iii) *Induced magnetic field* $B(\rho,\zeta)$ [Figs. 5.9 and 5.10]: The induced magnetic field is denser near the cylinder wall at $\rho = 1$ than the axis at $\rho = 0$ as H is increased. $B(\rho,\zeta)$ widens over ζ as either H is increased or N is decreased. For large N = 10 and small $H \lesssim 10$, B grows almost linearly with ρ in the interelectrode space, $-1 < \zeta < 1$.

iv) *Electric fields* $E_{\rho,\zeta}$ [Figs. 5.7, 5.8, 5.11 and 5.12]: The intensity of $E_{\rho,\zeta}$ grows rapidly near the ring electrodes ($\rho = 1$, $\zeta = \pm 1$) and the maximum of $E_{\rho,\zeta}$ shifts to the cylinder wall as H is increased. $E_{\rho,\zeta}$ extends more widely along the ζ-axis as either H is increased or N is decreased.

The graphs in Figures 5.3-5.12 are based on the Fourier series solutions for the Bessel functions of complex arguments, which are summed up to $n = n_{max}$ terms such that n_{max} satisfies $|f(\rho,\zeta)_{n_{max}-5} - f(\rho,\zeta)_{n_{max}}|/|f(\rho,\zeta)_{n_{max}}| \lesssim 10^{-3}$. The numerical values of complex Bessel functions J_0 and J_1 in the series solutions are computed based on the algorithms by Gautschi (1964). The Gibbs phonomena at discontinuities and the tendency of oscillation are suppressed by using the Lanczos convergence factors σ_n (Arfken 1970),

$$\sigma_n = \frac{\sin[n\pi/(n_{max}+1)]}{n\pi/(n_{max}+1)}, \quad \sigma_n = 1, 2, \ldots, n_{max}. \tag{5.48}$$

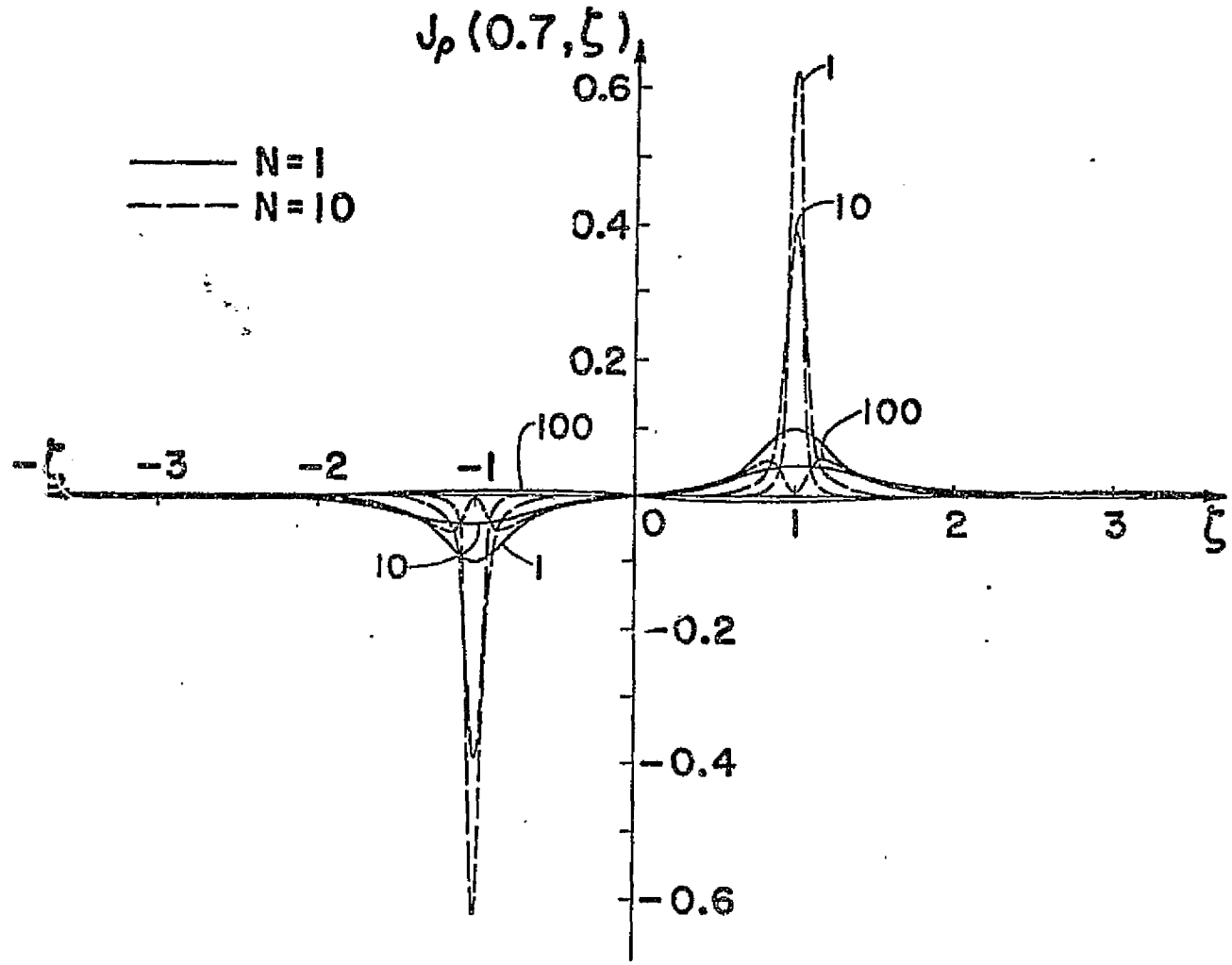

Fig. 5.5. $J_\rho(\rho,\zeta)$ versus ζ for $\rho = 0.7$, $N = 1$, 10 and $H = 1$, 10, 100.

ORIGINAL PAGE IS
OF POOR QUALITY

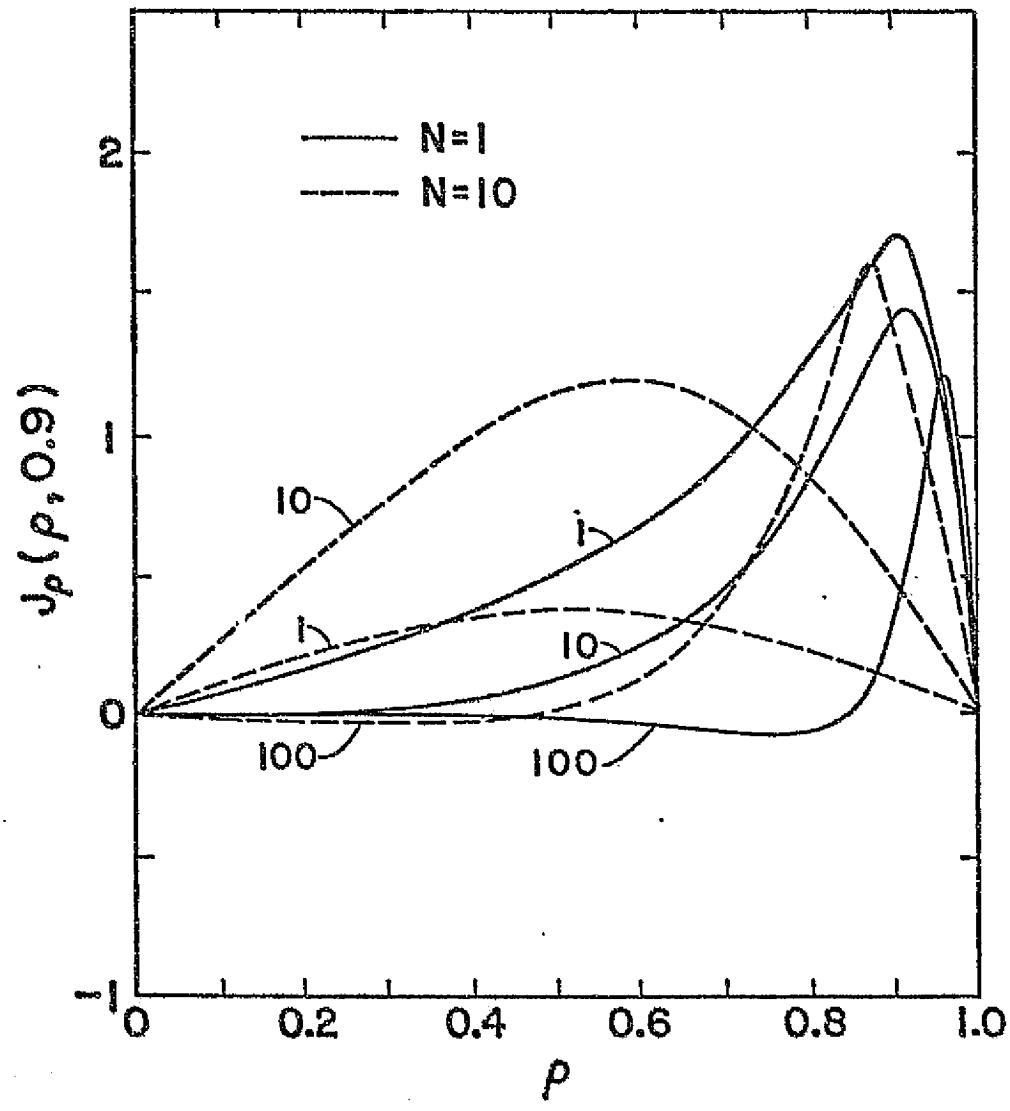

Fig. 5.6. $J_\rho(\rho,\zeta)$ versus ρ for $\zeta = 0.9$, $N = 1$, 10 and $H = 1$, 10, 100.

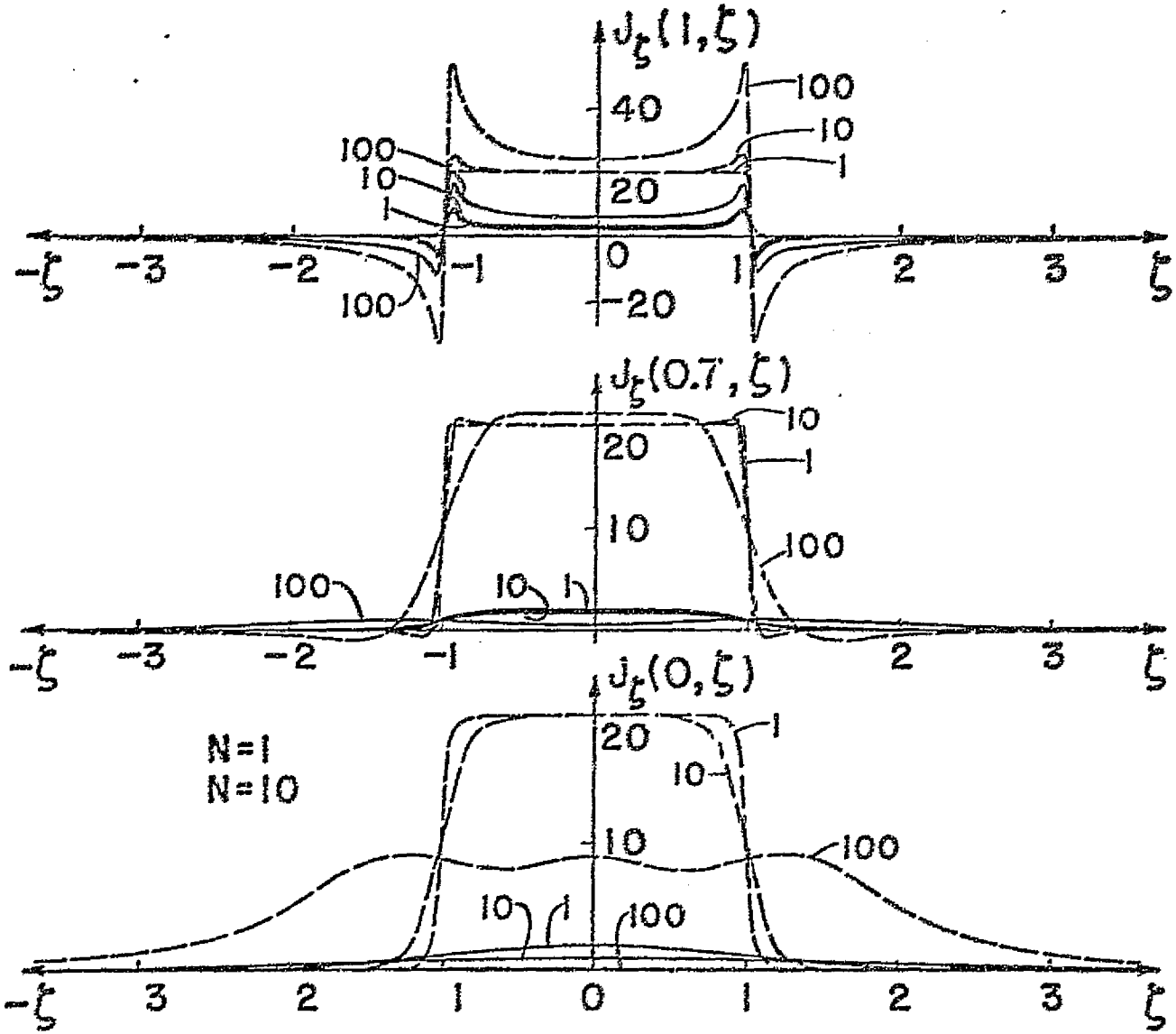

Fig. 5.7. $J_\zeta(\rho,\zeta)$ versus ζ for ρ = 1, 0.7, 0, N = 1, 10 and H = 1, 10, 100.

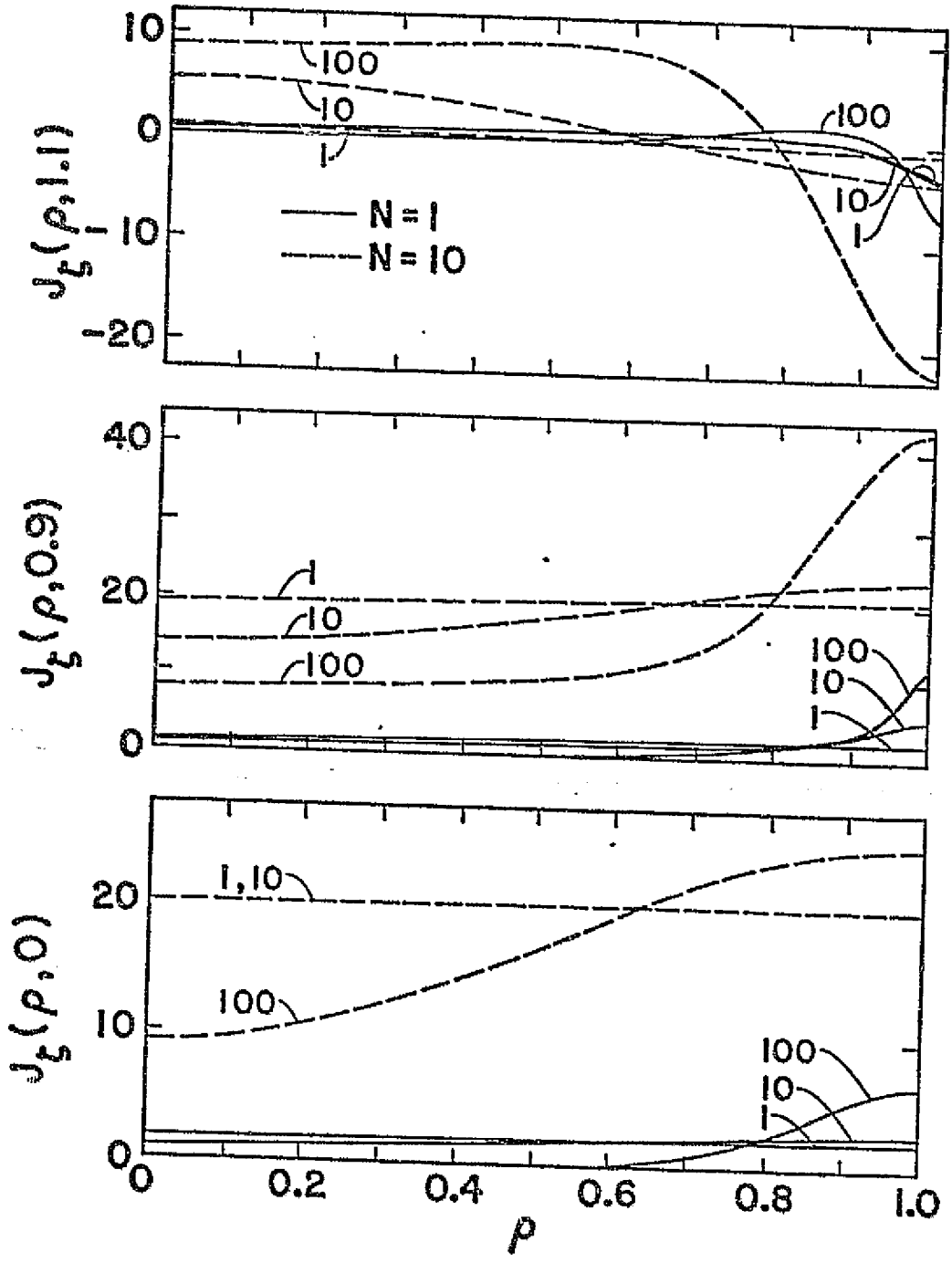

Fig. 5.8. $J_\zeta(\rho,\zeta)$ versus ρ for ζ = 1.1, 0.9, 0, N = 1, 10 and H = 1, 10, 100.

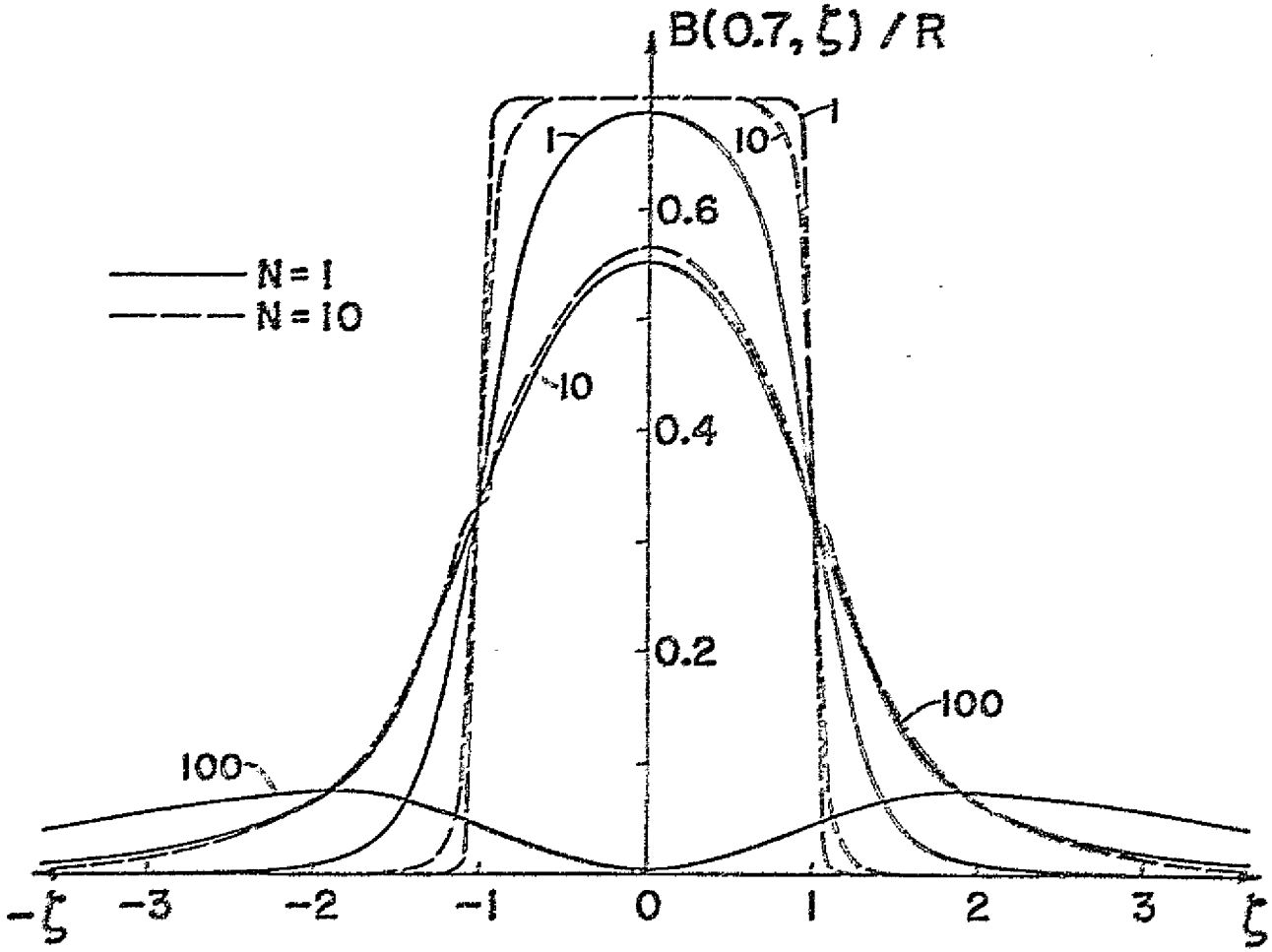

Fig. 5.9. $B(\rho,\zeta)/2$ versus ζ for $\rho = 0.7$, $N = 1$, 10 and $H = 1$, 10, 100.

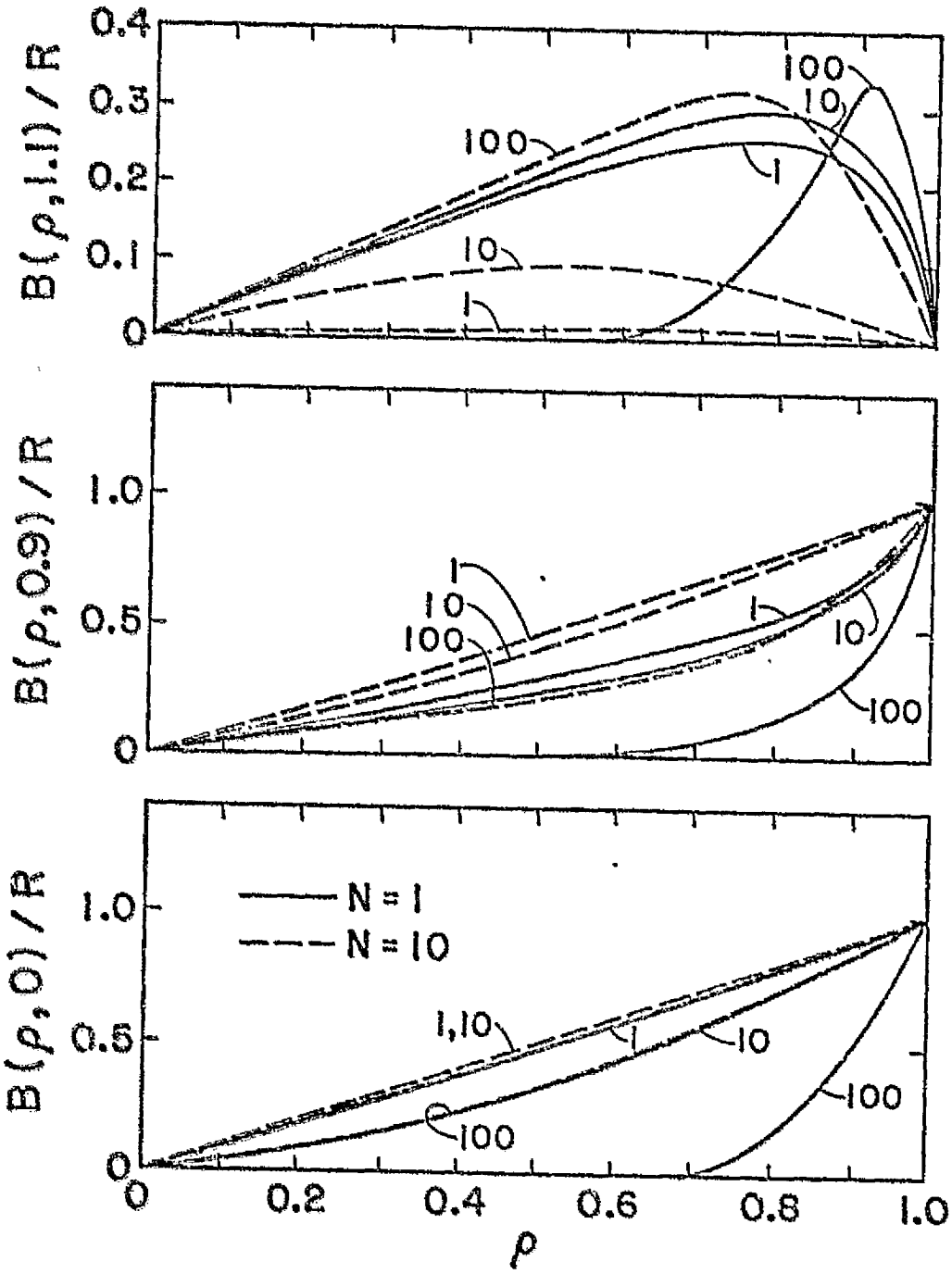

Fig. 5.10. B(ρ,ζ)/R versus ρ for ζ 1.1, 0.9, 0, N = 1, 10 and H = 1, 10, 100.

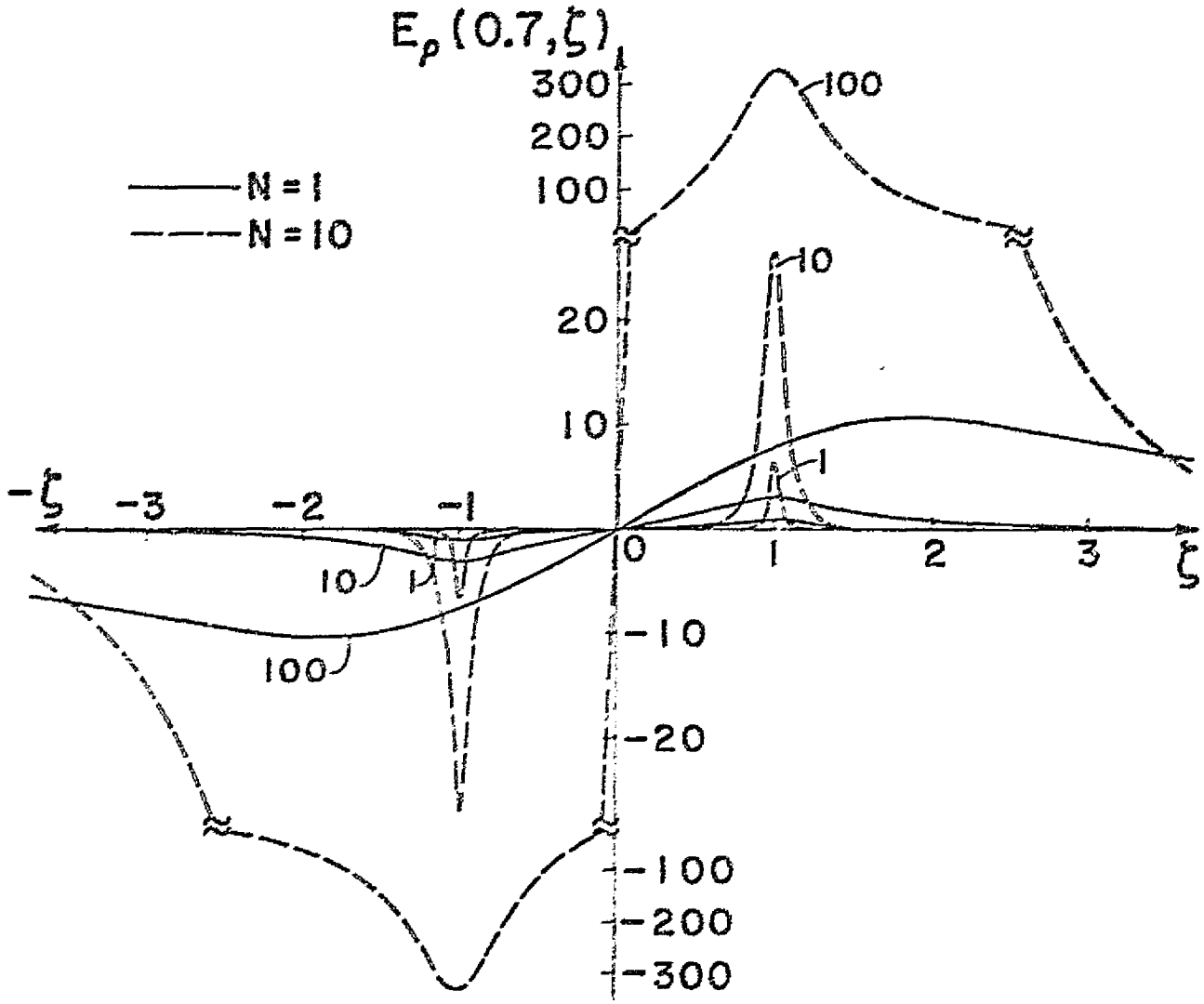

Fig. 5.11. $E_\rho(\rho,\zeta)$ versus ζ for $\rho = 0.7$, $N = 1, 10$ and $H = 1, 10, 100$.

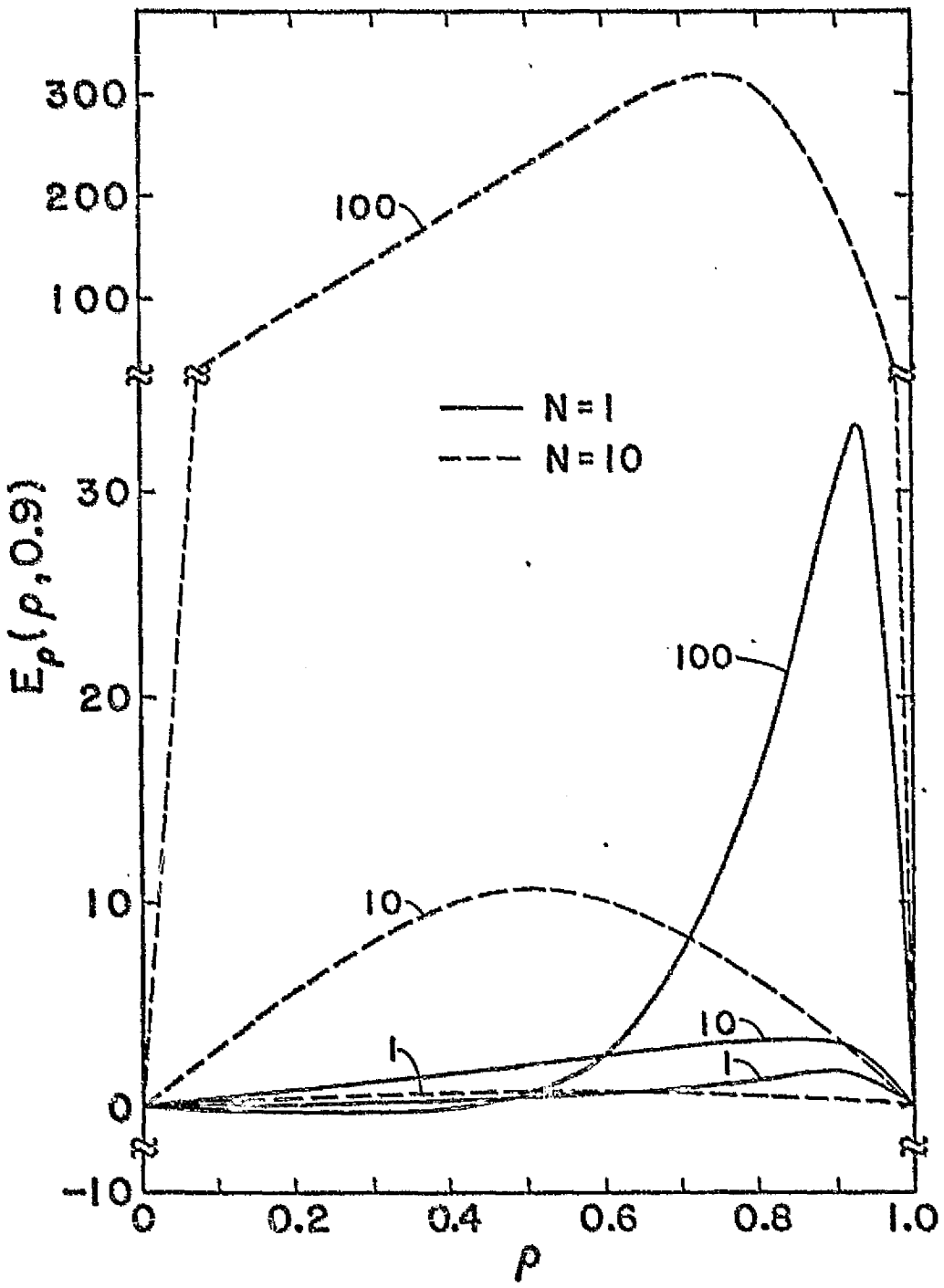

Fig. 5.12. $E_\rho(\rho,\zeta)$ versus ρ for $\zeta = 0.9$, $N = 1$, 10 and $H = 1$, 10, 100.

The graphical presentations of the plasma fields indicate that it is desirable for the ring electrodes to be located sufficiently apart in distance compared to the cylinder radius ($N = c/R_o > 1$), to ensure a significant Lorentz force and plasma rotation. As long as the end walls of the discharge chamber are placed sufficiently far from the ring electrodes ($\ell = L/c \gg 1$), velocity losses due to the boundary layers at the end walls are insignificant. The proposed centrifuge scheme results in supersonic rotational plasma velocities (which are not affected by the induced magnetic field) for moderate flow numbers H, N, ℓ that are realizable in practical applications. For example $|I| = 10^2$ amp, $B_o = 10^0$ Tesla, $\sigma = 10^2$ mho/m and $c = 10R_o = 10^{-1}$ m, the speed of plasma rotation is 10^4 m/sec in order of magnitude by Equation (5.15) and Figures 5.3 and 5.4 for $H = 100$ and $N = 10$.

In a practical centrifuge design for isotope separation, the multi-discharge centrifuge would be located at some stage in a cascade. The enriched and depleted isotope streams are introduced at one end of each centrifuge stage and removed at the other end. As long as the inflow of the isotope mixture and the removal of separated ions occur at a sufficiently slow rate, these flows can be neglected in the analysis of the plasma rotations.

CHAPTER VI

APPLICATION TO ISOTOPE SEPARATION

As shown in the previous chapters, the plasma centrifuge using electromagnetic forces permits to generate speeds of rotation of the order 10^4 m/sec for ordinary steady-state conditions, which are by two orders of magnitude larger than the achievable speeds of about 400 m/sec in the mechanical centrifuges. As a result of the high speed of plasma rotation, the plasma centrifuges could be used with advantage for the separation of isotopes. The spatial separation of the isotope ion and atom components according to their particle masses is ensured by the strong centrifugal force acting on the isotope elements at these high speeds of rotation. Two different kinds of isotope components get different rotational velocities according to the mass due to the intercomponent friction force. This frictional force together with the magnetic field results in a radial motion of the isotope components, the velocity of which is negligible compared with the velocity of rotation. The heavier components move outwards and the lighter inwards in the plasma centrifuge. The diffusion for such a multicomponent plasma transverse and parallel to a magnetic field in the presence of a centrifugal force has been discussed by Bonnevier (1966). For the plasma centrifuges, it is possible to apply his theory

to get approximate numerical results where the separation effect is taken into account.

As an illustration to the plasma centrifuge, the isotope separation ratio α is calculated for two isotopes of lighter mass m_i and heavier mass m_j with the same charges. The separation ratio at distances $0 < r \leq R_o - \delta$, where δ is the viscous boundary layer thickness, is proportional to the power $(m_j - m_i)V_\theta^2(r)/kT_o$ in both the mechanical and plasma centrifuges (T_o is the temperature of the isotope ions). The separation ratio α_m for the mechanical centrifuge is expressed by Cohen (1951)

$$\alpha_m \equiv \frac{n_j(r)/n_i(r)}{n_j(0)/n_i(0)} = \exp\left[\frac{(m_j - m_i)V_\theta^2(r)}{2kT_o}\right] , \tag{6.1}$$

while the separation ratio α_p for the plasma centrifuge is given by Bonnevier (1966)

$$\alpha_p \equiv \frac{n_j(r)/n_i(r)}{n_j(0)/n_i(0)} = \exp\left[\frac{(m_j - m_i)V_\theta^2(r)}{kT_o} \ln\left(\frac{R_o}{r}\right)\right] . \tag{6.2}$$

As a specific example, consider an uranium plasma centrifuge containing the heavier isotope ion(j) U^{238} and the lighter(i) U^{235} to obtain enriched U^{235} of about 3% from the natural abundance of 0.7% as nuclear fuel for reactors. For the enrichment of natural uranium with U^{235}, the centrifuge discharge would be burnt either between solid uranium electrodes or in an UF_6 atmosphere. Such uranium arc discharges can be operated at temperatures as low as ~ 4500°K. In this case, one has $m_{238} - m_{235} = 4.982 \times 10^{-27}$ kg, $kT_o = 6.213 \times 10^{-20}$ Joule. Hence, the isotope separation ratio for $r = R_o/2$ is

$$\begin{aligned} \alpha_p &\approx 1.057 \times 10^0 \quad \text{for} \quad V_\theta(r) = 10^3 \text{ m/sec} , \\ &\approx 4.013 \times 10^0 \quad \text{for} \quad V_\theta(r) = 5 \times 10^3 \text{ m/sec} , \\ &\approx 2.593 \times 10^2 \quad \text{for} \quad V_\theta(r) = 10^4 \text{ m/sec} . \end{aligned} \tag{6.3}$$

It is seen that the plasma centrifuges could produce considerably larger separation ratios α_p than α_m of the mechanical centrifuges for the maximum achievable velocity of about 400 m/sec. Consequently, the plasma centrifuge requires significantly fewer stages in a cascade to get desired concentrations of the isotopes in comparison with the mechanical centrifuges.

CHAPTER VII

COMPRESSIBLE PLASMA CENTRIFUGE WITH SECONDARY FLOWS

In this section, the theoretical analysis of the steady-state dynamics of a plasma centrifuge employing concentric cylinder electrodes and an axial magnetic field $\vec{B}_o$ is proposed. The plasma is produced by a radial discharge of current density $\vec{J}$ in the isotope mixture, and the rotation of the plasma is caused by the Lorentz-forces $\vec{J} \times \vec{B}_o$. Based on the compressible magnetogasdynamic equations, a mathematical method is proposed which permits to calculate the plasma fields, such as the velocity, mass and current densities, and the electromagnetic field in the centrifuge, as a superposition of primary and secondary fields. In this approach, the critical Reynolds number for the onset of secondary flows is determined as the eigen-value of the boundary-value problem for the secondary fields. Attention is given to the evaluation of the feasibility of plasma centrifuges as it is affected by secondary flows and viscous boundary layers.

7.1. Plasma Centrifuge Model with Secondary Flows

The subject of the consideration is a two-dimensional theory for a plasma centrifuge with electromagnetic and viscous forces, the Hall effect and secondary flows. As a centrifuge model, the previously considered type is chosen with concentric cylinder electrodes and axial magnetic field (Fig. 7.1). This centrifuge geometry is symmetric with

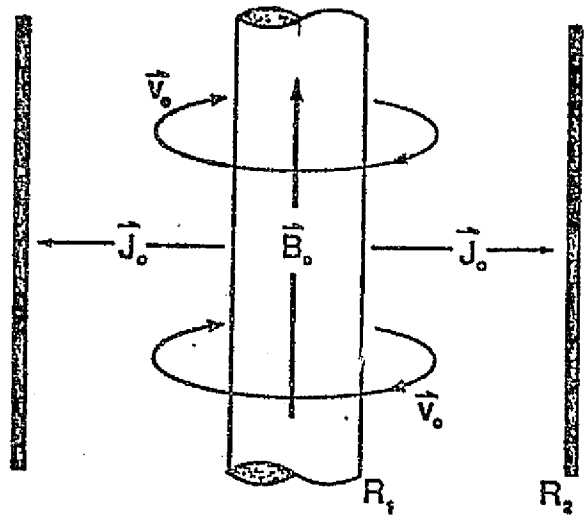

Fig. 7.1. Geometry of plasma centrifuge with cylinder electrodes at $r = R_{1,2}$ (V_o = primary velocity field, J_o = primary current density field).

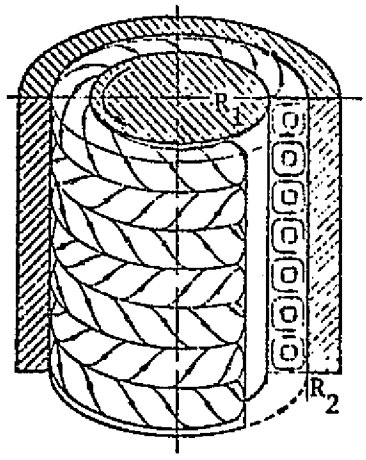

ORIGINAL PAGE IS
OF POOR QUALITY

Fig. 7.2. Qualitative representation of secondary flows.

respect to the z-axis and the plane $z = 0$. It should, therefore, make the inclusion of secondary flows into the analysis possible. The isotope mixture is contained in the interelectrode space $R_1 < r < R_2$ in form of a plasma sustained by a radial gas discharge between the cathode at $r = R_2$ and the anode $r = R_1$. The radial component of the current density $\vec{J}$ forms with the magnetic field $\vec{B}_o$ a volume force $\vec{J} \times \vec{B}_o$ the azimuthal component $(\vec{J} \times \vec{B}_o)_\theta = -J_r B_o$ of which produces the rotation in the circumferential direction $-\theta$. In the steady state, the $\vec{J} \times \vec{B}_o$ forces are balanced by viscous forces and inertia forces of the plasma motion. The resulting velocity field $\vec{V}(r,z)$ of the plasma can be represented as a superposition of a primary rotation field (o) and secondary velocity fields in the r, θ, and z -directions,

$$\vec{V}(r,z) = \{0, v_{o\theta}(r), 0\} + \{v_r(r,z),\ v_\theta(r,z),\ v_z(r,z)\}\ .$$

Generally, the axial extension Δz of the centrifuge is large compared to the radial extension $R_2 - R_1$ so that the primary fields (o) can be treated as one-dimensional, e.g., $v_{o\theta}(r,z) = v_{o\theta}(r)$. In particular, this assumption is rigorous for a hypothetical centrifuge of infinite axial extension, $\Delta z \to \infty$. Similarly, the plasma density, $\rho_p = \rho_p(r,z)$, current density, $\vec{J} = \vec{J}(r,z)$, and electric potential, $\Phi = \Phi(r,z)$, are a superposition of primary (o) and secondary fields.

The problem of secondary flows was first studied experimentally and theoretically for incompressible flow of liquids between rotating cylinders (Taylor 1923). A qualitative picture of the secondary flows in liquids between rotating cylinders is given in Fig. 7.2, which provides an impression of the complexity of these flows. In this case, radial and axial fluid motions have to be considered in addition to

azimuthal components of fluid motion, so that the Navier-Stokes equations become highly nonlinear. Both experiment (Taylor 1923) and bifurcation theory (Yudovich 1967) indicate that a critical Reynolds number λ_* exists for which the problem has a unique solution (Couette flow) for small Reynolds numbers λ compared with $\lambda_*(\lambda < \lambda_*)$, and three-dimensional solutions of steady secondary flows after the loss of stability for λ slightly larger than λ_* $(\lambda_* \leq \lambda)$. As the Reynolds number λ is further increased, more and more complicated types (n) of secondary flows occur as soon as λ becomes larger than λ_n (bifurcation), where λ_n are higher order eigen-values. Finally, for sufficiently large λ, no laminar flow solutions exist and the rotating flow becomes turbulent. The problem of secondary flows in incompressible fluids has not been resolved analytically or numerically to date.

The proposed plasma centrifuge model contains all major effects which i) enhance the rotation (electromagnetic forces, Hall effect) and ii) reduce the rotation (viscous forces, boundary layers, secondary flows) of the isotope mixture. Secondary flows occur because the centrifuge operates at high, supersonic speeds of rotation for which the Reynolds number λ is probably larger than the critical value λ_*. The momentum and energy dissipated in the secondary flows represents a loss mechanism which reduces the speed of azimuthal plasma rotation and the efficiency of the centrifuge. For these reasons, the secondary flows have to be included in the feasibility analysis of plasma centrifuges. As important is the determination of the critical Reynolds numbers λ_* at which bifurcation occurs, which are important design parameters for actual plasma centrifuges.

3.2. Analytical Method

The two-dimensional fields in the plasma centrifuge with secondary flows are described by a nonlinear boundary-value problem for the compressible, magnetogasdynamic equations. This problem is considerably more complex than that of the secondary flows of an incompressible liquid between rotating cylinders, since the number of coupled, nonlinear partial differential equations in compressible magnetogasdynamics is much larger. The solution of the nonlinear magnetogasdynamic equations for the primary plasma fields is first sought, and then the solution of the total plasma fields as a superposition of primary and secondary fields. The secondary fields will be expanded in Liapunov-Schmidt series (Vainberg and Trenogin, 1962), e.g.,

$$\vec{v}(r,z) = \sum_{m=1}^{\infty} (\lambda - \lambda_*)^{\frac{1}{2}m} \vec{v}_m(r,z), \quad |\lambda - \lambda_*| \ll 1,$$

for the secondary velocity field. This statement for solution permits real solutions of the secondary flows for Reynolds numbers $\lambda > \lambda_*$. Since $|\lambda - \lambda_*| \ll 1$ in the vicinity of the onset of secondary flows, $(\lambda - \lambda_*)^{\frac{1}{2}}$ serves as expansion parameter. Thus, in the vicinity of the onset of secondary flows, the nonlinear boundary-value problem for the secondary fields can be treated by the method of successive approximations. In this approach, the secondary fields in the m-th approximation ($m = 1, 2, 3, \ldots$) are described by coupled, linear differential equations, with coefficients and source terms which depend only on the solutions of the lower approximations $m = 1, 2, \ldots, m - 1$. In each approximation $m \geq 1$ to the coupled differential equations, the critical eigen-value λ_* appears as an eigen-value. Thus, the higher

approximations give not only corrections to the secondary flow fields but also to the critical Reynolds number λ_*. The secondary fields have to satisfy boundary conditions at the centrifuge walls, as well as periodicity conditions due to the spatial periodicity of the arrangement of the secondary flows. Although this method of solution is simple in principle, the actual integration of several coupled, inhomogeneous differential equations is difficult, and the degree of complexity grows with each approximation m.

It is proposed to analyze the plasma centrifuge depicted in Figure A.1 along the lines discussed above, in order to obtain solutions of the plasma fields as a superposition of primary and secondary fields. For the mathematical details, it is referred to Section A.3, which contains also physical extensions to the plasma centrifuge problem with secondary flows.

7.3. Theoretical Formulation

In the theoretical description of the rotating plasma in the centrifuge, it is permitted the inclusion of axisymmetric secondary flows $\vec{v}(r,z)$ superimposed on the main azimuthal plasma flow $\vec{v}_{0\theta}(r)$ so that the velocity field of the plasma is given by $\vec{V}(r,z) = \{v_r(r,z), v_{0\theta}(r) + v_\theta(r,z), v_z(r,z)\}$. In view of the extreme mathematical complexity of the analysis of secondary flows for compressible centrifuge flows, the assumptions of an isothermal partially-ionized plasma and small magnetic Reynolds number are made first. Accordingly, the plasma temperature is constant ($T = T_0$) and the induced magnetic fields can be neglected, $\vec{B}_0 = \{0, 0, B_0\}$ in this model. The proposed plasma centrifuge is described by the (isothermal) compressible magnetogasdynamic

equations and the conservation equation for the electric current density with Hall-effect ($\omega\tau \neq 0$), subject to the appropriate boundary conditions and periodicity conditions for the secondary flows. After normalization in accordance with the following substitutions,

$$r/R_c \to r, \quad z/R_c \to z,$$
$$\vec{V}/V_c \to \vec{V}, \quad \vec{B}_o/B_c \to \vec{B}_o, \quad \vec{J}/J_c \to \vec{J}, \quad \rho_p/\rho_c \to \rho_p, \quad \Phi/\Phi_c \to \Phi, \tag{7.1}$$

where the characteristic reference values are defined by

$$R_c \in (R_1, R_2), \quad V_c \equiv \sqrt{kT_o/m}, \quad B_c \equiv B_o,$$
$$J_c \equiv \sigma V_c B_c, \quad \rho_c \equiv \rho_o(r=R_1), \quad \Phi_c \equiv R_c V_c B_c, \tag{7.2}$$

the dimensionless magnetogasdynamic equations for the mass density (ρ_p), velocity ($\vec{V}$), current density ($\vec{J}$), and electric potential (Φ) fields become

$$\rho_p \vec{V}\cdot\nabla\vec{V} = -\nabla\rho_p + \lambda^{-1}[\nabla^2\vec{V} + \tfrac{1}{3}\nabla(\nabla\cdot\vec{V})] + H^2\lambda^{-1}\,\vec{J}\times\vec{B}_o\,, \tag{7.3}$$

$$\nabla\cdot(\rho_p\vec{V}) = 0\,, \tag{7.4}$$

$$\vec{J} = -\nabla\Phi + \vec{V}\times\vec{B}_o - \omega\tau\,\vec{J}\times\vec{B}_o\,, \tag{7.5}$$

$$\nabla\cdot\vec{J} = 0\,, \tag{7.6}$$

where

$$\lambda \equiv \rho_c V_c R_c/\mu, \quad H \equiv \sqrt{\sigma/\mu}\,R_c B_c$$

are Reynolds number and Hartmann number, respectively. The system (7.3)-(7.6) must satisfy the following boundary conditions,

$$\vec{V}(r,z)_{r=R_{1,2}} = \vec{0}, \quad -\infty < z < +\infty, \tag{7.7}$$

$$\int_{R_1}^{R_2} v_z(r,z)rdr = 0, \quad -\infty < z < +\infty, \tag{7.8}$$

$$\Phi(r,z)_{r=R_{1,2}} = \Phi_{1,2}, \quad -\infty < z < +\infty, \tag{7.9}$$

where $R_{1,2}$ and $\Phi_{1,2}$ are now dimensionless constants normalized by R_c Φ_c, respectively. The boundary conditions (7.7) and (7.8) consider that the plasma does not slip at cylinder electrodes, and that there is no velocity flux through any transverse plane z = constant, respectively. The boundary conditions (7.9) specify that an electric potential difference $\Phi_2 - \Phi_1$ is maintained across the perfectly conducting cylinder electrodes. Since the secondary flows are axisymmetric and periodic along the cylinder axis (α = axial wave number) the periodicity conditions for the secondary flows are

$$\begin{aligned} v_{r,\theta}(r, -z \pm 2\pi/\alpha) &= v_{r,\theta}(r,z) , \\ v_z\ (r, -z \pm 2\pi/\alpha) &= -v_z(r,z) . \end{aligned} \tag{7.10}$$

The formal perturbation theory is employed to analyze the behavior of the solutions in the vicinity of primary fields. All centrifuge $\vec{F}(r,z)$ are therefore sought in the form

$$\vec{F}(r,z) = \vec{f}_o(r) + \vec{f}(r,z) . \tag{7.11}$$

The primary fields $\vec{f}_o(r)$ are first considered and it is supposed that a small secondary field $\vec{f}(r,z)$ is superimposed on the initial steady-state field $\vec{f}_o(r)$. Substitution of the expression (7.11) into

Equations (7.3)-(7.9) yields a boundary-value problem for the initial steady state, and a linear eigen-value problem for the secondary flows by retaining only the first-order terms in the perturbation fields.

7.4. Solutions for Primary Fields

The following boundary-value problem for v_o (r) and $\phi_o(r)$ describes the zero-order steady state of the plasma centrifuge:

$$\frac{d}{dr}\left[\frac{1}{r}\frac{d}{dr}(r\, v_{o\theta})\right] - H_\perp^2\, v_{o\theta} = -H_\perp^2 \frac{d\phi_o}{dr}\,, \tag{7.12}$$

$$\frac{1}{r}\frac{d}{dr}\left(r\,\frac{d\phi_o}{dr}\right) = \frac{1}{r}\frac{d}{dr}(r\, v_{o\theta})\,, \tag{7.13}$$

where

$$v_{o\theta}(r)_{r=R_{1,2}} = 0\,, \tag{7.14}$$

$$\phi_o(r)_{r=R_{1,2}} = \Phi_{1,2}\,, \tag{7.15}$$

and

$$H_\perp^2 \equiv H^2/(1+\omega^2\tau^2)\,.$$

The remaining primary fields are consecutively determined by using the solutions for $v_{o\theta}$ and ϕ_o:

$$j_{or}(r) = (1+\omega^2\tau^2)^{-1}\left(-\frac{d\phi_o}{dr} + v_{o\theta}\right)\,, \tag{7.16}$$

$$j_{o\theta}(r) = \omega\tau\, j_{or}\,, \tag{7.17}$$

$$\frac{d\rho_o}{dr} - \frac{v_{o\theta}^2}{r}\rho_o = H^2\lambda^{-1}\, j_{o\theta}\,. \tag{7.18}$$

The steady-state solutions of Equations (7.12)-(7.18) are obtained in the form:

$$v_{o\theta}(r) = ar + br^{-1} + cr\ell nr \ , \tag{7.19}$$

$$\phi_o(r) = a(r^2/2) + b\ell nr + c[r^2/2 - H_\perp^{-2})\ell nr - r^2/4] + d \ , \tag{7.20}$$

$$j_{or}(r) = 2cH^{-2}r^{-1} \ , \tag{7.21}$$

$$j_{o\theta}(r) = \omega\tau \ j_{or}(r) \ , \tag{7.22}$$

$$\rho_o(r) = [2\omega\tau\lambda^{-1}c\int_{R_1}^{r} r^{-1}\exp(-\int_{R_1}^{r} r^{-1}v_{o\theta}^2 dr)dr + 1]\exp(\int_{R_1}^{r} r^{-1}v_{o\theta}^2 dr) \ , \tag{7.23}$$

where

$$a = -c[(R_2^2\ell nR_2 - R_1^2\ell nR_1)/(R_2^2 - R_1^2)] \ ,$$

$$b = c[R_1^2R_2^2\ell n(R_2/R_1)/(R_2^2 - R_1^2)] \ , \tag{7.24}$$

$$c = -(\Phi_2-\Phi_1)[(R_2^2-R_1^2)/4 - R_1^2R_2^2\ell n^2(R_2/R_1)/(R_2^2-R_1^2) + 2H_\perp^{-2}\ell n(R_2/R_1)]^{-1},$$

$$d = \Phi_2 - aR_2^2/2 - b\ell nR_2 - c[(R_2^2/2 - 2H_\perp^{-2})\ell nR_2 - R_2^2/4] \ .$$

Equations (7.20)-(7.23) exhibit clearly the effect of plasma rotation (7.19) on the plasma fields.

7.5. Eigen-value Problem for Secondary Fields

Linearization of Equations (7.3)-(7.9) according to Equation (7.11) yields for the secondary flows in the plasma the eigen-value problem:

$$\rho_o(\vec{v}_o\cdot\nabla\vec{v} + \vec{v}\cdot\nabla\vec{v}_o) + \rho(\vec{v}_o\cdot\nabla\vec{v}_o)$$
$$= -\nabla p + \lambda^{-1}[\nabla^2\vec{v} + \frac{1}{3}\nabla(\nabla\cdot\vec{v})] + H^2\lambda^{-1}\vec{j}\times\vec{e}_z \ , \tag{7.25}$$

$$\rho_o \nabla \cdot \vec{v} + \vec{v} \cdot \nabla \rho_o = 0 \ , \tag{7.26}$$

$$\vec{j} = -\nabla\phi + \vec{v} \times \vec{e}_z - \omega\tau \ \vec{j} \times \vec{e}_z \ , \tag{7.27}$$

$$\nabla \cdot \vec{j} = 0 \ , \tag{7.28}$$

where

$$\vec{v}(r,z)_{r=R_{1,2}} = \vec{0} \ , \quad -\infty < z < +\infty \ , \tag{7.29}$$

$$\int_{R_1}^{R_2} v_z(r,z) r dr = 0 \ , \quad -\infty < z < +\infty, \tag{7.30}$$

$$\phi(r,z)_{r=R_{1,2}} = 0 \ , \quad -\infty < z < +\infty. \tag{7.31}$$

$\vec{e}_z$ designates the unit vector in the z-direction. Substitution of the periodicity conditions (7.10) for the secondary flows into Equations (7.25)-(7.28) produces additional periodicity conditions in z for the remaining perturbation fields:

$$\begin{aligned} j_{r,\theta}(r, -z \pm 2\pi/\alpha) &= j_{r,\theta}(r,z) \ , \\ j_z(r, -z \pm 2\pi/\alpha) &= -j_z(r,z) \ , \\ \rho(r, -z \pm 2\pi/\alpha) &= \rho(r,z) \ , \\ \phi(r, -z \pm 2\pi/\alpha) &= \phi(r,z) \ . \end{aligned} \tag{7.32}$$

In view of periodicity conditions (7.10) and (7.32), the solutions for the linearized system are sought in the form

$$v_{r,\theta}(r,z) = \hat{v}_{r,\theta}(r)\cos\alpha z, \quad v_z(r,z) = \hat{v}_z(r)\sin\alpha z\ ,$$

$$j_{r,\theta}(r,z) = \hat{j}_{r,\theta}(r)\cos\alpha z, \quad j_z(r,z) = \hat{j}_z(r)\sin\alpha z\ , \tag{7.33}$$

$$\rho(r,z) = \hat{\rho}(r)\cos\alpha z, \quad \phi(r,z) = \hat{\phi}(r)\cos\alpha z\ .$$

By substituting the above trial solutions into the linearized system (7.25)-(7.31), the problem is reduced to a set of coupled ordinary differential equations subject to homogeneous boundary conditions:

$$(DD_* - \alpha^2)\hat{v}_r = \lambda[-f_1\hat{v}_\theta - f_2\hat{\rho} + D\hat{\rho}] - H_\perp^2[\omega\tau(-D\hat{\phi} + \hat{v}_\theta) - \hat{v}_r]$$
$$- \frac{1}{3}(DD_*\hat{v}_r + \alpha D\hat{v}_z)\ , \tag{7.34}$$

$$(DD_* - \alpha^2)\hat{v}_\theta = \lambda f_3\hat{v}_r + H_\perp^2(-D\hat{\phi} + \hat{v}_\theta + \omega\tau\hat{v}_r)\ , \tag{7.35}$$

$$(DD_* - \alpha^2)\hat{v}_z = -\lambda\alpha\hat{\rho} + \frac{\alpha}{3}(D_*\hat{v}_r + \alpha\hat{v}_z)\ , \tag{7.36}$$

$$[D_*D - (1 + \omega^2\tau^2)\alpha^2]\hat{\phi} = D_*(\hat{v}_\theta + \omega\tau\hat{v}_r)\ , \tag{7.37}$$

$$D_*\hat{v}_r + f_4\hat{v}_r + \alpha\hat{v}_z = 0\ , \tag{7.38}$$

where

$$\hat{v}_{r,\theta,z}(r)_{r=R_{1,2}} = 0\ , \tag{7.39}$$

$$D\hat{v}_r(r)_{r=R_{1,2}} = 0\ , \tag{7.40}$$

$$DD_*\hat{v}_\theta(r)_{r=R_{1,2}} = 0\ , \tag{7.41}$$

$$\hat{\phi}(r)_{r=R_{1,2}} = 0\ , \tag{7.42}$$

$$D\hat{\phi}(r)_{r=R_{1,2}} = 0\ , \tag{7.43}$$

and

$$D \equiv \frac{d}{dr} \ , \quad D_* \equiv \frac{d}{dr} + \frac{1}{r} \ ;$$

$$f_1(r) \equiv 2\rho_o \, v_{o\theta}/r \ , \quad f_2(r) \equiv v_{o\theta}^2/r \ , \quad f_3(r) \equiv \rho_o D_* v_{o\theta} \ , \tag{7.44}$$

$$f_4(r) \equiv (D\rho_o)/\rho_o \ .$$

The perturbation amplitudes of the current density fields are determined by using the solutions for $\hat{v}_r$, $\hat{v}_\theta$ and $\hat{\phi}$:

$$\hat{j}_r(r) = (1 + \omega^2\tau^2)^{-1}(-D\hat{\phi} + \hat{v}_\theta + \omega\tau\hat{v}_r) \ , \tag{7.45}$$

$$\hat{j}_\theta(r) = (1 + \omega^2\tau^2)^{-1}[\omega\tau(-D\hat{\phi} + \hat{v}_\theta) - \hat{v}_r] \ , \tag{7.46}$$

$$\hat{j}_z(r) = \alpha\hat{\phi} \ . \tag{7.47}$$

Equations (7.34)-(7.38) with the corresponding boundary conditions (7.39)-(7.43) constitute an eigen-value problem for the Reynolds number λ. For given system constants ($R_{1,2}$, μ, σ, ω, τ) and operating parameters (H, Φ_1, Φ_2), the eigen-value problem (7.34)-(7.43) has a sequence of positive eigen-values $\lambda_n(\alpha)$ for any axial wave number α. Among these eigen-values the smallest one, $\lambda_*(\alpha_*) = \min_{0<\alpha<\infty} \lambda_n(\alpha)$, for a certain value of α_*, is the critical Reynolds number, at which the secondary flows first set in.

The similar eigenvalue problems as shown here have frequently occurred in the analysis of axisymmetric neutral stability for either a hydrodynamic Couette flow or an MHD Couette flow. Indeed even in these simpler cases, the problems have never been completely solved by analytical methods. Either case has been analyzed using some techniques (Chandrasekhar 1961, Ovchinnikova and Iudovich 1966) of an

expansion in orthogonal functions, a variational method and Green's function solution or direct numerical computations by employing the Galerkin method (Kurzweg 1963), the Runge-Kutta method (Harris and Reid 1964), successive approximations (Sparrow et al. 1964) or a finite-difference technique (Chang and Sartory 1965).

The solutions of the eigenvalue problem (7.34)-(7.43) correspond to the first approximation (m=1) of the Liapunov-Schmidt series expansion (Section 7.2). In a similar way, the eigenvalue problems for the higher order expansion fields $\vec{v}_m$ ($m \geq 2$) can be formulated to obtain improved series solutions and eigenvalues λ for the secondary fields. Along these lines, a quantitative theory of the plasma centrifuge with secondary flows could be developed with an accuracy corresponding to the second approximation (m=2) of the Liapunov-Schmidt expansion.

In the above theoretical formulation of the plasma centrifuge problem, certain physical effects have been neglected in order to reduce the number of equations and to reduce the formalism. In the actual research, induced magnetic fields should be taken into consideration so that the results are applicable for arbitrary magnetic Reynolds numbers, $R = [B_{ind}/B_o] = \mu_o \sigma V_c L$. Because of the large thermal conductivity of plasmas, the heavy particle temperature T_o is quasi-homogeneous over most of the centrifuge space $R_1 < r < R_2$, i.e., temperature drops exist in the vicinity of the electrode walls. Thermal energy transport and dissipation should be taken into account if this is mathematically feasible. The theoretical approach proposed would make it also possible to solve the dynamics of secondary flows in ordinary, nonconducting gases, another still unsolved problem.

CHAPTER VIII

COLLISIONLESS PLASMA CENTRIFUGE

In this section, the problem of the collisionless plasma centrifuge is presented within the framework of the (steady-state) Vlasov-Maxwell equations. A one-dimensional configuration of a multicomponent rarefied plasma in an infinitely long cylinder aligned parallel to an external axial magnetic field is considered. In the charge-neutral approximation, a solution to the self-consistent Vlasov-Maxwell equations is obtained by assuming Maxwellian distributions for the plasma particles.

8.1. Model

As a model for a collisionless plasma centrifuge an electrically insulating cylinder R_o containing a mixture of isotope ions and electrons of masses m_i, $i = 1,2,..,e$ is chosen. The plasma state is produced by switching on a strong axial magnetic field $B(t) \to B_o \sim 1$ Tesla so that the associated induced electric field $E(t)$, which is in the azimuthal direction, breaks down the isotope mixture simultaneously. The ions and electrons are accelerated by the induced electric field so that they obtain mean mass velocities V_{oi} in the azimuthal direction. The resulting centrifugal forces (in a system of reference moving with the particles) distribute the isotope ions radially in accordance with their different masses m_i. The subject of the consideration is the

steady-state composition of the isotope mixture after the magnetic field B(t) has reached its "plateau" value B_o (Fig. 8.1).

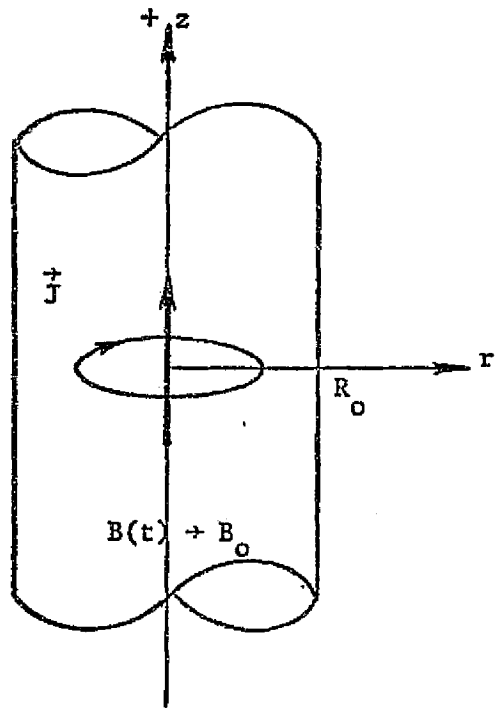

Fig. 8.1. Model of collisionless plasma centrifuge.

This centrifuge has to be operated at low particle densities (collisionless system without significant viscous losses at $r = R_o$), but at still high enough pressures to avoid a compression of the plasma immediately after breakdown by the Lorentz force $J_\theta B_z$ which is directed radially inwards (theta pinch effect). A pinch contraction of the plasma with a radial velocity $\vec{V}$ would produce even higher azimuthal particle velocities through the azimuthal $\vec{V} \times \vec{B}$ field but would render a controlled extraction of the isotope ions difficult within the typical pinch times $\Delta t \sim 10^{-6}$ sec. Another reason for avoiding θ-pinch

conditions is the shock heating of the ions to temperatures $T_o \sim 10^6$ °K. At such high ion temperatures, the random thermal forces would dominate the directed centrifugal forces and make an efficient isotope separation impossible.

Accordingly, in an experiment the centrifuge would have to be operated under conditions where the radial Lorentz force is small compared to the pressure gradient and the electron temperature T_e generated in the induced electrical breakdown is large compared to the ion temperature, T_o, $T_e \gg T_o \sim 10^3$ °K. Nonisothermal plasmas are readily realized at low filling pressure ($T_e \gg T_o$) since only a fraction $\sim m_e/m_i$ of energy is lost by an electron e in collision with an ion i. Since ideal collision and lossless plasmas do not exist, only a quasi-equilibrium can be reached in the isotope ion mixture after B(t) has risen to B_o, which should last for about $\Delta t \sim 10^{-3}$ sec, and permit extraction of the separated isotope species due to the long thermal relaxation time of the electrons. As a technical application, this collisionless plasma centrifuge would have to be operated under continuously repeated induction pulses $B(t) \to B_o$, in order to separate a significant amount of isotopes in a reasonable time.

8.2. Boundary-value Problem for Vlasov-Maxwell Equations

From the theoretical point of view, one is interested in analyzing the quasi-equilibrium state in the final external magnetic field B_o and the self-consistent electric, $\vec{E} = -\nabla\phi$, and magnetic, $\vec{B} = \nabla \times \vec{A}$ fields. For a quasi-infinitely long centrifuge, all fields are functions of r only, i.e., $\vec{E} = -\vec{e}_r \partial\phi/\partial r$ and $\vec{B} = \vec{e}_z \partial(rA)/r\partial r$. In the one-dimensional

steady state, the distribution functions $f_i(\vec{V},r)$ of the particles of type $i = 1,2,..,e$ are described by the coupled Vlasov-Maxwell equations (Section 2.2):

$$V_r \frac{\partial f_i}{\partial r} + [\frac{e_i}{m_i} V_\theta \frac{1}{r} \frac{\partial}{\partial r}(rA) - \frac{e_i}{m_i} \frac{\partial \phi}{\partial r} + \frac{V_\theta^2}{r}] \frac{\partial f_i}{\partial V_r}$$
$$- [\frac{e_i}{m_i} V_r \frac{1}{r} \frac{\partial}{\partial r}(rA) + \frac{V_\theta V_r}{r}] \frac{\partial f_i}{\partial V_\theta} = 0 , \tag{8.1}$$

where

$$- \frac{\partial}{\partial r} [\frac{1}{r} \frac{\partial}{\partial r}(rA)] = \mu_o \sum_i e_i \iiint_{-\infty}^{+\infty} V_\theta f_i \, d\vec{V} , \tag{8.2}$$

$$- \frac{1}{r} \frac{\partial}{\partial r}(r \frac{\partial \phi}{\partial r}) = \varepsilon_o^{-1} \sum_i e_i \iiint_{-\infty}^{+\infty} f_i \, d\vec{V} , \tag{8.3}$$

relate the vector potential $A(r)$ and the scalar potential $\phi(r)$ to its current density and space charge sources, respectively (V_r, V_θ, V_z are the cylindrical coordinates of the particles i in the velocity space).

The equations of motion for each particle species i,

$$m_i \frac{dV_r}{dt} = -e_i \frac{d\phi}{dr} + e_i V_\theta r \frac{1}{r} \frac{\partial}{\partial r}(rA) + m_i \frac{V_\theta^2}{r} ,$$

$$m_i \frac{dV_\theta}{dt} = -e_i V_r \frac{1}{r} \frac{\partial}{\partial r}(rA) - m_i \frac{V_r V_\theta}{r} , \tag{8.4}$$

$$m_i \frac{dV_z}{dt} = 0 ,$$

have the three integrals of motion:

$$H_i = \tfrac{1}{2}m_i(V_r^2 + V_\theta^2 + V_z^2) + e_i\phi \quad , \tag{8.5}$$

$$P_i \equiv P_{i\theta} = m_i V_\theta r + e_i A r \quad , \tag{8.6}$$

$$P_{iz} = m_i V_z \quad . \tag{8.7}$$

The Hamiltonian H_i, the generalized angular momentum $P_i \equiv P_{i\theta}$ and the generalized axial momentum P_{iz} are constants of motion for each isotope i. Knowing the complete set of integrals of motion, the general solutions of equations (8.1) are arbitrary functionals of H_i and P_i (P_{iz} does not enter explicitly due to the absence of the mean axial velocity):

$$f_i(\vec{V},r) = f_{oi} \exp(-\alpha_i H_i - \beta_i P_i) \quad . \tag{8.8}$$

The arbitrary constants f_{oi}, α_i and β_i are to be determined by Maxwellian boundary conditions at $r = R_o$,

$$f_i(\vec{V},r)_{r=R_o} = n_{oi}\left(\frac{m_i}{2\pi kT_i}\right)^{3/2} \times$$

$$\exp\{-m_i[V_r^2 + (V_\theta - V_{oi})^2 + V_z^2]/2kT_i\} \quad , \tag{8.9}$$

$$T_i \equiv T_o, \quad i = 1,2,\ldots \neq e; \; T_i \equiv T_e \gg T_o, \; i = e \quad .$$

Note that n_{oi} and V_{oi} are the particle densities and mean (azimuthal) mass velocities (rotation) of the i-particles at $r = R_o$. Since $T_e \gg T_o$ due to electron heating and $T_o \sim 10^3$ °K is of the order of the wall temperature, a distinction between temperatures $\|$ and $\perp$ to $\vec{B}_o$ is unnecessary.

Substitution of Equation (8.9) into Equation (8.8) yields

$$\alpha_i = 1/kT_i \ ,$$

$$\beta_i = -\omega_i/kT_i \ , \tag{8.10}$$

$$f_{oi} = n_{oi}\left(\frac{m_i}{2\pi kT_i}\right)^{3/2} \exp\left[-\left(\frac{m_i\omega_i^2R_o^2}{2} - e_i\phi_o + e_i\omega_iR_oA_i\right)/kT_i\right] \ ,$$

where

$$\omega_i \equiv V_{oi}/R_o, \quad \phi_o \equiv \phi(R_o), \quad A_o \equiv A(R_o) \ . \tag{8.11}$$

The particle density and azimuthal mean velocity of each isotope are given by

$$n_i(r) = \iiint_{-\infty}^{+\infty} f_i d\vec{V}$$

$$= f_{oi}\left(\frac{2\pi kT_i}{m_i}\right)^{3/2} \exp\left[\left(\frac{m_i\omega_i^2r^2}{2} - e_i\phi + e_i\omega_irA\right)/kT_i\right] \tag{8.12}$$

and

$$V_i(r) = \frac{1}{n_i(r)} \iiint_{-\infty}^{+\infty} V_\theta f_i d\vec{V} = \omega_i r \ . \tag{8.13}$$

Substitution of Equations (8.12) and (8.13) into Equations (8.2) and (8.3) yields a boundary-value problem for coupled nonlinear ordinary differential equations for the self-consistent potentials:

$$\frac{d}{dr}\left[\frac{1}{r}\frac{d}{dr}(rA)\right] = -\mu_o r \sum_i e_i\omega_i n_i(r) \ , \tag{8.14}$$

$$\frac{1}{r}\frac{d}{dr}\left(r\frac{d\phi}{dr}\right) = -\varepsilon_o^{-1} \sum_i e_i n_i(r) \ , \tag{8.15}$$

where

$$\frac{1}{r}\frac{d}{dr}(rA)\Big|_{r=R_o} = B_o \quad , \tag{8.16}$$

$$\frac{1}{r}\frac{d}{dr}(rA)\Big|_{r=0} = B_o + \frac{\mu_o}{2\pi}\sum_i e_i\omega_i N_i \ , \tag{8.17}$$

$$\frac{d\phi}{dr}\Big|_{r=R_o} = -\frac{1}{2\pi\varepsilon_o R_o}\sum_i e_i N_i \ , \tag{8.18}$$

$$\frac{d\phi}{dr}\Big|_{r=0} = 0 \ , \tag{8.19}$$

and

$$N_i \equiv 2\pi\int_0^{R_o} n_i \, r dr \tag{8.20}$$

is the total number of i particles per unit length. The boundary conditions (8.16)-(8.19) can be derived directly from Equations (8.14) and Equation (8.15) by integration, respectively. The boundary conditions (8.16) and (8.17) consider that the requirements of symmetry make the self-consistent magnetic field parallel to the cylinder axis at points inside the centrifuge and that it approaches zero at points outside the centrifuge. The boundary conditions (8.18) and (8.19) take into consideration that the radial electric field is due to the space charges.

8.3. Quasi-neutral solutions

In the limiting case of charge neutrality ($\sum_i e_i n_i = 0$), there are no internal space charges so that the electric field vanishes and only a magnetic field exists. In this case, by Equation (8.12),

$$\sum_i e_i f_{oi}\left(\frac{2\pi kT_i}{m_i}\right)^{3/2} \exp\left[\left(\frac{m_i\omega_i^2 r^2}{2} - e_i\phi + e_i\omega_i rA\right)/kT_i\right] = 0 \ , \tag{8.21}$$

from which

$$\frac{e_i\omega_i}{kT_i} \equiv a = \text{const}, \quad \frac{m_i\omega_i^2}{2kT_i} \equiv b = \text{const} ,$$
$$\phi(r) = 0, \quad \sum_i e_i f_{oi}\left(\frac{2\pi kT_i}{m_i}\right) = 0 . \tag{8.22}$$

Then, Equation (8.14) becomes

$$\frac{d}{dr}\left[\frac{1}{r}\frac{d}{dr}(rA)\right] = -\mu_o r \exp(br^2 + arA) \sum_i e_i f_{oi}\left(\frac{2\pi kT_i}{m_i}\right)^{3/2} \omega_i . \tag{8.23}$$

With the change of variables

$$\Psi \equiv br^2 + arA ,$$
$$\xi \equiv \frac{\lambda}{\sqrt{C}} r^2 , \tag{8.24}$$

where

$$\frac{\lambda^2}{C} = \frac{1}{4}\mu_o a \sum_i e_i f_{oi} \left(\frac{2\pi kT_i}{m_i}\right)^{3/2} \omega_i , \tag{8.25}$$

Equation (8.23) can be transformed to

$$\frac{d^2\psi}{d\xi^2} + e^{\psi} = 0 . \tag{8.26}$$

The general solution of Equation (8.26) has the form

$$e^{\psi} = \frac{2C\gamma e^{\lambda r^2}}{(1+\gamma e^{\lambda r^2})^2} , \tag{8.27}$$

where C, λ and γ are determined by Equation (8.25) and the appropriate boundary conditions:

$$\gamma = -(p - Q)/(p + Q) \ , \tag{8.28}$$

$$\lambda = \frac{e_i\omega_i}{2kT_i} \ Q \ , \tag{8.29}$$

where

$$p \equiv B_o + B_* + \frac{\mu_o}{2\pi} \sum_i e_i\omega_i N_i \ ,$$
$$Q \equiv \pm[(B_o + B_*)^2 + 2\mu_o \sum_i n_{oi}kT_i]^{\frac{1}{2}} \ . \tag{8.30}$$

B_* is the magnetic field which is necessary for particle i to rotate with the cyclotron frequency $\omega_i = e_iB_*/m_i$. It is noted that $(2\pi)^{-1} \sum_i e_i\omega_i N_i = I$ is the total current per unit length, and that $\sum_i n_{oi}kT_i = \sum_i n_{oi}m_i\overline{V_r^2}$ where $\overline{V_r^2}$ is a mean square velocity of each i. By the above expressions, the quasi-neutral solutions are finally given by

$$\phi(r) = 0, \quad V_i(r) = \omega_i r, \quad J_i(r) = e_i n_i \omega_i r,$$
$$n_i(r) = n_{oi} \frac{4Q^2}{Q^2-(B_o+B_*)^2} \frac{\gamma e^{\lambda r^2}}{(1+\gamma e^{\lambda r^2})^2} \ , \tag{8.31}$$
$$B(r) = -B_* + Q \frac{1-\gamma e^{\lambda r^2}}{1+\gamma e^{\lambda r^2}} \ .$$

It turns out, however, that the radial distribution of the isotope ions depends sensitively on the electric potential $\phi(r)$ since $e_i\phi/kT_o > 1$ for the ions $i \neq o$ ($kT_o \sim 75 \times 10^{-3}$ volt for $T_o = 10^3$ °K), i.e., it is not determined solely by the centrifugal forces $m_i V_{oi}^2/r$. For this reason, the theory should be extended to include space charge effects and to obtain the exact potential distribution $\phi(r)$. In view of the complexity of the underlying nonlinear (transcendental) differential equations, this extension has probably to be carried through within the frame of an appropriate perturbation theory.

APPENDIX: PREVIOUS RESEARCH ON ISOTOPE SEPARATION

For isotope separation, various methods have been suggested such as chemical methods (Urey 1939), diffusion methods (Furry et al. 1939), electromagnetic methods of mass spectrometry (Smith et al. 1947), and mechanical centrifuge methods (Humphreys 1939; Cohen 1951). In electromagnetic methods, ions are moving in different orbits and are deflected in a magnetic field according to their different charge to mass ratio. However, because of difficulties in producing intense ion beams and neutralization of ions by electrons, this method was not widely used in industry. In fact, it is used only for laboratory purpose for producing limited amounts of pure isotopes owing to its high resolution. For separation of isotopes with low mass, chemical methods are more effective than electromagnetic methods. When large quantities of pure materials are required, it is industrial practice to use gaseous-diffusion separation systems.

In recent years, other effective methods for isotope separation have been studied. In particular, plasma methods are promising for high precision technology and in new technological developments. Plasma separators can be designed to operate on the basis of plasma streams (Becker nozzle) and plasma rotation (plasma centrifuge). The Becker nozzle is being developed as a commercial isotope separation device. In principle, this device expands the isotope mixture through a supersonic nozzle and along a curved wall so that extremely large centrifugal forces result which separate the heavy isotope from the light (Becker et al. 1955). An extension of this principle is applied in the jet scheme in which two or more opposing supersonic nozzle flows deflect each other so that centrifugal forces occur again as a result of stream line curvature (Campargue 1970; Becker et al. 1973).

Although the plasma centrifuge concept was first proposed by Slepian (1956), a major research effort does not appear to exist in this field in the United States. There is a significant research program on plasma centrifuges in the U.S.S.R. (Berezov et al. 1976; Belorusov et al. 1976), which is classified. The interest of smaller countries, such as Sweden (Bonnevier 1966, 1971; Lehnert 1970, 1973), Japan (Okada et al. 1973), and Australia (George and Kane 1972; James and Simpson 1974, 1976), in plasma centrifuges appears to be due to the low cost of this type of separation device. From the theoretical point of view, the basic mechanism for plasma rotation by means of crossed electric and magnetic fields and Lorentz forces in rarefied and dense plasmas is understood qualitatively (Anderson et al. 1958; Gordeev 1959, 1961; Kessey 1964; Hanson and Cohen 1970; Vrba 1971; Witalis 1974; Ban and Sekiguchi 1976; Marlier 1977).

Proposed plasma centrifuges employ either low-density collisionless plasmas or high-density collision-dominated plasmas as working fluids. Experimental evidence on isotope separation in plasma centrifuges has been reported for both cases (Bonnevier 1971; James and Simpson 1974, 1976; Heller and Simon 1974; Berezov et al. 1976). Exact solutions for collisionless centrifuge plasmas are not known, which require evaluation of the self-consistent electromagnetic field interactions (Komarov and Fadeev 1962; Watson 1956). The disadvantages of collisionless centrifuges are relatively large electric power dissipation to produce high degrees of ionization of the isotope mixture and the small amounts of isotopes they permit to separate. On the other hand, collisionless centrifuges have minimum velocity losses at the walls due to the absence of ordinary hydrodynamic boundary layers. In high-density centrifuges,

only a small fraction of isotope such as cesium with a low ionization energy) has to be ionized to produce a partially ionized plasma state. The Lorentz force due to the interaction of the current density and magnetic field sets not only the charged plasma components but also the neutral plasma components in rotation, which are coupled through the intercomponent friction forces. The collision-dominated centrifuge excels through relatively low energy dissipation and large isotope densities. The velocity losses occurring in the viscous boundary layers at the walls are, however, of some disadvantage.

REFERENCES

Anderson, O. A., W. R. Baker, A. Bratenahl, H. P. Furth, J. Ise Jr., W. B. Kunkel and J. M. Stone, "Study and use of rotating plasma," Proc. 2nd UN International Conference on Peaceful Uses of Atomic Energy 32, 155 (1958).

Arfken, G., Mathematical Methods for Physicists (Academic Press, New York, 1970).

Ban, T. and T. Sekiguchi, "Experimental and theoretical studies on weakly-ionized, steady rotating plasma," Japan J. Appl. Phys. 15, 115, (1976).

Batchelor, D. B. and R. C. Davidson, "Kinetic description of linear theta-pinch equilibria," J. Plasma Phys. 14, 77 (1975).

Beams, J. W. and C. Skarstrom, "The concentration of isotopes by the evaporative centrifuge method," Phys. Rev. 56, 266 (1939).

Becker, E. W., K. Bier, and H. Burghoff, "The separation nozzle. A new apparatus for the separation of gases and isotopes," Z. Naturf. A. 10, 565 (1955).

Becker, E. W., W. Bier, P. Bley, U. Ehrfeld, W. Ehrfeld, and G. Eisenbeiss, "Developmental potential of the isotope separation nozzle method for the enrichment of U^{235}," Atomw. Atomt. 18, 524 (1973).

Belorusov, A. V., A. I. Karchevskii, Yu. A. Muromkin, and E. P. Pontanin, "Separation of gas mixtures and xenon isotopes in pulsed plasma centrifuge," Pisma V. Zh. Tekh. Fiz. 12, 664 (1976).

Berezov, D. V., I. I. Demidenko, N. S. Lomino, A. I. Morozov, and V. G. Padalka, "Separation of ions with large mass differences in a plasma," Sov. Phys. Tech. Phys. 20, 906 (1976).

Bonnevier, B., "Diffusion due to ion-ion collisions in a multicomponent plasma," Ark. Fys. 33, 255 (1966).

Bonnevier, B., "Experimental evidence of element and isotope separation in a rotating plasma," Plasma Phys. 13, 763 (1971).

Cambel, A. B., Plasma Physics and Magnetofluidmechanics (McGraw-Hill, New York, 1963).

Campargue, R., "Aerodynamic separation effect on gas and isotope mixtures induced by invasion of the free jet shock wave structure," J. Chem. Phys. 52, 1795 (1970).

Chadrasekhar, S., Hydrodynamic and Hydromagnetic Stability (Oxford at the Clarendon Press, 1961).

Chang, C. C. and T. S. Lundgren, "Flow of an incompressible fluid in a hydromagnetic capacitor," Phys. Fluids 2, 627 (1959).

Chang, T. S. and W. K. Sartory, "Hydromagnetic stability of dissipative vortex flow," Phys. Fluids 8, 235 (1965).

Channoll, P. J., "Exact Vlasov-Maxwell equilibria with sheared magnetic fields," Phys. Fluids 19, 1541 (1976).

Chen, F. F., Introduction to Plasma Physics (Plenum Press, New York, 1974).

Cohen, K., The Theory of Isotope Separation (McGraw-Hill, New York, 1951).

Cramer, K. R. and S. Pai, Magnetofluid Dynamics for Engineers and Applied Physicists (McGraw-Hill, New York, 1973).

Furry, W. H. and R. C. Jones, "On the theory of isotope separation by thermal diffusion," Phys. Rev. 55, 1083 (1939).

Gautschi, W., "Bessel functions of the first kind," Comm. ACM 7, 479, (1964).

George, D. W. and E. L. Kane, "Plasma centrifuging for isotope separation," IEE 90, 174 (1972).

Gordeev, G. V., "The influence of end boundaries upon the rotation of plasma in a magnetic field," Sov. Phys. Tech. Phys. 4, 683, (1959).

Gordeev, G. V., "The nonstationary rotation of a plasma in a magnetic field," Sov. Phys. Tech. Phys. 6, 195 (1961).

Hanson, J. P. and I. M. Cohen, "Magnetohydrodynamic rotation in an annulus," Univ. of Pennsylvania Report No. INDEC-80 (1970).

Harris, D. L. and W. H. Reid, "On the stability of viscous flow between rotating cylinders," J. Fluid Mech. 20, 95 (1964).

Haller, H. and M. Simon, "Neon isotope separation in a rotating plasma," Phys. Lett. 50A, 139 (1974).

Hong, S. H. and H. E. Wilhelm, "Magnetohydrodynamic instability of a cylindrical liquid metal brush," J. Appl. Phys. 47, 906 (1976).

Hong, S. H., "Transformation of the perturbation equations for the analysis of magnetohydrodynamic Couette flow stability," ZAMP 27, 483 (1976).

Hong, S. H. and H. E. Wilhelm, "Boundary-value problem for a counterrotating electrical discharge in an axial magnetic field," J. Appl. Phys. 49, 146 (1978).

Howatson, A. M., An Introduction to Gas Discharge (Pergamon Press, New York, 1965).

Hugh, W. F. and F. J. Young, The Electromagnetodynamics of Fluids (John Wiley & Sons, New York, 1966).

Humphreys, R. F., "Separation of bromine isotopes by centrifugation," Phys. Rev. 56, 684 (1939).

James, B. W. and S. W. Simpson, "Isotopic separation in a rotating plasma," Phys. Lett. 46A, 347 (1974).

James, B. W. and S. W. Simpson, "Isotope separation in the plasma centrifuge," Plasma Phys. 18, 289 (1976).

Kalikhman, L. E., Elements of Magnetogasdynamics (Saunders, Philadelphia, 1967).

Kessey, K. O., "Rotating electrically conducting fluids in a long cylinder," AIAA J. 2, 864 (1964).

Komarov, N. N. and V. M. Fardeev, "Plasma in a self-consistent magnetic field," Sov. Phys. JETP 14, 378 (1962).

Kurzweg, U. H., "The stability of Couette flow in the presence of an axial magnetic field," J. Fluid Mech. 17, 52 (1963).

Lehnert, B., "A partially ionized plasma centrifuge," Phys. Scrip. 2, 106 (1970).

Lehnert, B., "Rotating plasma," Nucl. Fusion 11, 485 (1971).

Lehnert, B., "The partially ionized plasma centrifuge," Phys. Scrip. 7, 102 (1973).

Marlier, S. F., "A steady rotating plasma disk," Appl. Phys. 14, 53, (1977).

Matalon, M. and S. Schweitzer, "Viscous MFD low Hartmann flow in an annular gap - a magnetic Prandtl number expandion," J. Franklin Inst. 297, 259 (1974).

Morozov, A. I. and L. S. Solovev, "A kinetic examination of some equilibrium plasma configurations," Sov. Phys. JETP 13, 927 (1961).

Okada, O., T. Dodo, and T. Kawai, "Separation of uranium isotope by plasma centrifuge," J. Nucl. Sci. Tech. 10, 626 (1973).

Ovchinnikova, S. N. and V. I. Iudovich, "Analysis of secondary steady flow between rotating cylinders," PMM 32, 858 (1968).

Schlichting, H., Boundary-Layer Theory (McGraw-Hill, New York, 1968).

Schwenn, R., "Measurement of radial distributions of electric-current densities and temperature in hydrogen arc with axial magnetic field," Z. Naturf. A. 25, 1601 (1970).

Shapiro, A. H., The Dynamics and Thermodynamics of Compressible Fluid Flow (Ronald Press, New York, 1954).

Slepian, J., "Hydromagnetic equations for two isotopes in a completely ionized gas," Phys. Rev. 112, 1441 (1958).

Smith, L. P., W. E. Parkins, and A. T. Forrester, "On the separation of isotopes in quantity by electromagnetic means," Phys. Rev. 72, 989 (1947).

Sparrow, E. M., W. D. Munro, and V. K. Jonsson, "Instability of the flow between rotating cylinders: the wide-gap problem," J. Fluid Mech. 20, 35 (1964).

Spitzer, Jr., L., Physics of Fully Ionized Gases (Interscience Publishers, New York, 1962).

Tayler, G. I., "Stability of a viscous liquid contained between two rotating cylinders," Phil. Trans. Roy. Soc. A223, 289 (1923).

Urey, H. C., "Separation of isotopes," Rep. Prog. Phys. 6, 48 (1939).

Vainberg, M. M. and V. A. Trenogin, "The methods of Lyapunov and Schmidt in the theory of non-linear equations and their further development," Usp. Mat. Nauk. 17, 104 (1962).

Vedenov, A. A., E. P. Velikhov, and R. Z. Sagdeev, "Stability of plasma," Sov. Phys.- Usp. 4, 332 (1961).

Vrba, P., "The theory of a rotating plasma in crossed electric and magnetic fields," Czech. J. Phys. B 21, 636 (1971).

Watson, G. N., Theory of Bessel Functions (Cambridge at the University Press, 1966).

Watson, K. M., "Use of the Boltzmann equation for the study of ionized gases of low density. I," Phys. Rev. 102, 12 (1956).

Wilhelm, H. E. and S. H. Hong, "Plasma rotation by electric and magnetic fields in a discharge cylinder," J. Appl. Phys. 48, 561 (1977).

Wilhelm, H. E. and S. H. Hong, "Boundary-value problem for plasma centrifuge at arbitrary magnetic Reynolds numbers," Phys. Rev. A 15, 2108 (1977).

Witalis, E. A., "Magnetically induced plasma rotation," Z. Naturf. A 29, 1138 (1974).

Yudovich, V. I., "The bifurcation of a rotating flow of liquid," Sov. Phys. Doklady 11, 566 (1967).

1. Report No.	2. Government Accession No.	3. Recipient's Catalog No.
CR-135079		

4. Title and Subtitle	5. Report Date
System Analysis of Plasma Centrifuges and Sputtering	May 1978
	6. Performing Organization Code
7. Author(s)	8. Performing Organization Report No.
H. E. Wilhelm and S. H. Kong	
9. Performing Organization Name and Address	10. Work Unit No.
Department of Electrical Engineering Colorado State University Fort Collins, CO 80523	11. Contract or Grant No.
	NGR 06-002-147
12. Sponsoring Agency Name and Address	13. Type of Report and Period Covered
National Aeronautics and Space Administration Washington, DC 20546	Contractor Report 1 Nov. 76 - 31 Oct. 77
	14. Sponsoring Agency Code

15. Supplementary Notes

Grant Manager, Maris Mantenieks
Spacecraft Technology Division
NASA Lewis Research Center
Cleveland, OH 44135

16. Abstract

System analyses of cylindrical plasma centrifuges are presented, for which the velocity field and electromagnetic fields are calculated. The effects of different electrode geometrics, induced magnetic fields, Hall-effect, and secondary flows are discussed. It is shown that speeds of 10^4 m/sec can be achieved in plasma centrifuges, and that an efficient separation of U_{238} and U_{235} in uranium plasmas is feasible. - The external boundary-value problem for the deposition of sputtering products is reduced to a Fredholm integral equation, which is solved analytically by means of the method of successive approximations.

17. Key Words (Suggested by Author(s))	18. Distribution Statement
Plasma Centrifuges Isotope Separation Sputtering Deposition	Unclassified - Unlimited

19. Security Classif. (of this report)	20. Security Classif. (of this page)	21. No. of Pages	22. Price*
Unclassified	Unclassified	137	

*For sale by the National Technical Information Service, Springfield, Virginia 22161

NASA-C-168 (Rev. 10-75)